2010

Extending the chronology for Blombos Cave, South Africa: Further evidence for the origins of modern human behaviour

Elspeth H. Hayes
University of Wollongong

Extending the chronology for Blombos Cave, South Africa: Further evidence for the origins of modern human behaviour

Abstract

Behavioural modernity, however defined, is considered to be the key distinctive feature separating *Homo sapiens* from earlier hominid lineages. While the fossil and genetic records imply that modern human morphology evolved in Africa between 250 and 150 thousand years (ka) ago, there is currently no unification regarding the timing or geographical origins of modern human behaviour (MHB). An increasing body of evidence suggests modern behaviour was present during the African Middle Stone Age (MSA). Defining the origins of MHB requires accurate and precise chronologies of when they first emerged.

Blombos Cave in South Africa has yielded a collection of well-preserved cultural material from within the MSA layers. These include bone tools, shell beads, engraved ochre slabs and an assemblage of stone artefacts which are believed to represent a dynamic tool industry, the Still Bay (SB). More recently, ochre containers which may contain evidence for the ingredients used to produce paint, have been found in the lower layers of the cave, along with a tool kit, such as bone spatulas, that suggest an even earlier origin of MHB. The likely symbolic significance of these artefacts implies cognitive sophistication of MSA hominids and modern human behaviour previously only asserted in LSA people.

Examination of both sediments and anthropogenic deposits within the MSA levels have allowed the MSA layers of Blombos Cave to be subdivided into separate phases and layers. Each of these has been systematically dated in this study using optically stimulated luminescence (OSL) dating techniques. The improved temporal resolution of this site contributes to the debates regarding the key mechanisms behind the emergence of MHB. Two leading theories regarding the emergence of MHB include: 1) environmental change, and 2) demographic change.

OSL ages of sediments associated with these MSA levels suggest the SB industry occurred between 70 and 80 ka ago, with the other symbolic behaviours being recognised at ~110 ka. Such ages imply that MHB was present in southern Africa during the MSA and that it occurred sporadically, possibly as an outcome of increased human population and environmental conditions that were happening concurrently.

Degree Type

Thesis

Degree Name

Bachelor of Science (Honours)

Department

School of Earth & Environmental Sciences

Advisor(s)

Zenobia Jacobs

Keywords

optically stimulated luminesce, OSL, Still Bay, Howieson's Poort

FACULTY OF SCIENCE

EXTENDING THE CHRONOLOGY FOR BLOMBOS CAVE, SOUTH AFRICA: FURTHER EVIDENCE FOR THE ORIGINS OF MODERN HUMAN BEHAVIOUR

ELSPETH HANNAH HAYES

"THIS THESIS IS PRESENTED AS PART OF THE REQUIREMENTS FOR THE AWARD OF THE DEGREE OF BACHELOR OF SCIENCE (HONS) OF THE UNIVERSITY OF WOLLONGONG."

OCTOBER 2010

The information in this thesis is entirely the result of investigations conducted by the author, unless otherwise acknowledged, and has not been submitted in part, or otherwise, for any other degree or qualification.

_____

Elspeth. H. Hayes

13th October 2010

ABSTRACT

Behavioural modernity, however defined, is considered to be the key distinctive feature separating *Homo sapiens* from earlier hominid lineages. While the fossil and genetic records imply that modern human morphology evolved in Africa between 250 and 150 thousand years (ka) ago, there is currently no unification regarding the timing or geographical origins of modern human behaviour (MHB). An increasing body of evidence suggests modern behaviour was present during the African Middle Stone Age (MSA). Defining the origins of MHB requires accurate and precise chronologies of when they first emerged.

Blombos Cave in South Africa has yielded a collection of well-preserved cultural material from within the MSA layers. These include bone tools, shell beads, engraved ochre slabs and an assemblage of stone artefacts which are believed to represent a dynamic tool industry, the Still Bay (SB). More recently, ochre containers which may contain evidence for the ingredients used to produce paint, have been found in the lower layers of the cave, along with a tool kit, such as bone spatulas, that suggest an even earlier origin of MHB. The likely symbolic significance of these artefacts implies cognitive sophistication of MSA hominids and modern human behaviour previously only asserted in LSA people.

Examination of both sediments and anthropogenic deposits within the MSA levels have allowed the MSA layers of Blombos Cave to be subdivided into separate phases and layers. Each of these has been systematically dated in this study using optically stimulated luminescence (OSL) dating techniques. The improved temporal resolution of this site contributes to the debates regarding the key mechanisms behind the emergence of MHB. Two leading theories regarding the emergence of MHB include: 1) environmental change, and 2) demographic change.

OSL ages of sediments associated with these MSA levels suggest the SB industry occurred between 70 and 80 ka ago, with the other symbolic behaviours being recognised at ~110 ka. Such ages imply that MHB was present in southern Africa during the MSA and that it occurred sporadically, possibly as an outcome of increased human population and environmental conditions that were happening concurrently.

ACKNOWLEDGEMENTS

Completion of this thesis would not have been possible without the help and support of several individuals. I would firstly like to thank my supervisors, Dr Zenobia Jacobs and Professor Bert Roberts, for all your help and support over the past year. Thank you for allowing me to explore a highly significant (and fascinating!) area of research and for giving me the amazing opportunity to travel overseas. I must give additional thanks to Zenobia, for all the hours and effort you put that allowed me to finalise this thesis. Your patience and enthusiasm was invaluable.

Thank you to my friends and colleagues working beside me in the OSL lab, not only for fielding my many impromptu questions but also for making this past year an enjoyable experience. To Terry Lachlan and Gitte Jensen, who introduced me to the OSL lab in the early days, your insights were most helpful. I would also like to thank Jose Abrantes, Paul Carr and Nathan Jankowski, for all the help with sample preparation and XRF analyses, and particularly Nathan, whose efforts in regards to this project have been greatly appreciated. Thank you to Stephanie Kermode, for always offering your help and support, and for encouraging me throughout the year.

Finally I would like to say a big thank you to Professor Chris Henshilwood and the team at Blombos, for allowing me to stay at this beautiful location and teaching me about the significance of Blombos. Thank you to my supervisors and Brain Jones, who accompanied me on this research trip. It was a fantastic experience and I am grateful to have been involved.

TABLE OF CONTENTS

Chapter 1: Background and study design

1.1 Introduction 2
1.2 Study site: Blombos Cave, South Africa 4
1.2.1 Description and site location 5
1.2.2 Site stratigraphy, sediments and layers 5
1.2.3 Archaeological context 9
1.2.4 Previous chronologies for deposits at Blombos Cave 12
1.3 Significance and innovation 12
1.4 Aims 14
1.5 Chapter summary 14

Chapter 2: Archaeology and modern human origins

2.1 Introduction 18
2.2 Models of behavioural evolution 19
2.3 Indicators of modern human behaviour 20
2.4 Standardisation of tool industries 21
2.4.1 Still Bay and Howieson's Poort MSA tool industries 22
2.5 Significance of Still Bay and Howieson's Poort MSA tool industries 24
2.5.1 Bone points 24
2.5.2 Special purpose tools: Projectiles and geometrics 26
2.6 Implications of improved technology 28
2.6.1 Specialised hunting of large prey items 28
2.6.2 Exploitation of marine resources 30
2.6.3 Range extension and dispersal into new regions 30
2.6.4 Long-distance exchange networks and procurement of raw materials 31
2.7 Symbolic expression during the MSA 27
2.7.1 Personal ornaments: Beads 32
2.7.2 Engravings 34
2.7.3 Use of pigment 34
2.8 Significance of SB and HP Industries 36
2.9 Mechanisms of behavioural change 36
2.9.1 Demographic change 37

2.9.2 Environmental change 37
2.10 Dating in archaeology 38
2.10.1 Introduction to luminescence dating 39
2.10.2 Conditions for luminescence dating 39
2.10.3 Optically stimulated luminescence and the age equation 41
2.10.4 OSL measurements on Blombos Cave sediments 43
2.11 Chapter summary 43

Chapter 3: Materials and methods

3.1 Introduction 46

3.2 Sample collection 46
3.3 Sample preparation 48
3.4 Single-grain OSL 51
3.5 Single-grain equipment 52
3.6 Single aliquot regenerative-dose procedure (SAR) 53
3.6.1 Background 53
3.6.2 SAR measurements on Blombos samples 55
3.7 Single-grain analysis 58
3.7.1 Single-grain rejection criteria 58
3.8 De distribution analysis 61
3.8.1 Radial plots, overdispersion and age models 61
3.8.2 Central age model (CAM) 64
3.8.3 Finite mixture model (FMM) 64
3.9 Radionuclide measurements and dose rate determinations 64
3.9.1 Thick-source alpha counting (TSAC) 66
3.9.2 X-ray fluorescence (XRF) 67
3.9.3 Risø GM-25-5 beta counting 67
3.9.4 *In situ* gamma spectrometry 68
3.10 Dose rate determination and corrections 70
3.10.1 Conversion from elemental concentration to dose rate 71
3.10.2 Moisture content correction 71
3.10.3 Correction for grain size and HF etching 72
3.11 Cosmic-ray dose rate 72

3.12 Calculation of total dose rate and application of the age equation 73
3.13 Chapter summary 74

Chapter 4: Equivalent dose (D_e) results

4.1 Introduction 76
4.2 OSL characteristics 76
4.2.1 Optical decay curves 77
4.2.2 OSL signal brightness 78
4.2.1.1 OSL signal brightness distribution 78
4.2.1.2 OSL absolute signal brightness 83
4.2.3 OSL dose response curve shapes 85
4.3 Equivalent dose (D_e) determination 86
4.3.1 Varying the size of the test dose 87
4.3.2 Varying the size of the signal integration range 90
4.3.3 Uncertainties on the D_e 95
4.4 Analysis and interpretation of D_e distributions 95
4.4.1 D_e distribution of SB samples 96
4.4.2 D_e distribution from samples from BBC M2 (lower), M3 & M4 levels..97
4.4.3 D_e distributions for calcrete layers 100
4.4.4 Conclusions 100
4.5 Operator variance 105
4.6 Chapter summary 108

Chapter 5: Dosimetry results

5.1 Introduction 112
5.2 Elemental concentration comparisons 112
5.2.1 ^{40}K comparisons 112
5.2.2 U comparisons 113
5.2.3 Th comparisons 118
5.3 Environmental dose rate comparisons 118
5.3.1 Comparison of beta dose rates 118
5.3.2 Comparison of gamma dose rates 119
5.4 Final dose rates 124

5.5 Chapter summary 126

Chapter 6: Final ages and archaeological significance

6.1 Introduction 130
6.2 Final age determination 130
6.3 Significance of ages obtained 132
6.3.1 Ages for Still Bay levels 132
6.3.2 Ages for layer CP/CQA – the ochre container levels 133
6.3.3 Ages for layer CS – the deepest and oldest archaeological levels 136
6.4 Driving forces behind behavioural modernity 136
6.4.1 Environmental change 136
6.4.2 Demographic change 137
6.5 Conclusions 139

References 141

LIST OF FIGURES

Figure 1.1A. Map of South African Middle Stone Age archaeological sites 6
Figure 1.1B. Blombos Cave floor plan 6
Figure 1.2 a. Photograph of the Blombos Cave and immediate surroundings 7
Figure 1.2 b. Photograph of the entrance of Blombos Cave 7
Figure 1.3. Stratigraphical diagram of Blombos Cave 10
Figure 1.4A-D. Photographs of some of the modern behavioural indicators identified at Blombos Cave 12
Figure 2.1. Map showing the locations of sites that show evidence of early modern human behaviour 21
Figure 2.2. Still Bay and Howieson's Poort artefacts 25
Figure 2.3. Bone tools as identified from several sites of early modern human behaviour 27
Figure 2.4. Points discovered at Sibudu Cave with photographs of associated residues 29
Figure 2.5. Bone fragments identified from Klasies River 31
Figure 2.6. Shell beads identified from sites of early modern human behaviour 33
Figure 2.7. Geometric engravings on ochre, bone and ostrich eggshell from sites of early modern human behaviour 35
Figure 2.8. Still Bay and Howieson's Poort Industry ages plotted with oxygen isotope records 40
Figure 2.9. Schematic of the basic principles behind OSL dating 42
Figure 3.1 a-b. Sample locations at Blombos Cave 48
Figure 3.2A-C. Illustration of single-grain equipment 54
Figure 3.3 a. Flow chart showing the conventional SAR protocol 56
b. Hypothetical sensitivity–corrected dose response curve 56
Figure 3.4A. Natural OSL decay curve for a moderately bright quartz grain 59
Figure 3.4B. OSL dose response curve 59
Figure 3.5a-d. Representative radial plots of single grain D_e values from different types of D_e distributions 63
Figure 3.6A-B. ^{232}Th and ^{238}U decay series chains 69
Figure 3.7. Different penetration spheres of alpha, beta, gamma and cosmic radiation 73
Figure 4.1a-c. OSL decay curves for one representative sample from each phase at Blombos Cave 79

Figure 4.2a-c. Decay rates of grains from samples collected from each layer measured in this study 80
Figure 4.3a-c. Cumulative light plots for all Blombos samples measured in this study 82
Figure 4.4. Four dose response curves for the four brightest grains of BBC10-3 from the Still Bay layers 87
Figure 4.5a-c. Pie graphs representing the percentage of grains rejected using different criteria 89
Figure 4.6. Percentage of quartz grains resulting in a measurable test dose OSL signal versus the percentage of usable grains after implementation of rejection criteria 92
Figure 4.7a-c. Radial plots of Blombos sample BBC09-3 using three different test doses 93
Figure 4.8a-d. D_e values shown as radial plots for individual grains of sample BBC09-3 after using different integration intervals 94
Figure 4.9 a-g. Radial plots for all seven Still Bay samples 98
Figure 4.10 a-i. Radial plots for samples collected from within the BBCM2 (lower), BBCM3 and BBCM4 levels of Blombos Cave 101
Figure 4.11 a-e. Radial plots for all five samples comprising the archaeologically-sterile calcrete layers 103
Figure 4.12. Photograph showing the fresh exposure from within the geological calcrete units where samples have been removed 104
Figure 4.13. Radial plots of the same two samples as analysed by two separate operators 107
Figure 6.1 Still Bay sample ages plotted against corresponding sea level and oxygen isotope stages 138

LIST OF TABLES

Table 1.1. Previous OSL, TL, ESR and ^{14}C dates achieved for Blombos Cave 13
Table 2.1. Archaeological signatures of modern human behaviour as observed in the MSA 22
Table 3.1. Sample names and location 49
Table 3.2. Steps of the SAR protocol used in the measurement of Blombos samples 60
Table 3.3. Sample and flux weights used in XRF analysis of major elemental constituents 70
Table 3.4. Factors to convert elemental concentrations (ppm or %) to dose rate values (Gy/ka) for alpha, beta and gamma radiation 72
Table 4.1. Number of grains pertaining to certain brightness characteristics for each sample ..84
Table 4.2. Distribution of rejected grains according to the formal rejection criteria 88
Table 4.3. Measurement results for Blombos sample BBC09-3 after receiving different size test doses 92
Table 4.4. Results of the D_e analysis, including model used, number of grains and final D_e and overdispersion values 106
Table 4.5. Number of accepted grains, D_e values and overdispersion ratios for Still Bay samples analysed by two operators 108
Table 5.1A-C. Elemental concentration comparisons using XRF and TSAC for K, U & Th concentrations 114
Table 5.2. Th/U rates from TSAC 117
Table 5.3. Beta dose rates 120
Table 5.4. Gamma dose rates 122
Table 5.5. Previously published *in situ* gamma measurements obtained from within Blombos Cave 123
Table 5.6. Total dose rates 125

Table 6.1. Final dose rates, D_e values and ages for all samples analysed in this study 134
Table 6.2. D_e values and ages obtained for the Still Bay samples after analysis by two different operators 135

Chapter 1

Chapter 1- Background and study design

1.1 Introduction

Few topics in palaeoanthropology have generated as much interest and debate than the anatomical and behavioural origins of modern humans (*Homo sapiens*). Although we are relatively confident that humans attained anatomical modernity more than 150 thousand years (ka) ago (that is to say, they were anatomically identical to present-day humans), we cannot be certain as to when our ancestors achieved the cognitive sophistication we associate with ourselves today, and what the key mechanism could be behind our apparent behavioural shift. Recent evidence obtained from new fossil and archaeological discoveries (as well as the reinterpretation of old ones) have provided valuable new insights into the course of modern human evolution. Innovations in research areas such as climate change and phylogenetic analysis, as well as improvements in dating procedures and the development and application of new dating techniques, continue to reveal important information as to the behavioural origins of our distant ancestors.

Previously, modern human behaviour (MHB) was commonly thought to be associated with a cultural 'revolution', whereby anatomically modern humans (AMH) expanded from Africa into Europe approximately 40-50 ka ago much later than when *Homo sapiens* had originated as an anatomical entity. Recent archaeological evidence from numerous sites within Africa and the Levant, however, suggest the emergence of behaviourally modern *Homo sapiens* occurred during the African Middle Stone Age (MSA), at least 30 ka earlier than previously asserted. One of the most striking features of this evidence is the emergence of two distinctive stone tool industries recorded in the southern African MSA. These are named the Still Bay (SB) and the Howieson's Poort (HP) industries and are represented not only by the emergence of complex tool assemblages, but also a range of associated symbolic artefacts indicative of modern cognition.

Evidence of the SB industry has been identified at a small number of sites throughout southern Africa, with a large collection uncovered at the site of Blombos Cave in South Africa. Currently, this site provides the most compelling evidence to suggest an early origin for MHB in Africa. In addition to the SB artefacts, this site has yielded several indisputable markers of behavioural modernity, reflecting an ability to plan for the future, symbolic consciousness, abstract thought and technological innovation.

This thesis will describe key findings from Blombos, its significance, and how they contribute to debates regarding the origins of behavioural modernity. A detailed chronology will be produced for the archaeological deposits of the site, using single-grain optically stimulated luminescence (OSL) dating. This will produce a complete timeline for behavioural innovation as identified at this site, and thereby improve the chronological resolution of the existing evidence for MHB. Such data will contribute towards determining whether behavioural innovations at this site were attained 1) gradually through cumulative change, 2) more quickly during a brief, punctuated event, or 3) in a more sporadic fashion. This information will provide insights into the possible mechanisms behind our acquisition of modern behaviour.

Chapter 1 will outline the study site, the location, stratigraphy and archaeological context of Blombos Cave and describe in more detail the archaeological evidence associated with MHB that have been identified. The existing OSL, thermoluminescence (TL), electron spin resonance (ESR) and radiocarbon (^{14}C) chronologies for the site will be outlined and the gaps within this chronology will be brought to attention. The aims and significance of this thesis will also be provided.

Chapter 2 is a synthesis of the current literature and will begin by introducing the two models of behavioural modernity and how this may be recognised within the archaeological record. Evidence of modern behavioural markers identified at certain MSA archaeological sites will be presented, with particular reference to the emergence of two revolutionary MSA stone tool industries: the SB and the HP. Proposed mechanisms triggering behavioural adaptations will be discussed with particular emphasis on climatic and demographic variables. The importance of providing accurate chronologies for these behavioural markers will also be outlined with specific reference to OSL dating techniques, which appear most suitable for dating sediments from Quaternary settings.

Chapter 3 will outline the methodology used in this study, including an explanation of the methods involved in sample collection, sample preparation, instrumentation, data collection and analysis. This will include a detailed description of the measurement and analytical methods used, such as the single aliquot regenerative-dose (SAR) procedure and the statistical age models.

Chapters 4 and 5 will present the results of the single-grain OSL analysis for sediments comprising Blombos Cave by presenting the equivalent dose (D_e) and dose rate (D_r) values, respectively. Chapter 4 will present the D_e values (i.e. the latent luminescence signal built up as

a function of time) as measured on each single grain of quartz. It will outline the percentage of grains that were unable to be used in the final age determinations and give reasons pertaining to their rejection. The final accepted D_e values will be presented in the form of a radial plot, which will provide a visual means of evaluating the D_e distributions. The shape of the radial plot and the number of rejected grains will be discussed, and what these imply about the depositional history and the inherent characteristics of the material being dated. Experimental techniques used to determine the significance of the test dose values and integration intervals will also be discussed, along with experiments on operator variance.

Chapter 5 will present the final D_r determinations for the site, outlining the amount of beta (β), gamma (γ) and cosmic radiation produced by the surrounding sediments. These have been determined using a number of methods and combinations of these methods, which will be discussed. The relative proportions of radionuclides potassium (^{40}K), uranium (^{238}U) and thorium (^{232}Th) will also be presented as measured by two separate techniques: thick-source alpha counting and X-ray fluorescence. The data obtained from both the D_e and D_r analyses will be combined to determine ages for Blombos sediments and to produce a chronology for the site.

Chapter 6 displays the final age determinations and discusses the chronology of the site with reference to 2 key issues: 1) the first appearance of modern behavioural markers at Blombos Cave, and 2) the contemporaneous climatic and demographic conditions in relation to the appearance and disappearance of symbolic innovations, and their possible meaning in relation to MHB. The chapter will conclude by outlining which model of behavioural modernity is most strongly supported by the current archaeological evidence, and recommendations will be made for future research in this field.

1.2 Study Site: *Blombos Cave, South Africa*

Archaeological evidence from Blombos Cave in South Africa provides (currently) the most substantial body of evidence supporting an origin of MHB earlier than 50 ka ago. This small archaeological cave site has yielded several pieces of evidence supporting a MSA origin for MHB, and is just one of a number of sites in southern Africa that contains evidence of MSA occupation (Fig. 1.1). Archaeological markers of behavioural modernity found within the cave are described here along with current chronological information.

1.2.1 *Description and site location*

Blombos Cave is a small sandstone cave (Fig. 1.2 a-b) situated along the southern Cape coast of South Africa, approximately 300 km east of Cape Town (34°25'S, 21°13'E), 34.5 m above mean sea level and 100 m inland from the Indian Ocean (Henshilwood et al., 2001b). The cave itself is an erosional feature formed as a result of wave-cutting into the calcified sediments of the Mio/Pliocene Wankoe Formation (part of the Breadasdorp Group) that lies above a basal layer of the Table Mountain Sandstone (Henshilwood et al., 2001b; Grine & Henshilwood, 2002; Jacobs et al., 2003a; d'Errico et al., 2005). The interior of the cave contains 55 m^2 of visible deposit with a further 18 m^2 forward of the drip line. The front entrance of the cave has an estimated depth of ~4 to 5 m of deposits, and ~3 m at the rear of the cave (Henshilwood, 2004). The cave interior has been sub-divided into 1 x 1 m squares that are strategically labelled to illustrate the cave layout (Fig. 1.1b). Each square is assigned a letter based on its horizontal position within the cave, followed by a number indicating its vertical position. The squares are further divided into four even sections, which are labelled clockwise from a to d, beginning at the top left hand corner of the square.

1.2.2 *Site stratigraphy, sediments and layers*

Currently, the Blombos stratigraphic sequence consists of six phases of Later Stone Age (LSA) and MSA occupation, with an additional three phases of non-anthropogenic sedimentary deposits (Jacobs et al., 2006a) (Fig. 1.3). The LSA phases are separated from MSA layers by a thick, archaeologically sterile layer of aeolian sand. This layer is referred to as the BBC Hiatus, and its stratigraphic position makes it a key unit, as it provides a minimum age for the MSA deposits (Jacobs et al., 2003a). The LSA sequence situated directly above this has been dated using radiocarbon (^{14}C) dating to ~2 ka before present (BP).

The MSA layers are divided into five phases: BBCM1, BBCM2 upper, BBCM2 lower, and BBCM3 and BBCM4. These will be referred to as M1, M2 (u), M2 (l), M3 and M4, respectively. The naming of these phases has changed slightly over the last year or so, and since the publication of the original excavation, because at least four more field seasons have been conducted. This resulted in a more finely resolved understanding of the stratigraphy and a larger artefact assemblage that has informed the divisions. In the section below, I will describe the stratigraphy as understood in 2010.

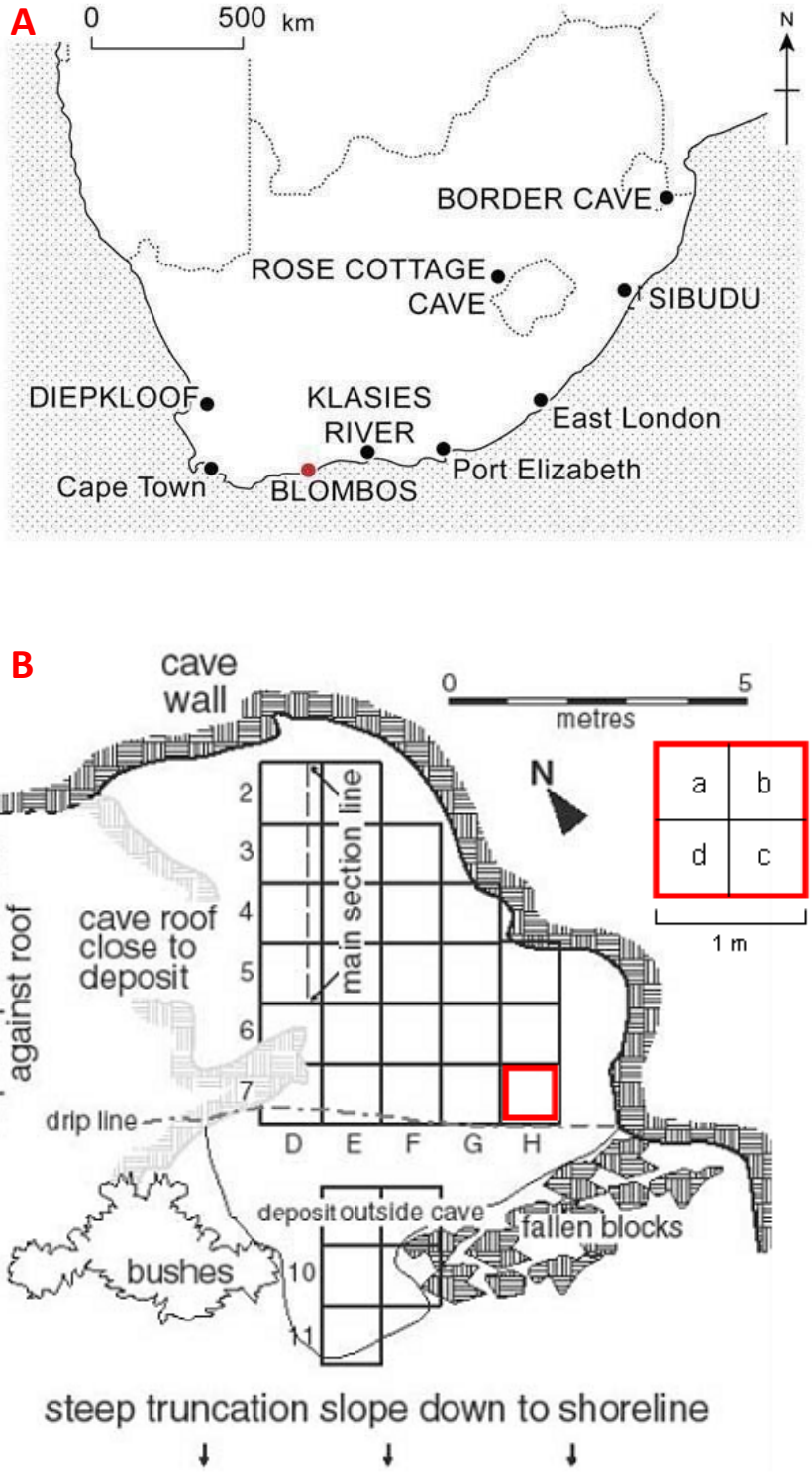

Figure 1.1: A) A map of southern Africa indicating some of the better known MSA archaeological sites in South Africa, including Blombos Cave (from Jacobs et al., 2008). **B)** Blombos Cave floor plan. The cave area has been divided up into smaller areas of $1m^2$; which have further been divided up into four sections and labelled according to their horizontal and vertical positioning.

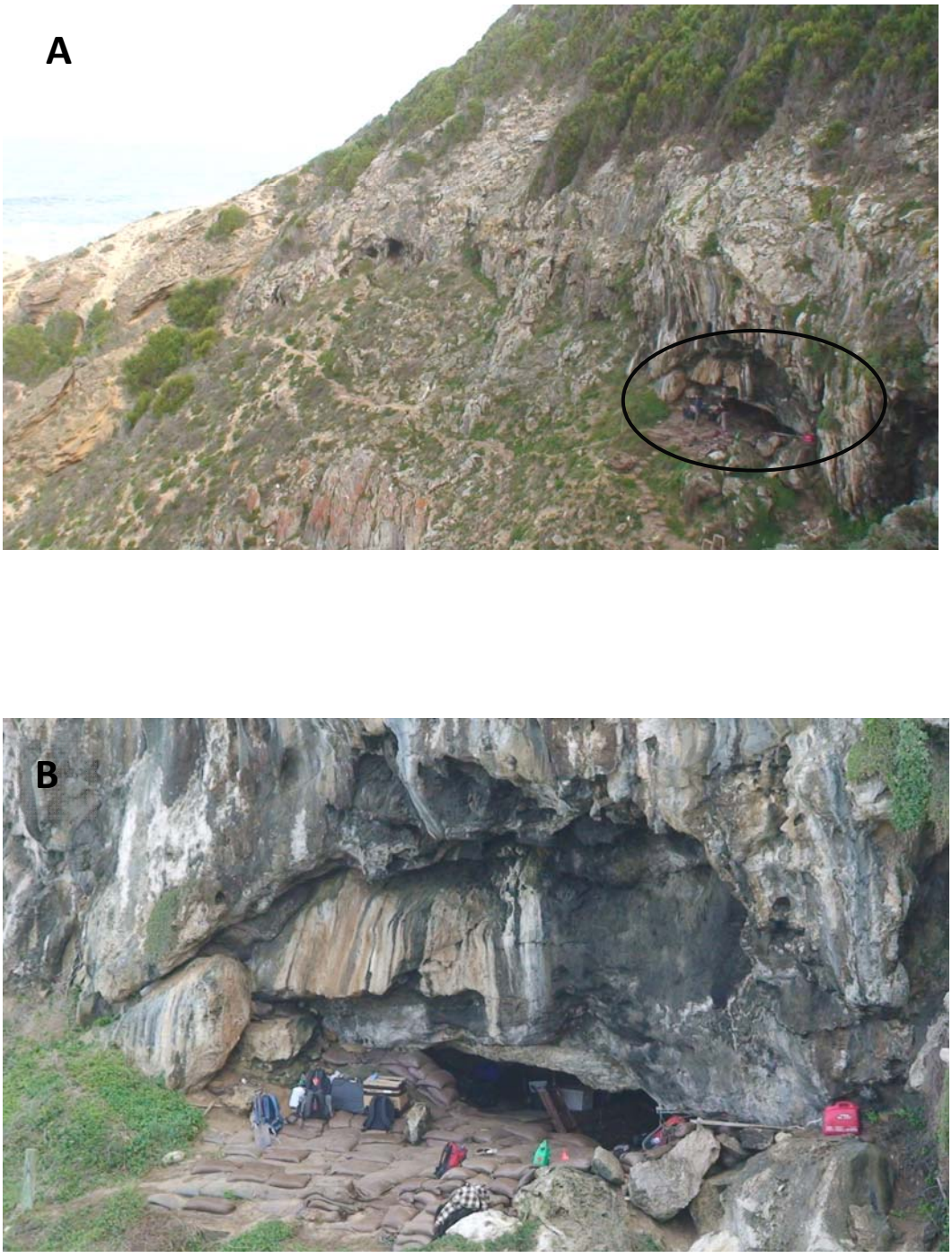

Figure 1.2: a) View of Blombos Cave and the immediate surroundings. b) Entrance of Blombos Cave (photographs: Richard G. Roberts).

The M1 phase contains the four uppermost MSA layers, directly below the BBC Hiatus. This phase, together with the upper four layers of the M2 phase, is referred to as the 'Still Bay' phase as it contains lanceolate bifacially shaped points, the *fossil directeur* of the SB industry.

The M1 phase has been dated using single-grain OSL dating of sedimentary quartz grains, TL dating of burnt stones and ESR dating of bovid teeth to between 75 and 70 ka (Jones, 2001; Jacobs et al., 2006a; Tribolo et al., 2006). Presence of behavioural indicators at this time suggests modern cognitive abilities that are conventionally not associated with MSA people.

The M2 upper phase (~85 to 75 ka) lies directly below the M1 phase and is comprised of four layers (CFA, CFB, CFC and CFD) (Fig. 1.3). It contains a large number of bone tools, probably used as awls or projectile points (Henshilwood et al., 2007), with additional SB stone points. In the latest understanding of the stratigraphy and archaeological content of these layers, the M2 (u) phase is now also considered part of the SB phase. Only one OSL age for the M2 (u) (layer CFD) has been reported previously (see Table 1.1).

The M2 lower phase contains four layers (CGAA, CGAB, CGAC, CGB). These levels contain high densities of shellfish remains, large hearths and a number of bone tools.

Directly below the M2 phase is the M3 phase which is made up of nine layers (CH-CP). This phase is still largely unpublished, and many more layers have been revealed during the most recent excavations. Large roof-fall blocks made it difficult to excavate these layers, but some of the most obstructive of these blocks have been removed to facilitate further excavations of the deeper deposits.

The upper layers (CH, CI and CJ) of the M3 phase contain vast quantities of well-preserved shellfish remains, evidence of burning in the form of hearth features and charcoal, and also high densities of ochre, including several pieces that display deliberately engraved surfaces (Henshilwood et al., 2009). The middle layers (CK, CL, CM and CN) are thin sandy layers with only ephemeral evidence for occupation. Layer CO is distinctly different from the overlying and underlying layers, as it is a rubbly layer consisting mostly of small pieces of roof spall. The upper part of layer CP is a sterile sand layer. Immediately below the upper CP sterile layer is layer CPA. When this layer was first excavated, it was bright red in colour, as a result of the large ochre content, which occurs mostly in fine, powdered or ground form. This layer is also archaeologically quite rich, containing further evidence for MHB alongside a more traditional stone tool kit. The sediments below this rich archaeological unit (layer CQ) is again

sterile and is positioned above a thick (~15 to 20 cm) layer of calcrete. This calcrete layer is culturally sterile. It can be traced horizontally across the entire excavated area (analogous to the sterile dune sand (BBC Hiatus) overlying the entire MSA) and separates layers CQ and CR. Little dating work has been done on the M3 layers at Blombos. A multi-grain OSL age of ~140 ka was reported by Jacobs et al. (2006a).

The remainder of the layers (CR and CS) make up the new M4 phase. Little material has been excavated, as large roof fall has again retarded progress. Nonetheless, layer CR is present immediately below the calcrete layer and contains evidence for occupation in the form of stone tools, shell and bone. Directly below this level is another thick (~10 cm) calcrete layer, separating layer CR from the underlying layer CS. At this stage, it is still uncertain whether or not this layer is sterile, or whether it may represent the deepest excavated occupation level. No dating work has been reported for these levels.

1.2.3 *Archaeological context*

The M1 and M2 (u) phases represent the SB phase, which is characterised by numerous indicators of MHB. These include over 400 SB stone tools (Henshilwood et al., 2001b), bone artefacts (Henshilwood & Sealy, 1997; Henshilwood et al., 2007), shell beads, which probably worn for jewellery (Henshilwood et al., 2004; d'Errico et al., 2005), and 13 pieces of deliberately engraved ochre with a cross-hatch pattern (Henshilwood et al., 2002, 2009) (Fig 1.4 a-d). In addition, a permanent pre-molar crown from an anatomically modern individual, as well as two heavily worn human deciduous teeth, were recovered from this phase (Grine et al., 2002). From the deeper layers of the cave – that is, the lowest layer of the M3 (layer CPA) – equally significant indicators of MHB have been identified, including the presence of ochre containers that may contain evidence for the ingredients used to produce paint for body and cave art, and also the tool kit (such as bone spatulas), used to produce and mix it. High densities of powdered ochre also characterise this layer. While these new discoveries are potentially very significant, the newly uncovered phases from which these finds have been obtained are yet to be dated.

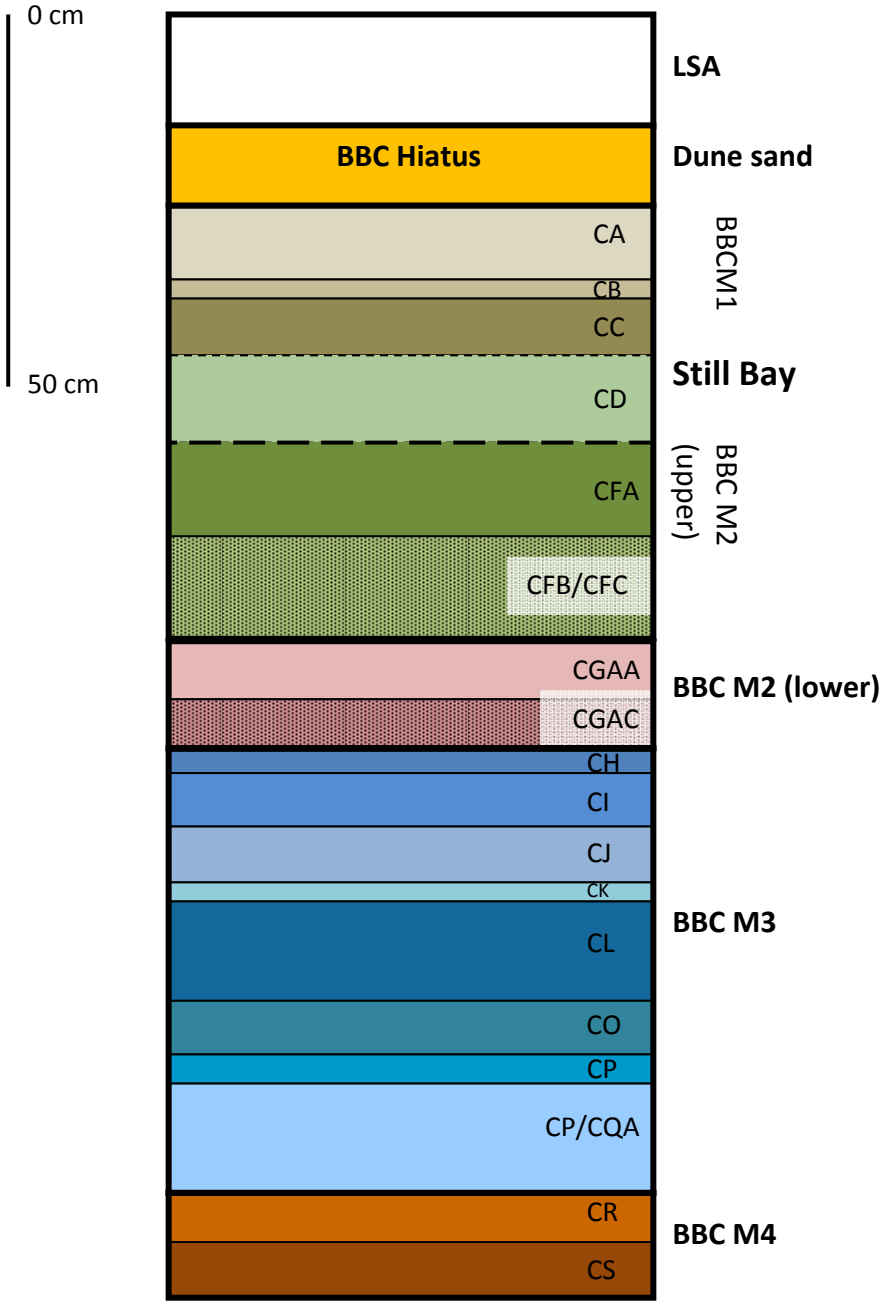

Figure 1.3: Stratigraphic diagram of the internal layers comprising Blombos Cave. The green layers represent the SB level, which is composed of the M1 and M2 (u) phases (separated in this diagram by broken black line). The pink, blue and brown layers represent the M2 (l), M3 and M4 levels, respectively. Black dots indicate hearth layers.

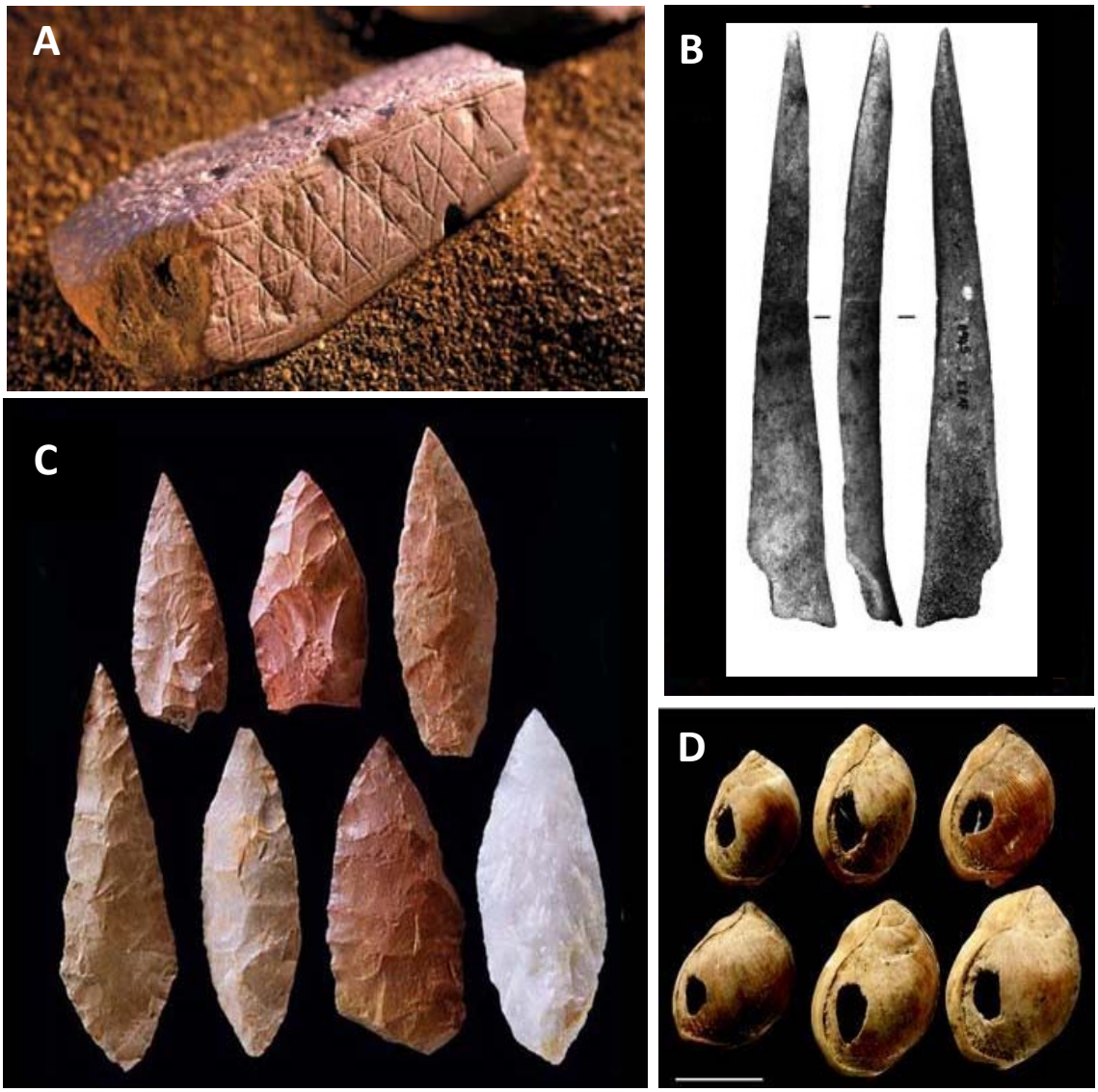

Figure. 1.4: Indicators of MHB identified in the M1 SB phase of Blombos Cave. These include: A) engraved ochre with elaborate geometric designs (from Zielinski, 2008) B) 28 bone artefacts including 25 awls and 3 points (from Henshilwood et al., 2001a), C) SB stone points, (from Henshilwood et al., 2001c) D) shell beads with deliberate perforations (from Henshilwood et al., 2004).

1.2.4 *Previous chronologies for the deposits at Blombos Cave*

Using a combination of OSL, TL, ESR and ^{14}C dating methods, ages have been produced for several of the layers comprising Blombos Cave and are outlined in Table 1.1. TL dating of burnt lithics unearthed in the M1 phase, along with OSL dating of sedimentary quartz grains and ESR dating of bovid teeth, have generated mean ages of 74 ± 5 ka, 75.6 ± 3.4 ka,and 62 ± 6 ka to 82 ± 6 ka, respectively (Jones, 2001; Jacobs et al., 2006a; Tribolo et al., 2006). The latter two ages represent the early uptake (EU) modelled ages and the linear uptake (LU) modelled ages as achieved through ESR dating. ^{14}C dating was also attempted for this phase, but the ages obtained were infinite, as these layers lie beyond the radiocarbon barrier, that is, before the ~40 ka practical limit of the technique. Radiocarbon dating was instead applied to the uppermost sequence of the cave, the LSA phase (directly above the BBC Hiatus). Radiocarbon analysis on pieces of both charcoal and shell provided a mean age of ~2 ka BP for this phase (Henshilwood et al., 2001a).

While OSL, TL and ESR ages derived from the M1 phase of the cave are in agreement with one another; chronological gaps within the entire cave sequence still exist (see Table 1.1). In order to increase the resolution of the chronology of the upper, already excavated, MSA levels at Blombos Cave, it is necessary to systematically date all the layers within each phase and apply the same methods to the recently excavated lower levels of the sequence. Only one age has been provided for the M2 (u) phase (which completes the SB phase) and the M3 phase, and there are still gaps in the M2 (l) phase. No ages have been published for the M4 phase. Obtaining an age for these lower sedimentary phases, which contain the artefacts of interest, may confirm an older age for the origins of MHB in southern Africa (although we do not know how much older).

1.3 Significance and innovation

Blombos Cave provides some of the earliest known evidence of MHB. A detailed chronology of this site will provide valuable insights as to the timing and geographic origins of MHB, and when certain technologies first appear within the archaeological record. This will contribute to the current debate about what may have triggered the abrupt appearance and disappearance of some of the markers found in the archaeological record. Based on the ages obtained (as well as previously published ages), we may infer whether MHB was acquired

Phase		Layer	Age (ka)	Method	Material	Reference
LSA			0.1 ± 0.01	OSL	sediment	Jacobs et al. 2003b
			290 ± 20 BP; 1840 ± 50 BP	^{14}C	charcoal	Jacobs, 2004
			1880 ± 50 BP; 1940 ± 50 BP; 2000 ± 40 BP	^{14}C	shell	Jacobs, 2004; Henshilwood et al. 2001b
BBC Hiatus			67.8 ± 4.2	OSL	sediment	Jacobs et al. 2003b
			64 ± 10♦; 81 ± 14♦♦	ESR	bovid teeth	Jones, 2001
STILL BAY	M1	CA	67 ± 7; 81 ± 10; 77 ± 8	TL	burnt stone	Tribolo et al. 2006
			63 ± 8♦; 57 ± 7♦	ESR	bovid teeth	Jones, 2001
			79 ± 12♦♦; 74 ± 11♦♦	ESR	bovid teeth	Jones, 2001
		CB	68 ± 10♦	ESR	bovid teeth	Jones, 2001
		CC	73 ± 3	OSL	sediment	Jacobs et al. 2006a
			68 ± 6; 82 ± 8	TL	burnt stone	Tribolo et al. 2006
			70 ± 7*; 86 ± 11♦♦	ESR	bovid teeth	Jones, 2001
		CD	50 ± 5♦; 70 ± 9♦♦	ESR	bovid teeth	Jones, 2001
	M2 (u)	CFA				
		CFB				
		CFC				
		CFD	77 ± 3	OSL	sediment	Jacobs, et al. 2006a.
M2 (l)		CGAA	82 ± 4	OSL	sediment	Jacobs, et al. 2006a
		CGAB				
		CGAC	81 ± 4	OSL	sediment	Jacobs et al. 2006a
			76 ± 7	TL	burnt stone	Tribolo et al. 2006
		CGB	85 ± 6	OSL	sediment	Jacobs et al. 2006a
M3		CH				
		CI	99 ± 6	OSL	sediment	Jacobs et al. 2006a
		CJ				
		CK				
		CL				
		CM				
		CN				
		CO				
		CP				
M4		CQ				
		CR				
		CS				

* EU modelled ESR, ♦♦ LM modelled ESR

Table 1.1: ESR, OSL, TL and ^{14}C ages produced for Blombos Cave, along with material being dated and references.

gradually over the last ~200 ka, evolving alongside anatomical developments, or whether it may have occurred in a more mosaic fashion, in tandem with environmental and/or demographic changes that can be gleaned from long-term environmental proxies and genetic information. We can also conclusively eliminate the possibility that behavioural modernity occurred rapidly at 50 ka. This will contribute towards current debates about what the 'triggers' may have been for the punctuated presence of particular innovations observed in the archaeological record. Such insight will enhance our understandings of the place, time and cause of the origins of MHB.

1.4 Aims

The aim of this research project is to obtain reliable age estimates using single-grain OSL dating for as many as possible of the MSA sedimentary layers identified at Blombos Cave. Dating these layers will enable us to finely resolve the chronology of the occurrence of MHB observed at the site. The specific aims of this project are:

1. to date the new finds in the deeper and recently excavated deposits, to push back the timing of MHB
2. to collect and date samples from previously excavated layers, to more finely resolve the existing evidence for MHB from this site, and
3. to integrate the new Blombos chronology with ages of modern human behavioural indicators at other archaeological sites across Africa and in the Levant, and to use this chronology to facilitate comparisons of the archaeological record with the demographic and environmental records for the same time period.

The expected outcome of this research is to show that MHB was present in southern Africa from at least 100 ka ago or more. This will add to the mounting evidence that indicates that MHB has its roots in the African MSA and that it was most likely acquired gradually over a long period, and in tandem with, changes in modern human anatomy.

1.5 Chapter summary

Blombos Cave in South Africa presents an opportunity to assess the origins and timing of MHB. Not only does this site display several indisputable markers of behavioural modernity,

but it also provides an abundance of potentially datable sediments so the chronology of the site, and thus the timing of the origins of MHB, may be finely resolved. This will contribute to debates regarding the antiquity of MHB as well as the possible mechanisms behind these revolutionary behavioural adaptations.

Chapter 2

Chapter 2- Archaeology and modern human origins

2.1 Introduction

It is generally considered that *Homo sapiens* is unique in their possessing language and symbolic consciousness and that we originated from a non-linguistic, non-symbolic ancestor. There is, however, currently a debate about whether or not we differed in our behaviour from Neanderthals (or even 'Hobbits' – *Homo floreniensis*) (e.g., d'Errico, 2003; Brumm et al., 2006; Zilhão, 2007). Some researchers consider that Neanderthal behaviour embraced the full range of 'modern' technology, subsistence and symbolism (e.g., d'Errico 2003, 2008; Zilhão, 2007), whereas others argue that significant differences in behaviour existed between the two species (Mellars, 2005). So the fundamental question remains: did *Homo sapiens* have superior and more complex behaviour than that of other species, which gave us a competitive advantage? If so, then how can we recognise it in the archaeological record?

While many authorities agree that a behavioural transformation resulted in the expansion and dispersal of modern *Homo sapiens* throughout Africa and the Old World, they are currently divided as to when modern behavioural traits first appear in the archaeological record, whether it is unique to our species, and what the possible triggers could be for this perceived behavioural shift. Unravelling this mystery relies on our ability to identify markers of behavioural modernity within the archaeological record and to produce accurate chronologies of when these markers first appear.

Much of the difficulty in pinning down MHB lies with defining modern behaviour. Any definition of modern behaviour has to begin with a *conceptual* definition (what is modern behaviour?) and from which an *operational* definition (how can it be recognised in the archaeological record?) needs to be developed. For example, symbolism has emerged as an important component of MHB. Symbolism commonly includes evidence for art, language and personal ornamentation (e.g., Chase & Dibble, 1987; Davidson & Noble 1989, 1993; Noble & Davidson, 1996; Wurz, 1999; Chase, 2001, 2006; Deacon, 2001; Henshilwood & Marean, 2003; Wadley, 2003; Klein 2008). But, how do you recognise language, for example, in the archaeological record (d'Errico et al., 2003; Chase, 2006;) and are all shells that have been pierced evidence for personal ornamentation (e.g., Henshilwood et al., 2004; Vanhaeren et al.,

2006; Bouzouggar et al., 2007; Klein, 2008)? If a consensus view can be obtained on what constitutes MHB, then identification of reliable markers may be determined.

This chapter addresses the interpretations regarding the timing and origins of behavioural modernity by reviewing the current evidence as identified in the archaeological record. An overview of the OSL dating procedures is also provided, as this method has proven to be especially useful in the analysis of Quaternary settings and, thus, may provide valuable insights into this elusive topic.

2.2 Models of behavioural evolution

Over the past two decades, one topic in particular has dominated the palaeo-anthropological debate: the origins of 'modern' humans (*Homo sapiens*). While fossil and genetic evidence confirm that the origin of AMH occurred in sub-Saharan Africa during the MSA, between approximately 250 and 100 ka ago (see Cann et al., 1987, Vigilant et al., 1991; Hammer, 1995; Ingham, 2000; White et al., 2003, Forster and Matsumura 2005, McDougall et al., 2005; Atkinson et al., 2009), there is currently no consensus as to the timing and origins of MHB.

In general, the term 'behavioural modernity' is used to describe the point at which AMH began to demonstrate not only fully modern cognitive ability, but also the fully modern capacity for culture (Klein, 1995). This is reflected in an ability to communicate symbolically and may be identified through the presence of certain archaeological signatures (McBrearty & Brooks, 2000) (see Section 2.3 and Table 2.1). Currently, there are two models associated with the emergence of modern human behaviour. The first proposes that behavioural innovations are related to a cultural 'revolution', whereby AMH expanded from Africa into Europe between ~50 and 40 ka ago, and subsequently replaced non-modern or 'archaic' populations. In this scenario, behavioural innovation is perceived as highly episodic and asynchronous with anatomical evolution, and perhaps triggered by biological changes causing a neural advance and the onset of language (Klein, 2008). Evidence for this model is associated with the abrupt burst of innovative technologies and symbolic artefacts observed in the European Upper Palaeolithic (UP) archaeological record at this time. Occurring alongside this transition is the African LSA, which is characterised by sophisticated blade tool assemblages, bone artefacts, personal ornaments and the emergence of symbolic artworks, all of which are indicative of MHB. The

assumption is that a lack of these features prior to the LSA reflects a lack of the required cognitive abilities (Zilhão, 2007).

An alternative model proposes that the behaviour of modern humans changed gradually, whereby behavioural modernity was acquired slowly over the last 200 ka, developing alongside modern anatomical adaptations. An earlier origin for the appearance of behavioural modernity was previously overlooked as material evidence supporting claims that MHB existed prior to 40 ka is rare and often ambiguous. However, a growing number of archaeological sites within Africa and the Levant continue to yield evidence that modern behavioural traits were present in the archaeological record as far back as 100 ka (e.g., Yellen et al., 1995; McBrearty & Brooks, 2000; Henshilwood et al., 2001a, 2001b; Vanhaeren et al., 2006; Bouzouggar et al., 2007; d'Errico et al., 2008, 2009; Bar-Yosef Mayer, 2009; Brown et al., 2009; Villa et al., 2009; Texier et al., 2010), or possibly even earlier (Marean et al., 2007). The sites in southern Africa provide numerous indicators of behavioural innovation, including the emergence of two sophisticated blade-based stone tool industries, the SB and HP. Such indicators represent early manifestations of sophisticated cognition and enhanced cultural complexity not traditionally associated with MSA hominids.

2.3 Indicators of modern human behaviour

While genetic and fossil evidence provide valuable insights into the timing and geographical origins of anatomically modern humans, determining exactly when and how AMHs attained behavioural modernity relies on careful evaluation of the archaeological record. However, recognising exactly when our ancestors made the transition from one cognitive state to the other has proven to be exceedingly complicated. This is in part due to the fact that early symbolic markers are often difficult to interpret (Henshilwood et al., 2009) and that MHB is poorly defined (Reynolds, 1991; Henshilwood & Marean, 2003). For this reason, it is essential that the literature converges on a number of common ingredients that characterise MHBs so that they may be recognised in the archaeological record.

According to an extensive review by McBrearty and Brooks (2000), indicators that reflect advanced cognitive abilities representative of modern behaviour can be characterised by four traits concerning both adaptation and cognition. These include evidence of i) abstract thinking, ii) planning depth, iii) economic and technological innovations, and iv) symbolic

expression. Acquisition of these traits can be identified through specific archaeological signatures (Table 2.1) including ecological, technological, economical and symbolic aspects (McBrearty & Brooks, 2000). These may be expressed in the form of art and ornamentation, the use of novel materials to form artefacts (such as bone, shell and ivory), the standardisation and emergence of different stone tool varieties, and the emergence of trade and exchange networks. Although these criteria have been used in this thesis as a method of identifying the presence of MHB, it should be noted that discrepancies still exist amongst the scientific community as to whether or not these traits do in fact represent behavioural modernity. Using the above criteria, evidence of such behaviour occurring in MSA contexts is described below, with particular reference to certain archaeological sites on the African continent.

2.4 Standardisation of tool industries

The production of standardised tool categories is a distinguishing feature of behavioural modernity, reflecting greater social complexity and an assortment of regional traditions (Byers, 1994; Noble & Davidson, 1996; McBrearty & Brooks, 2000; Brown et al., 2009). According to McBrearty and Brooks (2000), points best represent the presence of regional artefact styles, reflecting specific stylistic information and a standard template of manufacture. Regionally successful designs tend to be closely replicated within a community, allowing hunters to use tools produced by a variety of craftsman over several generations. Such craftsmanship reflects the ability and use of language, as communication is required to replicate and create successful designs (Chase, 1990; Byers, 1999).

MSA examples of standardised tool industries are represented by SB bifacial points and HP backed tool assemblages. An important feature of these two industries is the spatial synchronicity of their start and end dates across a vast range of archaeological sites, and their range of associated innovative behavioural artefacts (Jacobs et al., 2008c, Jacobs & Roberts, 2009a). Sites containing evidence for these industries span over two million km^2, as shown in Fig. 2.1.

Table 2.1: Archaeological signatures of modern human behaviour as observed in the African MSA (*after McBrearty and Brooks, 2000)*

Ecology

- Range extension to previously unoccupied regions (tropical lowland forest, islands, the far north in Europe and Asia)
- Increased diet breadth

Technological

- New lithic technologies (e.g., blades, microblades, backing)
- Standardisation within formal tool categories
- Hafting and composite tools
- Tools in novel materials (e.g., bone, antler)
- Special purpose tools (e.g., projectiles, geometrics)
- Increased number of tool categories
- Greater control of fire

Economy and social organisation

- Long-distance procurement and exchange of raw materials
- Curation of exotic raw materials
- Specialised hunting of large, dangerous animals
- Scheduling and seasonality in resource exploitation
- Site reoccupation
- Intensification of resource extraction, especially aquatic and vegetable resources
- Long-distance exchange networks
- Group and individual self-identification through artefact style
- Structured use of domestic space

Symbolic behaviour

- Regional artefact styles
- Self adornment (e.g., beads and ornaments)
- Use of pigment
- Notched and incised objects (bone, eggshell, ochre, stone)
- Image and representation
- Burials with grave goods, ochre, ritual objects.

2.4.1 *SB and HP MSA tool industries*

The SB industry may be identified throughout the southern Cape coast of South Africa and at other South African and Namibian sites such as Sibudu and Apollo 11. The SB industry is characterised by finely flaked lanceolate points composed of high quality materials such as chert, quartzite and silcrete (McBrearty & Brooks, 2000; Brown et al., 2009) (Fig. 2.2 a,b). The HP industry extends over a wider range of southern Africa, and is made of fine-grained lithic

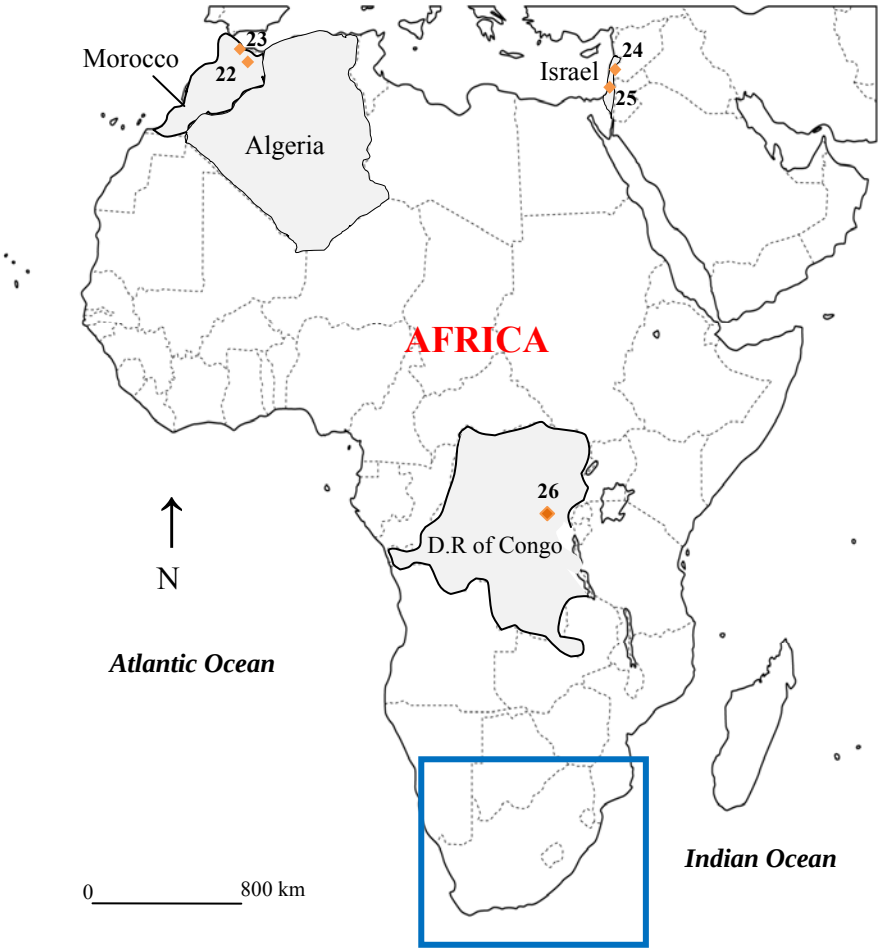

South African Sites:

1. Klein Kliphuis
2. Diepkloof Rock Shelter
3. Peers Cave
4. Blombos Cave
5. Boomplass
6. Pinnacal Point
7. Nelson Bay Cave
8. Klasies River Mouth
9. Howiesons Poort Cave
10. Umhlatuzana Rock Shelter
11. Sibudu Cave
12. Border Cave
13. Rose Cottage Cave
14. Ntlonoona Tsoana
15. Sehonghong Moshebis
16. Mellkane

Namibia sites:

17. Bremen 1C
18. Haalenberg
19. Aar 1
20. Pockenbank
21. Apollo 11

Moroccan sites:

22. Tafarolt (Grotte des Pigeons)
23. Ifri n'Ammar

Israeli sites

24. Qafzeh
25. Skhul

D. R. Of Congo sites

26. Katanda

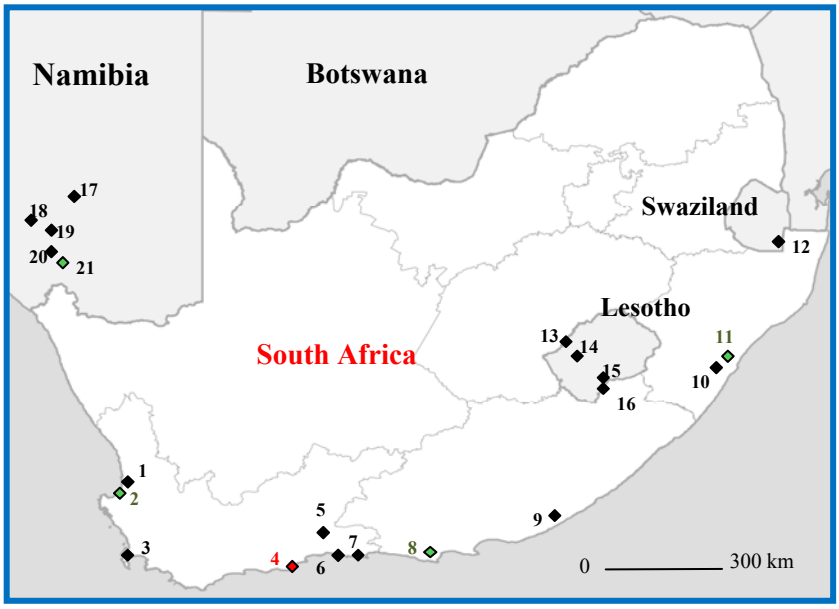

Figure 2.1: Locations of various African and Levantine archaeological sites as mentioned in the text (site names are listed with their corresponding numbers). Inset shows sites containing SB and HP artefacts as identified throughout southern Africa. Red and black diamonds represent sites containing SB and HP artefacts, respectively, green diamonds signify sites containing both HP and SB artefacts.

materials including blade-like tools that have been blunted ("backed") on one side and hafted to produce a composite weapon (Fig. 2.3 c-e) (Jacobs & Roberts, 2009a, 2009b). These industries have been allocated the bracketing ages of 72 to 71 ka and 65 to 60 ka respectively, using OSL dating (Jacobs & Roberts, 2009a; Jacobs et al., 2008a).

2.5 Significance of the SB and HP industries

In general, blade-based tool industries are typically only associated with UP and LSA archaeological sites, with the majority of MSA sites exhibiting flake-based stone tool industries (Ambrose, 1998). However, the SB and HP industries represent the emergence of more complex blade-based tool assemblages, including the construction of several different forms of weapons and sophisticated hunting equipment conventionally not associated with MSA populations (McBrearty and Brooks, 2000; Mellars, 2006; Brown et al., 2009). These include bone points, projectile weapons, standardised geometric shapes, and various forms of composite tools produced by hafting of compound materials (Fig. 2.4 a-e).

2.5.1 *Bone Points*

The shaping of bone and other organic materials into finely made tools was previously only associated with the European UP after 40 ka and only with African archaeological sites after 25 ka (Henshilwood et al., 2001a). However, discoveries from the sites of Katanda in the Semliki Valley, Democratic Republic of Congo (Fig. 2.3 c) (Brooks et al., 1995; Yellen et al., 1995), and the South African sites of Sibudu Cave (Backwell et al., 2008; Lombard, 2008), Klasies River (d'Errico & Henshilwood, 2007), Peers Cave, Blombosch Sands (d'Errico & Henshilwood, 2007) and Blombos Cave (Fig.2.4a) (Henshilwood et al., 2001a; Henshilwood & Sealy, 1997) (Fig. 2.1) have now placed bone tools in African MSA contexts. These tools, which are associated with both the SB and HP industries, have been allocated ages using various dating techniques and are thought to be somewhere between 60 and 80 ka in age (Feathers & Migliorini, 2001, Henshilwood et al., 2002, Jacobs et al., 2006b, 2006c, Tribolo et al., 2006; Backwell et al., 2008). Presence of bone points at these sites provides compelling evidence for the early employment of multi-component spears or harpoons (Lombard, 2005),

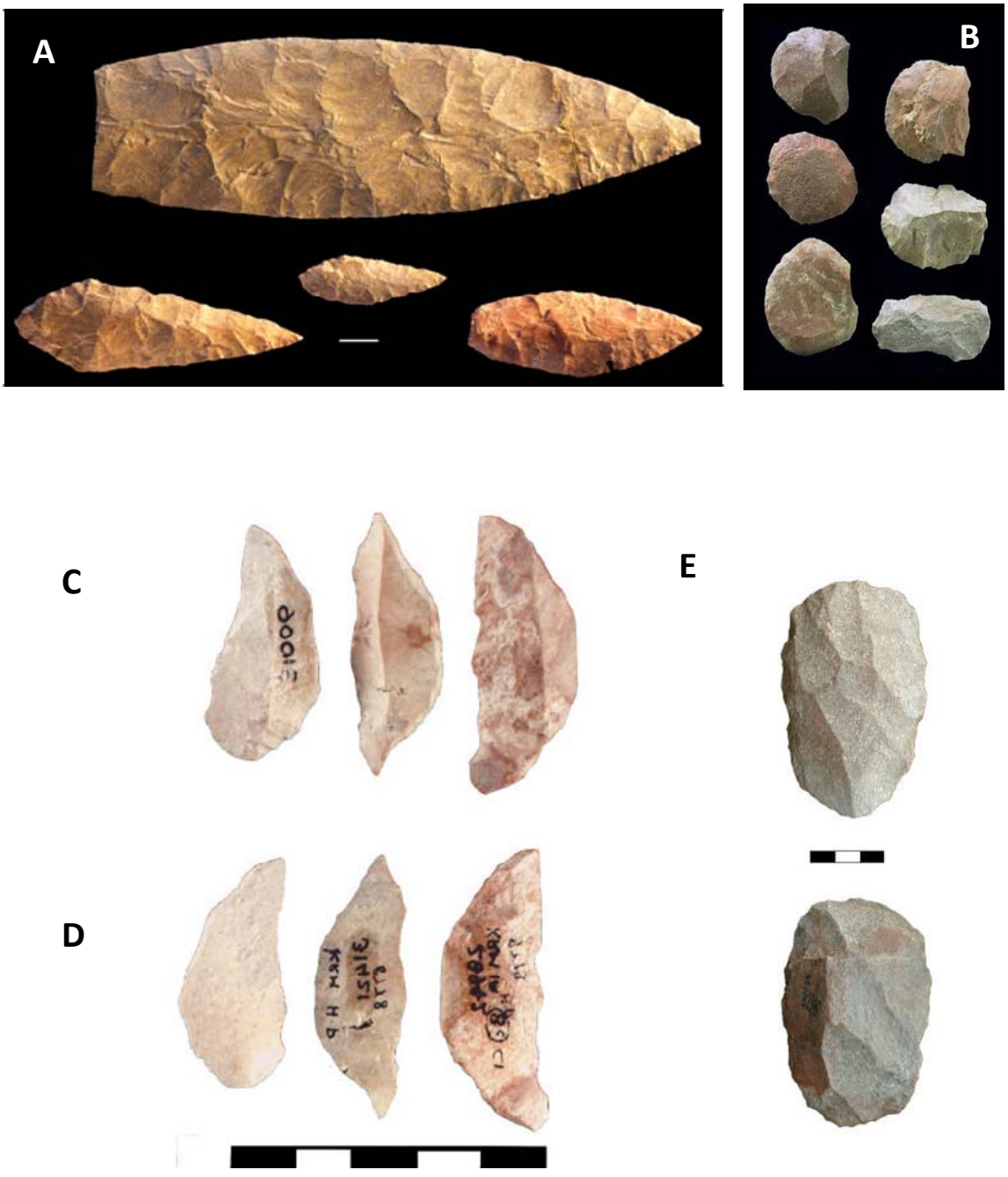

Figure 2.2: SB (A-B) and HP (C-E) artefacts; A) SB stone points (from Jacobs & Roberts, 2009b), B) SB scrapers, C) HP backed artefacts (ventral face), D) HP backed artefacts (dorsal face), E) HP blade core (upper and lower surfaces) from Wurz (2000).

most likely for the procurement of large animals and fish (see Section 2.6.1, 2.6.2) (Robbins & Murphy, 1994). In addition to this, recovered faunal remains indicate that MSA humans living in Blombos Cave were wide ranging and hunted both large and small mammals, shellfish and scavenged and/or hunted large fish and reptiles (Henshilwood et al., 2001b; d'Errico, 2005).

2.5.2 *Special purpose tools: Projectiles and geometrics*

The manufacture of raw material into standard geometric shapes to compose compound implements is associated with MSA tool industries (Brown et al., 2009). The earliest evidence for this sort of technology outside southern Africa comes from 65 ka layers within Mumba Rock Shelter in Tanzania (McBrearty & Brooks, 2000). Such craftsmanship represents an advance over simple flakes and blades, and indicates a modern approach to technology.

Retouched points from several African MSA sites may have been deliberately shaped and hafted to produce projectile weapons. Wynn et al. (2009) note that human hunters had begun hafting stone points onto the end of their spears as early as 200 ka ago and that the practice was routine in most MSA settings (McBrearty & Brooks, 2000). HP tools identified at Sibudu Cave, South Africa, reveal microscopic fractures consistent with hafting and contain 70 ka residues signifying the use of compound adhesives (Lombard, 2008; Wadley et al., 2009). Based on both residue analysis and use-wear patterns observed, it is most likely that the Sibudu HP tools were hafted onto wooden shafts used for the processing of raw animal material (Lombard, 2005, 2008) (Fig. 2.4). Microscopic residues associated with SB points from other South African sites, such as Blombos Cave, also imply the production of hafted or composite tools.

The abandonment of flake-based tool industries and the replacement of hand-held implements by hafted or composite tools represent a profound technological reorganisation implying sophisticated cognition (McBrearty and Brooks, 2000; Lombard, 2005). Furthermore, the manufacture of compound adhesives associated with the production of composite tools reflects the ability of MSA hominids to multitask and express abstract reasoning (Wadley et al., 2009; Wynn, 2009).

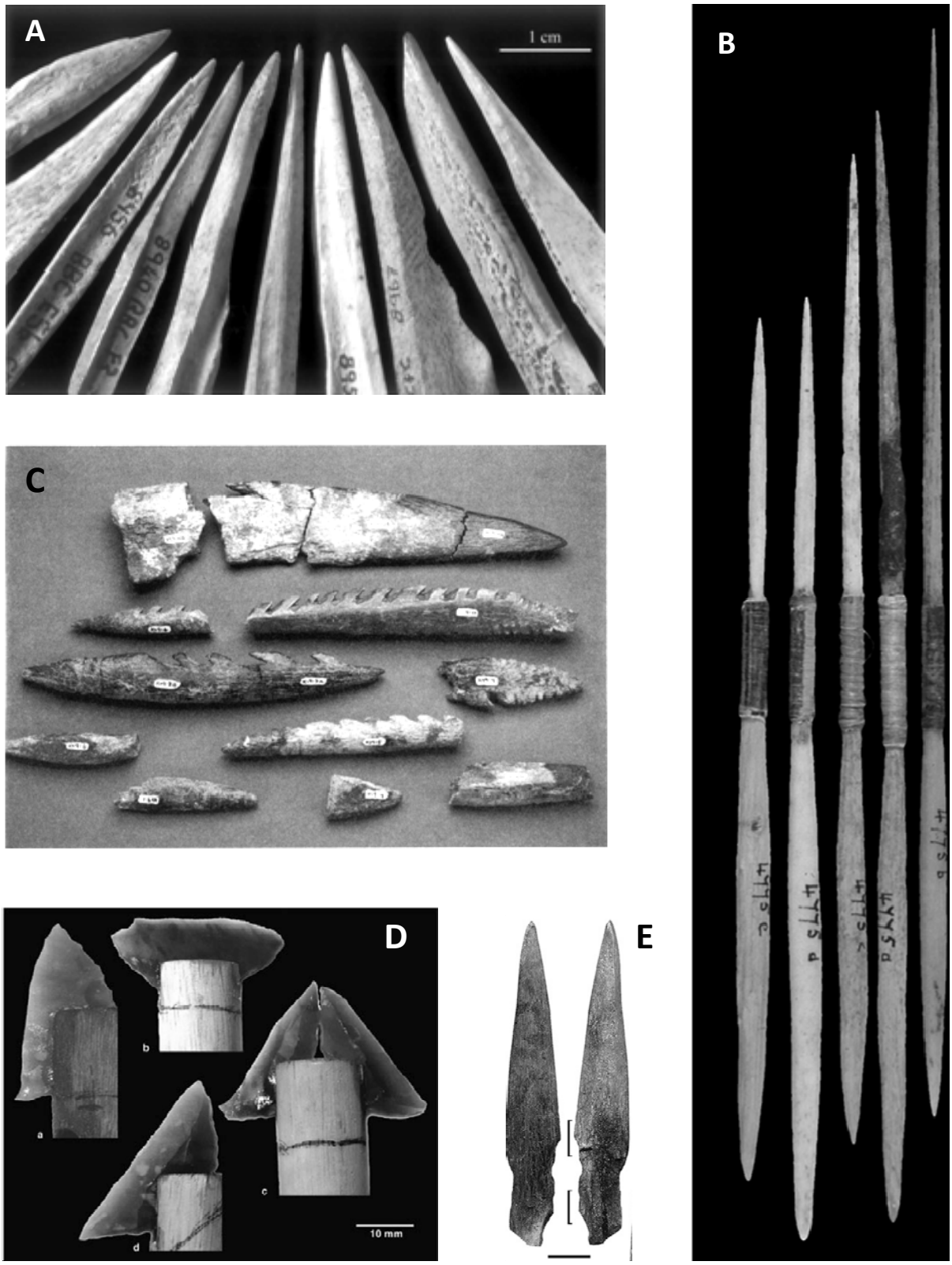

Figure 2.3: A) bone tools from Blombos Cave (from d'Errico, 2003). B) Arrow heads composed of thin arrow points connected to thicker shaft (binned with vegetal thread) (from d'Errico, 2007). C) Worked bone from Katanda (from Yellen, 1995). D) hypothetical recreations of HP tools attached to wooden handles, based on the location of adhesive residues identified on tool fragments (configurations assembled by Marlize Lombard and Justin Pargeter in Jacobs & Roberts 2009b). E) Bone points from M1 phase of Blombos Cave (from d'Errico et al. 2007)

2.6 Implications of improved technology

2.6.1 Specialised hunting of large prey items

The use of hafted or composite tools suggests that MSA hominids also indulged in weapon-assisted hunting of large game (Milo, 1998). Previously, it was argued that MSA hominids were opportunistic scavengers who lacked the ability to hunt large mammals (Klein, 1995, 1999; Binford, 1998). However, evidence from a large number of sites, including Klasies River and Die Kelders in South Africa, suggest that MSA hominids hunted bovids of all size classes and that they were skilful hunters (Marean, 1998; Milo, 1998; Plug, 2004). This is reflected in the presence of large mammal bones that have revealed microscopic cut marks and embedded tool fragments indicative of butchery (Fig. 2.5 a,b) (Milo, 1998). According to Milo (1998), primary predators and aggressive scavengers are usually entitled to the meatiest portions of bovid carcasses, including the upper hind quarters, ribs and thoratic vertebrae, as well as the upper forequarters. Butchery patterns identified on the faunal remains recovered from Klasies River suggest inhabitants had unrestricted access to these areas on bovid carcasses of all size classes, indicating either active hunting or very aggressive confrontational scavenging. The latter of the two is less likely as carnivore-damaged bone is scarce in relation to sample size (Lombard, 2005). Of particular interest is the recovery of a relatively large (10.6 x 4.4 mm) quartz fragment embedded in a cervical vertebra of a large bovid at Klasies River, most likely the tip of a stone point (Fig. 2.5 a). This animal was identified as an adult *Pelorovi antiquuss* (extinct giant buffalo) with an estimated body weight of >900 kg. Stereomicroscopic analysis reveals the embedded point was most likely introduced when the animal was still alive, providing evidence for weapon-assisted hunting of large game at this site. More recently, devices such as traps, snares and other non-selective capture techniques have been identified at Sibudu, likely used during the HP and possibly even the SB industries (Wadley, 2010). Presence of such devices indicates enhanced working memory and complex cognition demonstrated by the ability to envision actions removed from human supervision – i.e., they are out-of-sight but not out-of-mind (Wadley, 2010).

Age profiles of faunal remains identified at Sibudu Cave indicate that most of the bones come from adult animals, with some sub-adults (Lombard, 2005), thereby sanctioning the suggestion by Klein (1995, 1999) that MSA hominids are only capable of hunting juvenile or older animals, those more vulnerable to predation, disease or accidents. Furthermore, the active hunting or scavenging of large game requires the formation of socially mediated task

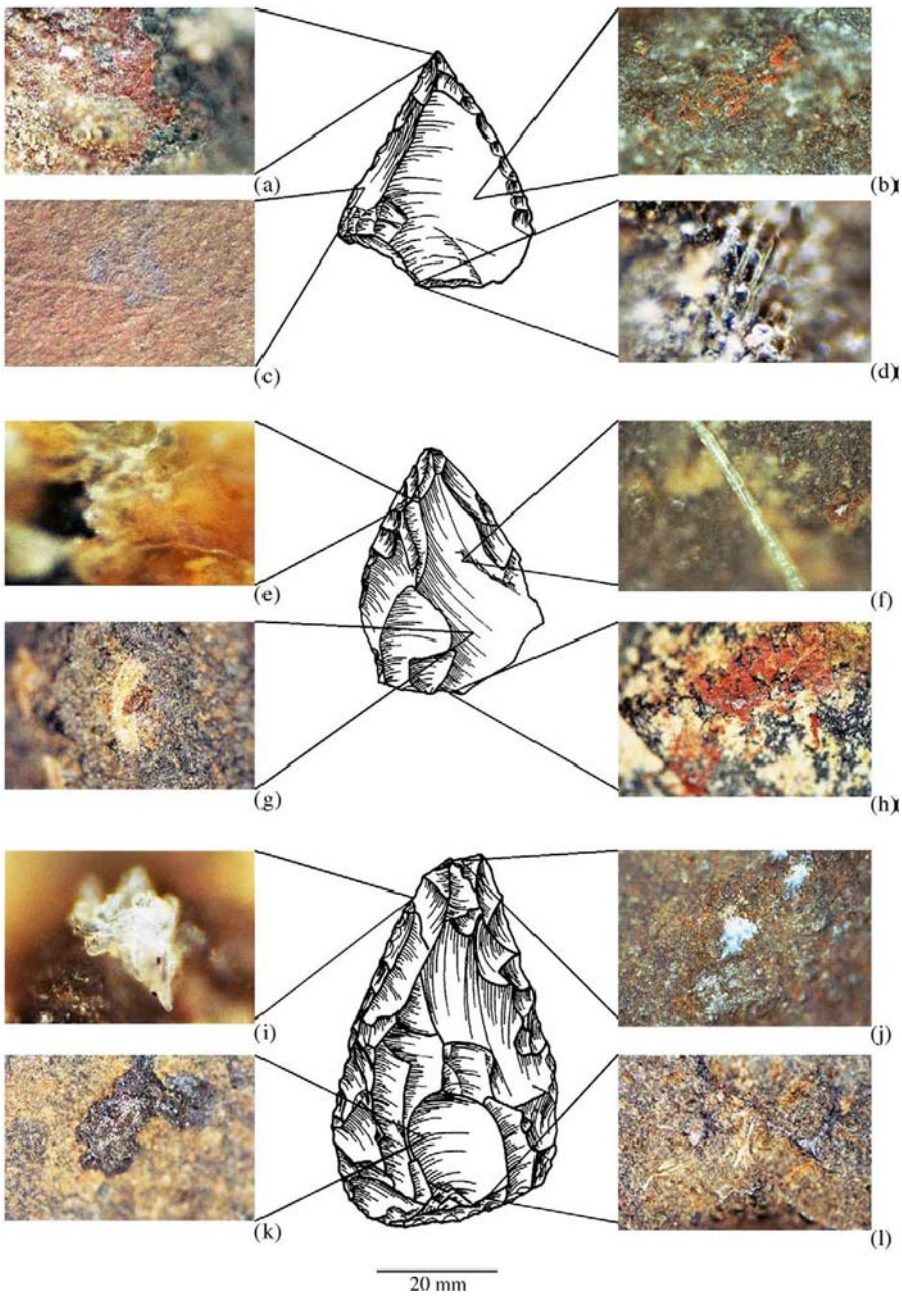

Fig. 2.4: Three points discovered at Sibudu Cave are illustrated with associated residues. **(a)** A thick blood residue deposit near the tip of the tool, **(b)** a diagonally deposited ochre smear on the medial portion, **(c)** a transverse striation associated with ochre and plant exudate (the grey stain) on the proximal surface, **(d)** bark cells on the proximal edge, **(e)** animal tissue on the distal surface, **(f)** animal hair on the medial surface, **(g)** woody residue trapped under a resin deposit on the proximal surface **(h)** a thick ochre deposit near the proximal edge associated with a diagonal striation and polish; the brown residue in the upper right corner of the micrograph is resin and the whitish deposit is macerated wood, **(i)** collagen with brown spots on the distal edge, **(j)** fatty deposit near the tip, **(k)** thick resinous deposit with wood imprint, and **(l)** woody fibres and resin associated with polish near the proximal edge of the tool. (from Lombard, 2005).

groups necessary to accomplish labour intensive tasks, which reflect both strategic planning and social networking skills equal to those of their LSA successors (Milo, 1998).

2.6.2 *Exploitation of marine resources*

Absence of clear fishing paraphernalia within MSA contexts has questioned the deliberate exploitation of marine resources by MSA hominids (McBrearty & Brooks, 2000). Despite this, intentional acquisition of marine resources may be inferred on the basis of stratigraphic context or the known habitat preferences of certain species. As such, fish remains identified within 75 to 50 ka year-old aeolian sediments at White Paintings Rock Shelter in Botswana may be interpreted as the product of deliberate fishing practices (Robbins & Murphy, 1994, 2000). Likewise, bones recovered from the upper horizon at site 440 in southern Sudan represent deep-sea species not associated with the riparian location (McBrearty & Brooks, 2000). Evidence from the South African sites of Blombos Cave (Henshilwood & Sealy, 1997), Pinnacle Point (Marean et al., 2007) and Klasies River (Milo, 1998) also imply that humans expanded their diet to include marine resources by ~164 ky ago (Marean et al., 2007). This is reflected in the presence of large shell middens associated with the systematic exploitation of marine shell resources (Milo, 1998). Finally, fish remains identified within open-air river boundary sites at Katanda, Democratic Republic of Congo, suggest that MSA hominids exploited large fish (> 35 kg) by at least 75 ka ago (Yellen et al., 1995; McBrearty & Brooks, 2000). Improved technology would have aided the capture and preparation of marine fishes, allowing MSA hominids to exploit marine resources as they developed highly sophisticated subsistence strategies.

2.6.3 *Range extension and dispersal into new regions*

The expansion of human populations into challenging environments by means of improved technology is reflected by numerous African MSA occupational sites located across a diverse range of environments (Jacobs & Roberts, 2009a) (Fig. 2.1). Sites containing HP and SB stone tools exist across a series of geographic and climatic boundaries, including mountainous terrains as observed in Lesotho, semi-arid regions such as Namibia, as well as numerous sites along the South African coastline. The extension of AMH into these new

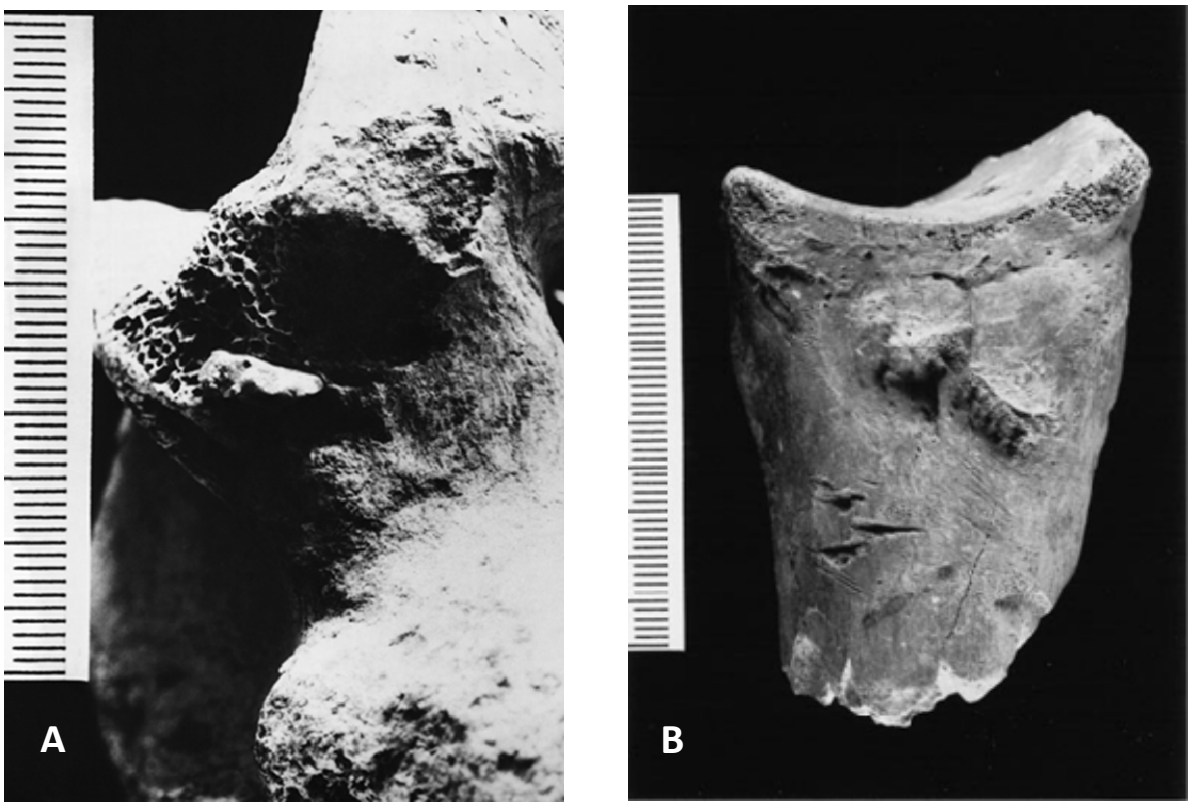

Figure 2.5: Magnification of bone fragments from Klasies River Mouth implying butchery. **A)** Quartz fragment identified as the tip of a spear head lodged into the cervical vertebrae of a large adult *Pelorovi antiquus.* **B)** Clearly identifiable cut marks overlain by at least five chop marks on the anterolateral shaft of an eland proximal radius (from Milo, 1998).

environments illustrates improved adaptive abilities of MSA hominids and their ability to exploit a new collection of resources (Clark, 1993).

2.6.4 *Long-distance exchange networks and procurement of raw materials*

The exchange of goods and the development of trade networks have long been considered a hallmark of MHB (Klein, 1995). Evidence of increased trading and exchange networks between adjacent hominid groups is reflected in the apparent technological synchronicity of the MSA SB and HP industries recorded at different sites of the same age (Jacobs & Roberts, 2009a). The sites represented in Fig. 2.1 are characterised by both SB and HP artefacts, yet span an area of two million km^2 (Jacobs & Roberts, 2009a). Furthermore, SB

and HP artefacts are often identified at sites where the production material is absent. For example, HP artefacts identified at the site of Klasies River represent the use of fine-grained lithic materials not identified locally (Minichillo, 2008). This trend implies that tools were either obtained through discrete trade networks or that materials for manufacture were collected on long-distance procurement journeys.

Evidence of this trend occurring outside southern Africa is reflected in the presence of obsidian artefacts located at several MSA sites in East Africa. Examination of the elemental and chemical composition of artefacts recovered in Kenya and Tanzania suggests that the obsidian came from a single source in the central Kenyan Rift Valley (McBrearty & Brooks, 2000). This implies artefacts were manufactured at one site and were subsequently dispersed by means of isolated exchange networks. The development of such trade industries during the African MSA implies social sophistication integral to MHB (McBrearty & Brooks, 2000).

2.7 Symbolic expression during the MSA

Symbolically mediated behaviour is a commonly accepted indicator of behavioural modernity and coincides with the emergence of both the SB and HP industries. Such behaviour may be expressed in the form of art and ornamentation, personal decoration and the adornment of specialised artefacts made from novel materials such as bone, ivory, shell and ochre.

2.7.1 *Personal ornaments: Beads*

Evidence for the emergence of symbolic culture during the African MSA is associated with the abundant occurrence of deliberately perforated marine shell beads, most likely worn as jewellery. The beads were unlikely collected for human consumption, as they are far too small to provide a sufficient amount of food to warrant collection (Henshilwood, 2004; Henshilwood et al., 2004; Vanhaeren et al., 2006). Estuarine shells identified at the sites of Qafzeh and Skhul in Israel (Vanhaeren et al., 2006; Bar-Yosef et al., 2009), Oued Djebbana in Algeria (Vanhaeren et al., 2006), Taforalt, Ifri n'Ammar and Rhafas in Morocco (Bouzouggar et al., 2007; d'Errico et al., 2009) and Blombos Cave and Sibudu in South Africa (Henshilwood et al., 2004; d'Errico et al., 2005) (Fig. 2.6 a-d) provide evidence for the use of personal ornamentation. These have each

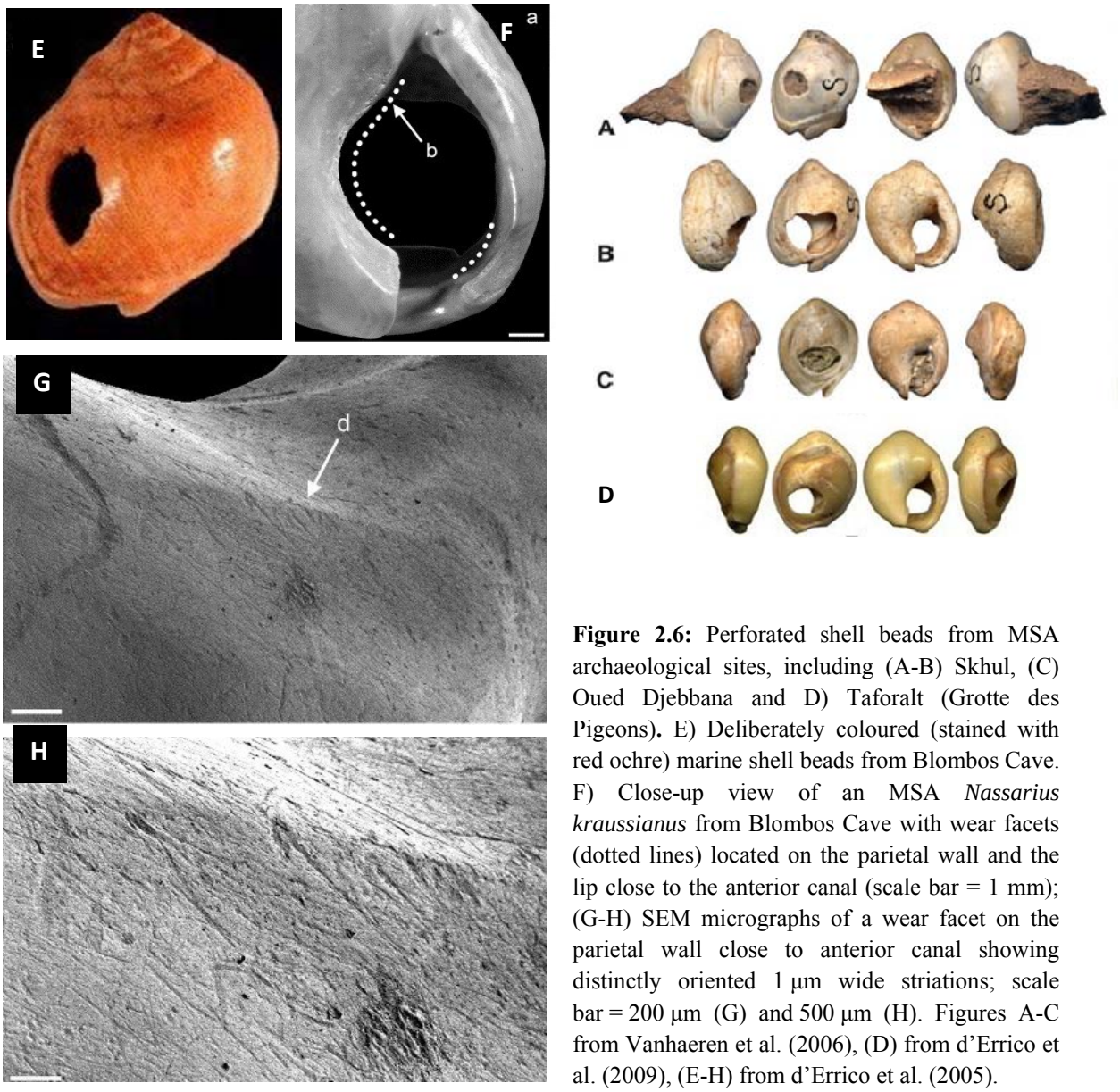

Figure 2.6: Perforated shell beads from MSA archaeological sites, including (A-B) Skhul, (C) Oued Djebbana and D) Taforalt (Grotte des Pigeons)**.** E) Deliberately coloured (stained with red ochre) marine shell beads from Blombos Cave. F) Close-up view of an MSA *Nassarius kraussianus* from Blombos Cave with wear facets (dotted lines) located on the parietal wall and the lip close to the anterior canal (scale bar = 1 mm); (G-H) SEM micrographs of a wear facet on the parietal wall close to anterior canal showing distinctly oriented 1 µm wide striations; scale bar = 200 µm (G) and 500 µm (H). Figures A-C from Vanhaeren et al. (2006), (D) from d'Errico et al. (2009), (E-H) from d'Errico et al. (2005).

been allocated ages ranging from 75 to 100 ka, placing them distinctly in MSA contexts. The shells at Blombos Cave display deliberate perforations and microscopic use-wear patterns signifying they were once strung as beads, probably to be worn as jewellery (Fig. 2.6 f-h) (d'Errico et al., 2005). It is unlikely that the perforations identified on the shells are the result of natural processes, because few natural specimens displaying corresponding perforations (Henshilwood et al., 2004; d'Errico et al., 2005; Vanhaeren et al., 2006). In addition, beads found at the Moroccan sites appear to have been deliberately coloured by heating over an open fire (d'Errico et al., 2009), a trend that is also observed in the Blombos finds, with beads apparently

stained with ochre (Fig. 2.6 e) (Henshilwood, 2004; Henshilwood et al., 2004). The significance of beadwork is that it represents an adaptive technology specific to humans, used to communicate social messages to other individuals through a shared symbolic language (d'Errico et al., 2009).

2.7.2 *Engravings*

One of the earliest well-documented expressions of symbolic behaviour includes the engraving of mobile items such as ostrich eggshell, ochre and bone. The Diepkloof Rock Shelter in South Africa (Fig. 2.1) has yielded 270 fragments of deliberately engraved ostrich eggshell (Fig. 2.7 a) dated at ~60 ka (Jacobs et al., 2008c; Texier et al., 2010). Similarly, Blombos Cave and Klein Kliphuis in South Africa have provided several pieces of engraved ochre displaying robust geometric designs (Fig. 2.7 b,c) (Henshilwood et al., 2002, 2009, Mackay & Welz, 2008). These engravings are estimated to be ~75 ka and 55 to 65 ka in age, respectively, based on OSL ages of associated sediment (Blombos) (Henshilwood et al., 2002, 2009; Jacobs et al., 2008b; Mackay & Welz, 2008). Intentional symbolic engravings of bone have also been identified at both Blombos Cave, Klasies River and Katanda (Yellen, 1995; d'Errico et al., 2001; Henshilwood et al., 2001a; d'Errico & Henshilwood, 2007) including deliberate markings on bone tools (Fig. 2.7 d) (Henshilwood et al., 2001a; d'Errico & Henshilwood, 2007). The deliberate use of geometric or iconographic representations through engraved objects reflects not just the ability of MSA humans to create a single geometric pattern, but also the development of a graphic tradition and the ability to use symbols to mediate social interactions (Henshilwood et al., 2002; Henshilwood et al., 2009; Texier et al., 2010). Such behaviour is a clear expression of symbolic communication associated with the presence of MHB.

2.7.3 *Use of pigment*

Evidence for the systematic use of pigment to create artworks or body decoration has become a consistent feature in MSA sites (d'Errico et al., 2003). The presence of ochre 'crayons' is associated with numerous archaeological sites, in some cases, as far back as 120 ka (Marean et al., 2007). Large quantities of ochre have been retrieved from sites such as Apollo 11, Boomplass, Hollow Rock Shelter, Border Cave, Klasies River, Umhlatuzana Rock Shelter, Rose Cottage Cave, Bushman Rock Shelter, Olieboompoort and Sibudu Cave (Lombard, 2007). These are associated with the SB and HP tool industries. The apparent increase in the systematic

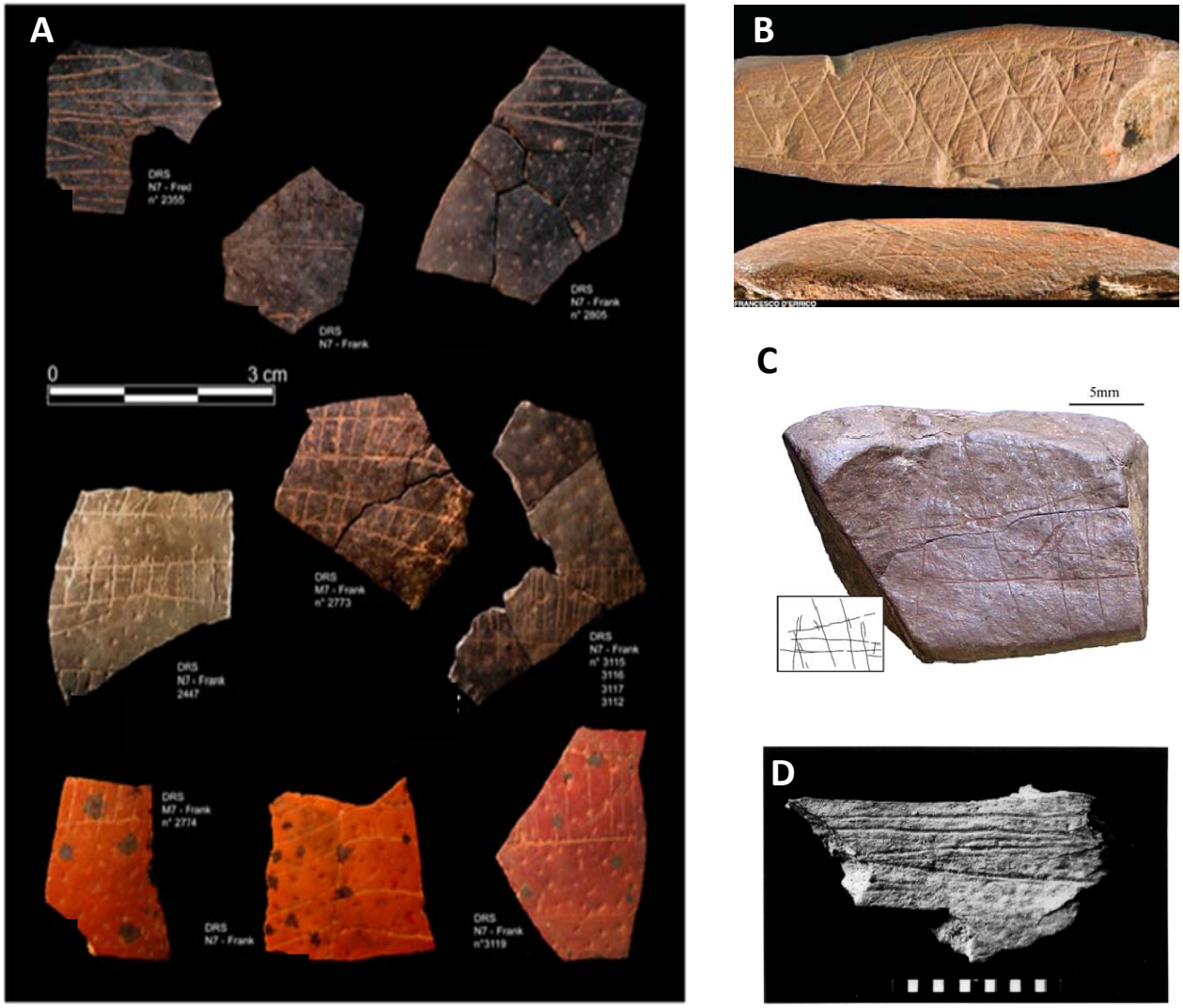

Figure 2.7: Geometric engravings from A) ostrich eggshell fragments from Diekloopf Rockshelter (from Texier et al, 2010), B) ochre slabs from Blombos (photo courtesy of F. d'Errico), C) ochre fragments from Klein Kliphuis (from Mackay & Welz, 2008) and D) incised bone fragment from Klasies River (from after Henshilwood & Sealey, 1997).

use of ochre in accordance with these industries reflects a period of heightened symbolic communication indicative of MHB (Wurz, 2000). As such, the presence of an ochre container at Blombos Cave most likely used to produce and mix paint, is potentially very significant, possibly indicating an even earlier origin of MHB.

Not only does the use of pigment represent symbolic behaviour, but may also have a functional use. Wadley et al. (2009) have tools with red ochre stains that imply the use of multi-component glue using ingredients including plant gum and red ochre. The ochre stains are present only on those parts of the tools that were once attached to hafts and, as such, are likely the remnants of some form of adhesive. Whether through symbolic expression or functional use, use of pigment is believed to be an indication of MHB.

2.8 Significance of SB and HP Industries

While it has long been recognised that the production of blade-based tool technologies such as the SB and HP industries during the African MSA are indisputable markers of behavioural modernity (McBrearty & Brooks, 2000), these revolutionary MSA industries and their associated artefacts virtually disappear from the record after 60 ka, succeeded by far less sophisticated forms of technology (Jacobs & Roberts, 2009a). Little is known about the period post-dating this dynamic phase of behavioural innovation owing to the rarity of post-HP and SB MSA occupational sites in southern Africa (Jacobs et al., 2008a). So far, there has been no documented evidence for the use of personal ornaments reliably dated to between 70 and 40 ka in Africa or Eurasia (d'Errico et al., 2009), and beads only reappear in the archaeological record at around 40 ka, following a 20 ka hiatus (d'Errico et al., 2005, 2008). The sporadic appearance and disappearance of such behavioural markers implies that behavioural innovation is highly episodic in human evolution (Tattersall, 2008).

2.9 Mechanisms of behavioural change

Several possible mechanisms have been proposed for the sporadic appearance of both the SB and HP industries and their associated artefacts. Currently, there are two opposing views: 1) demographic change, and 2) rapid environmental change. The former associates human cognitive advancements with what is now considered to be a period of expanded human population size and settlement density in Africa (Jacobs & Roberts, 2009b), whereas advocates of rapid environmental change perceive behavioural innovation as an outcome of corresponding climatic fluctuations (Thackeray, 2009).

2.9.1 *Demographic change*

Examinations of contemporary African mitochondrial DNA (mtDNA) sequences provide an estimate of the total African population size through time (Atkinson et al., 2008, 2009). Investigations carried out by Atkinson et al. (2008, 2009) suggest that human population growth occurred between 86 and 61 ka, corresponding with the rise and fall of both the SB and HP industries and the rapid appearance and disappearance of their associated symbolic markers. Other analyses of mtDNA sequences confirm the timing of this African population expansion (e.g., Watson, 1997), and indicate that a remarkable increase in population took place between 80 and 60 ka (Mellars, 2006). MtDNA distributions in Asian and European populations also reveal a clearly defined peak in population growth at between 60 and 40 ka, coinciding with the abrupt burst of innovative technologies observed in the European UP archaeological record (Mellars, 2006). The apparently rapid increase in African populations some 30 ka earlier may explain why indicators of MHB appear first in the African record (Mellars, 2006). This research has demonstrated a correlation between population expansion and behavioural innovation, the significance of which warrants investigation. Jacobs & Roberts (2009a) argue that population growth was associated with enhanced connectivity of communities, thereby facilitating the transfer of raw materials through the establishment of sophisticated trade networks. Evidence of increased trading and exchange networks between adjacent human groups at times of population expansion is reflected in the presence of high-quality stone artefacts and imported shell ornaments recorded at different sites of the same age (Ambrose, 1998). This pattern is reflected in those sites containing SB and HP artefacts as identified in Fig. 2.1 (refer to Section 2.6.4), which indicate materials were traded over vast distances among MSA hominid groups.

2.9.2 *Environmental change*

The intense climatic fluctuations that occurred during oxygen isotope stage (OIS) 4, between 74 and 60 ka, have been proposed as a possible mechanism behind the rise and fall of both the SB and HP industries (d'Errico et al., 2009; Fisher et al., 2010). Precise chronologies for the start and end of these revolutionary industries allow for direct comparisons to be made between the duration of their associated behavioural and technological innovations with specific climatic regimes. Past climatic records obtained through analysis of ice cores and lacustrine deposits (e.g. Dansgaard et al., 1993; Partridge et al., 1997; Scholz et al., 2007) indicate that the HP industry thrived during a period when temperatures were several degrees warmer

(Thackeray, 2009). However, no such warming trend is observed for the duration of the SB industry, and climatic records indicate that two subsequent warm intervals followed the HP industry, yet these are not associated with periods of technological or behavioural innovation (Jacobs & Roberts, 2009c) (Fig. 2.8). Furthermore, the dispersal of technological innovations associated with these industries occurred synchronously over a diverse range of climatic and ecological zones (Jacobs & Roberts 2009a, 2009c). As such, climate variation alone cannot be deemed as a significant factor, although we cannot discount the important role of climate as a backdrop against which changes may occur.

By mapping the demographic history of early modern humans, along with changes in climate, we are able to determine whether or not a correlation exists between the onset of behavioural modernity and demographic or environmental changes. Confirming one of these theories as a possible mechanism for the abrupt appearance of innovative technologies will have important implications as to whether MHB was acquired gradually, sporadically, or in one punctuated event.

2.10 Dating in archaeology

Accurate chronologies for MSA human occupation sites following the HP, and during both the SB and HP industries, are essential in the investigation of the origins of behavioural modernity and the key mechanisms behind these periods of behavioural innovation (Jacobs et al., 2008b). One method in particular, luminescence dating, has proven to be particularly useful in the reconstruction of Quaternary chronologies, especially as most of the of the MSA lies beyond the range of radiocarbon dating (Jacobs & Roberts, 2007, 2009). These numerical dating techniques, which includes OSL and TL dating, not only provides ages for materials that are abundant at archaeological sites, but also cover an archaeologically significant age range from just a few years to several hundred thousand years (Feathers, 1997) with typical precisions of 5-10% (Roberts & Jacobs, 2008). Several different luminescence-based dating procedures have been applied to sediments associated with southern African MSA sites. These include TL and OSL analysis of quartz from White Paintings Rock Shelter, Botswanna (Feathers, 1997), Apollo 11, Namibia (Jacobs et al., 2008b), of Lesotho and the South African sites of Die Kelders (Feathers & Bush, 2000), Sibudu Cave, Klasies River, Sehonghong, Ntloana Tsoana, Melikane Diekloof, Sehangong, Ntloana Tsoana, Rose Cottage Cave, Pinnacle Point and Blombos Cave (Jacobs et al., 2003b, 2006b,2008b; Tribolo et al., 2006; Marean et al., 2007;

Pienaar et al., 2007; Tribolo et al., 2009) (see Fig. 2.1 for site locations) as well as TL and OSL analysis of quartz and infrared stimulated luminescence (IRSL) analysis of Potassium-feldspars and polymineral fine grains at Klasies River and Duinefontein, South Africa (Feathers, 2002, Jacobs et al., 2003a). The following section describes luminescence dating techniques, with particular emphasis on OSL, which is the method used in this thesis to date quartz sediments from relevant layers of Blombos Cave.

2.10.1 *Introduction to luminescence dating*

Luminescence dating describes a collection of numerical dating methods in which ages are obtained by measuring the cumulative effect of ionising radiation on a given material (Aitken, 1998; Jacobs & Roberts, 2007). These methods are dependent on the observation that a crystalline material will emit light at a measurable intensity following some sort of stimulation, usually in the form of heat (such as in TL), or light (such as in OSL) (Feathers, 1997; Wintle 2008). Irradiation resulting from the natural decay of radioisotopes, specifically uranium (U), thorium (Th) and their daughter products, and potassium (K) (with minor contributions from cosmic radiation), causes the accumulation of electrons at defects in crystalline materials, typically quartz and feldspars (Duller, 2004; Feathers, 1996; Stokes, 1999; Wallinga, 2002). These minerals act as dosimeters and absorb incoming alpha (α), beta (β) and gamma (γ) radiation emitted during the process of radioisotope decay (Aitken, 1998). Upon stimulation, the electrons are released, causing the material to emit a faint yet measurable light; the intensity of which is proportional to the amount of stored energy, and thus time since the electron traps last emptied.

2.10.2 *Conditions for luminescence dating*

For luminescence dating methods to be applicable to sedimentary deposits, three conditions are essential. These include i) the presence of a natural dosimeter that will adequately record radiation; ii) sources of natural radioactivity and; iii) a zeroing event (Jacobs, 2004). The time elapsed since the latter is essentially the event being dated and is achieved when the trapped electron population within a material is subsequently emptied or 'zeroed'. If a material is heated to above 400°C, or if it is exposed to a sufficient amount of sunlight, the trapped

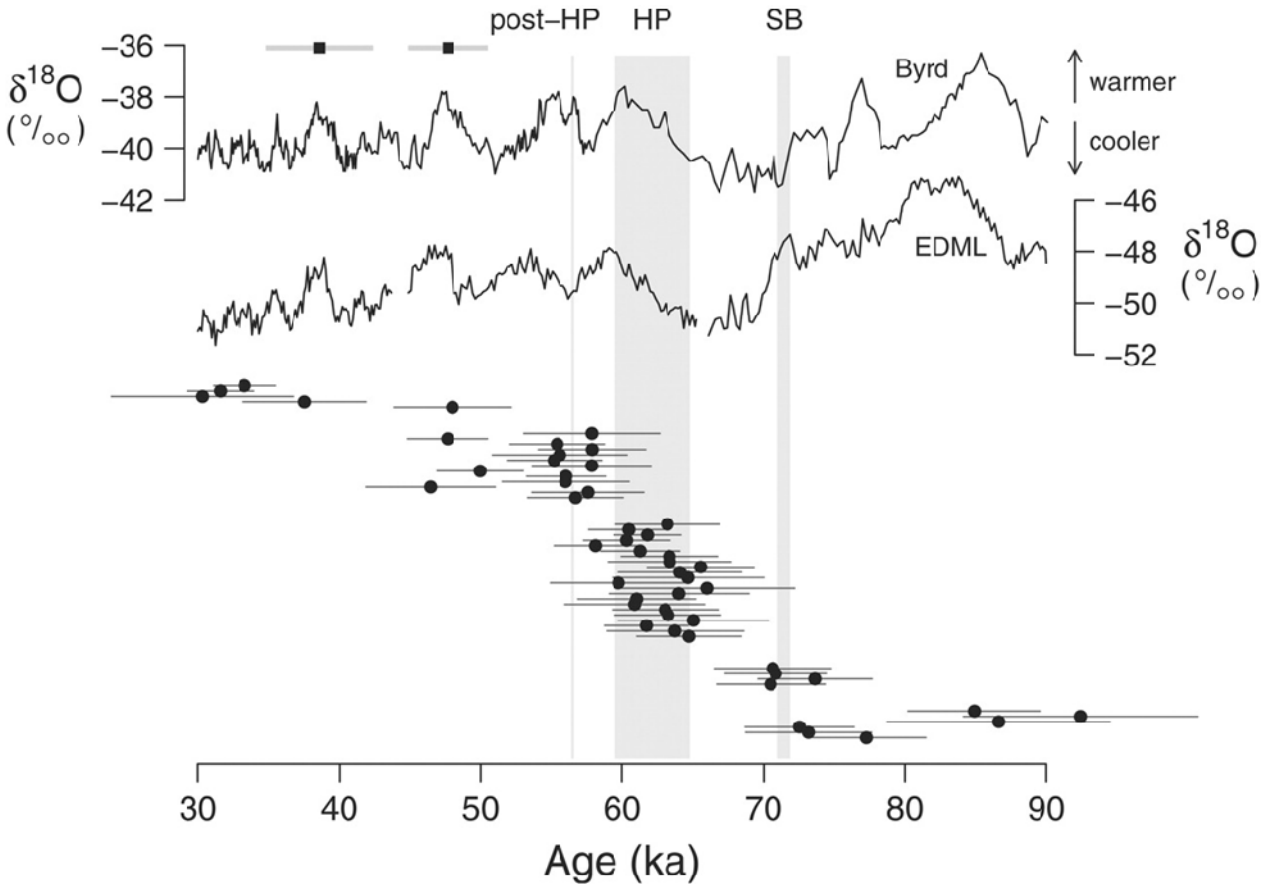

Figure 2.8. Age estimates (with 95% confidence intervals) plotted beside oxygen isotope data (‰, per mille) from the Byrd and European Project for Ice Coring in Antarctica (EPICA) Dronning Maud Land (EDML) ice cores from Antarctica. Records are plotted against time, and have been synchronised with Greenland ice core data. The EDML data are lowess-smoothed to 100-year resolution. Vertical grey bands illustrate estimates of the HP and SB periods as well as the pulse immediately post-HP, as determined by Jacobs et al. (2008c). (From Jacobs & Roberts, 2008b)

electron charge is reduced to zero, thereby resetting the luminescence 'clock'. For instance, the initial firing of pottery or the deliberate burning of flints and stones in a hot fire will sufficiently empty the trapped electron charge, while aeolian sediments will receive sufficient bleaching during transportation to reset the luminescence signal. Fluvial deposits may also be optically reset in this way, although not as effectively (Aitken & Valladas, 1992). Once the luminescence signal has been reset, natural radiation from the surrounding environment will gradually cause the electron population to build up again until another zeroing event occurs and energy is subsequently released in the form of luminescence (Fig. 2.9).

The sedimentary minerals that have proven to be particularly applicable to OSL dating methods include quartz and potassium-rich feldspars (Huntley et al., 1985; Wintle 1993, 1996). Feldspars, however, have been shown to be less reliable for dating then quartz as some varieties spontaneously lose their trapped charge, or fade, providing anomalously low ages (Wintle, 1973; Huntley & Lamothe, 2001). Researchers have also investigated optical dating on calcite, zircon and sodium-rich feldspars, however, quartz and K-feldspars are still the preferredminerals used as dosimeters (Wintle, 2008).

2.10.3 *OSL and the age equation*

In OSL, the intensity of the luminescence signal is representative of the time since the mineral grains were last exposed to sunlight (Huntley et al., 1985; Aitken, 1998; Jacobs & Roberts, 2007; Duller, 2008). Following deposition, buried mineral grains are exposed to incoming radiation from the surrounding sediment and a latent luminescence signal is gradually built up as a function of accumulating stored energy (Aitken & Valladas, 1992). When stimulated by light in the laboratory, a measureable OSL signal is produced, the intensity of which is proportional to the radiation dose the mineral has received since burial. This is referred to as the equivalent dose, D_e, and is also known as the palaeodose. The rate at which this radiation is supplied to the mineral is referred to as the environmental dose rate, D_r, and corresponds to the rate in which the trapped charge population was accumulated (Stokes, 1999). Obtaining accurate age estimates requires an equally sound approximation of the D_e and D_r. The natural radiation

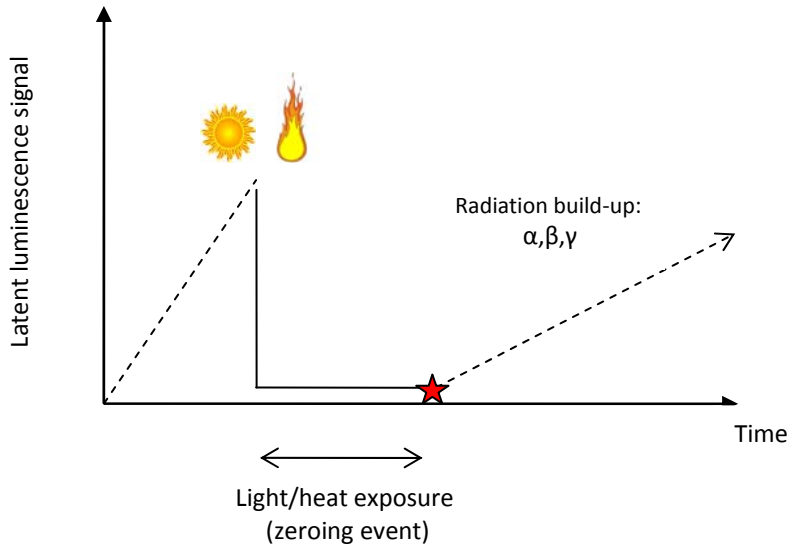

Fig. 2.9: Latent luminescence signal as a function of time. Ionising radiation causes the build up of energy within a crystalline material. Upon stimulation by heat or light, energy is released in the form of luminescence in a measurable intensity proportional to an age. The dashes lines represent burial time. The star represents the event being dated.

supply is predominately comprised of gamma, beta, and alpha radiation derived from the natural decay of radioactive elements ^{238}U, ^{235}U, ^{232}Th and their decay products, and ^{40}K, with minor contributions from ^{87}Rb (Aitken, 1985). The SI unit for absorbed radiation dose is measured the gray (Gy), where 1 Gy = 1J kg^{-1} (Jacobs & Roberts, 2007). To determine the optical age of the sediment, the following equation may be applied:

$$\textbf{Age (ka)} = \frac{\text{Equivalent dose or Palaeodose (Gy)}}{\text{Environmental dose rate (Gy/ka)}}$$

From the ages obtained, one can infer by association the ages of site occupation, manufacture of artefacts, and accumulation of faunal remains, based on the depositional age of the surrounding sediment (Jacobs & Roberts, 2007).

2.10.4 *OSL measurements on Blombos Cave sediments*

Two issues vital to our understanding of the Blombos Cave MSA artefacts involves the reliability of the dating of the MSA deposits and the stratigraphic integrity of the layers in which these significant artefacts are found (Jacobs, 2004).

According to Jacobs (2004), there are 3 potential problems associated with the use of OSL dating techniques on sediments from Blombos that may hamper the reliability of the age estimates. These problems relate to:

1. Lack of adequate bleaching or zeroing of the OSL signal prior to sediment deposition (this may cause an overestimation of the age).
2. Contamination of the well-bleached sediments with poorly bleached or unbleached decomposed roof material (causing an overestimate of the age).
3. Mixing of sediments among major stratigraphic units (which will result in either an under or over estimate of the age).

The use of single-grain OSL measurements should allow these three potential problems to be recognised and dealt with appropriately, and as such the most reliable age estimates will be derived.

2.11 Chapter summary

MSA archaeological sites make a significant contribution to debates surrounding the timing and origins of modern human behaviour. The occurrence of the remarkably advanced SB and HP industries throughout southern Africa implies that behavioural modernity was present among MSA hominids. The occurrences of SB stone tools in association with symbolic artefacts at Blombos Cave in South Africa indicate that this site was occupied by behaviourally modern *Homo sapiens.* Determining exactly when this site was occupied requires an accurate chronology for the site, and an appropriate dating method to be employed. The use of single-grain OSL measurements on sediments collected from Blombos Cave may provide a finely resolved chronology of the site, as this method has proven to be particularly useful at archaeological sites of a similar age.

Chapter 3

Chapter 3- Materials and Methods

3.1 Introduction

Determination of the optical ages for sediments collected from Blombos Cave, South Africa, was undertaken at the OSL facility at the University of Wollongong, New South Wales, Australia. Standard laboratory procedures were used in both the preparation and measurement of the samples so that an accurate OSL age could be derived. This chapter describes the materials and methods used to obtain such ages, the results of which are presented in Chapter 4.

3.2 Sample collection

A total of 32 sediment samples were collected for OSL dating from Blombos Cave during three field seasons in April 2008[1], April 2009[1] and April 2010. Twenty-one of these samples were processed for the purpose of this study, the remaining 10 samples having already been measured and analysed by Dr Zenobia Jacobs (ZJ). Sampling carried out during the 2008 field season focussed on the recently excavated previously un-dated lower phases of the cave that make up the M3 stratigraphic phase. A single sample has previously been dated from the uppermost layer of this phase, layer CH/CI (Jacobs et al, 2006c). It is from near the base of this phase that the most recent and still unpublished indicators of modern human behaviour have been recognised (layer CPA) (see Section 1.2.2). Fourteen samples were collected at this time, the majority of which were dated by ZJ. Four of these samples have been dated by the present author, three directly related to ochre containers in layer CPA (BBC08-1, BBC08-2, BBC08-5) and one from the very base of the M3 phase (BBC08-14).

Sampling carried out during the 2009 field season focused on the M4 phase and the geological units that separate the M3 and M4 phases. These sediments represent the deepest excavated layers in the cave. These phases are separated by two thick and laterally extensive calcrete layers. A total of 6 samples were collected from these phases: two from the top calcrete layer (BBC09-1 and BBC09-2), two samples from the bottom calcrete layer (BBC09-3 and BBC09-4) and two samples (BBC09-5 and BBC09-6) were collected from the deepest

[1] Samples collection from the 2008 and 2009 excavations was carried out by Dr. Zenobia Jacobs.

archaeological layer CS. A single layer (CR) containing archaeological materials occurs between the two calcrete layers. The location of some of these samples are shown in Fig. 3.1 a.

Sampling carried out over the 2010 field season focussed exclusively on the SB layers, i.e., M1 and M2 (u), with the exception of two samples collected from just below these phases (the uppermost layers of the M2 (l) phase). A total of 8 samples were collected, including 3 samples from the M1 phase (BBC 10-1 – 3), 5 samples from the M2 (u) phase (BBC 10-4 – 6) and 2 samples from the M2 (l) phase (BBC10-7 – 8). Prior to this study only two samples (ZB4 & ZB10) from the M1 and M2 (u) phases had been dated using OSL (Jacobs et al., 2006c). Dates obtained from these newly collected samples will enable a much more finely resolved chronology to be produced for the SB industry as identified at Blombos. The location of each of these 8 samples is indicated in Fig. 3.1 b. All samples analysed and collected for this thesis are listed in Table 3.1 alongside the stratigraphic layer and square location. All samples in this study were collected along the south section wall (Fig. 1.1B), immediately below the cave opening.

All sampling was carried out in a manner that prevented the exposure of the sample to light, a process which will otherwise lead to zeroing of the OSL signal. Thirteen of the 18 samples were collected using a plastic tube one inch in diameter and 15 cm long. After cleaning the section wall at the point of sampling, the tube was gently hammered into the cave face using a rubber mallet. This approach allows the sediments within the middle region of the tube to remain covered until the luminescence signal is able to be measured in the laboratory under the appropriate lighting conditions. Once the tubes were extracted from the cave face, they were immediately sealed on both ends and concealed in two thick black plastic bags to prevent any light exposure during transport from the field to the laboratory.

The remaining five samples (all from the calcrete layers) were collected as block samples. These samples were removed by gently tapping the edge of a calcrete layer with a hammer, and knocking off a block of sufficient size. All samples were tightly wrapped in black plastic for transport to the laboratory. The location of some of the samples are shown in Fig. 3.1 a).

Additional sediments were collected for each of the samples and used for laboratory-based radioactivity measurements and assessment of their moisture content. These were

Figure 3.1a: Locations of samples collected from the archaeologically-sterile calcrete layers and the M4 levels of Blombos Cave. The black circle and the black arrow indicate the location of sample tubes (BBC10-5, 6) collected from the M4 layer – layer CS. The red stars signify the location of the calcrete blocks in which samples were broken off. Two calcrete samples are not shown in the photograph but were sampled to the west. Samples BBC08-1,2 & 5 were sampled directly above the calcrete layer (layer CPA) but are not shown in this photograph. Stratigraphic position of the latter samples in layer CPA is shown in Figure 1.3.

immediately placed into small sample bags and sealed with duct tape to prevent moisture loss.

3.3 Sample preparation:

Once in the laboratory, samples were prepared for dating under subdued red light in order to preserve the OSL signal. Tubes were carefully opened and the end sediments removed in order to eliminate any light-exposed grains. During sampling we recognised that for 3 of the 8 samples collected in 2010 (BBC 10-5, BBC 10-7 and BBC 10-8), the tubes had accidently

OSL sample name	Sratigraphic layer	Excavation square
BBC M1& BBC M2(upper) (Still Bay phase)		
BBC10-1	CA	H6d
BBC10-2	CC	H6d
BBC10-3	CD	H6d
BBC10-4	CFA	H6d
BBC10-5(a)	CFB (hearth layer)	H6d
BBC10-5(b)	CFA	H6d
BBC10-6	CFB (hearth layer)	H6d
BBC M2 (lower)		
BBC10-7(a)	CGAA	H6d
BBC10-7(b)	CGAB/CGAC (hearth layer)	H6d
BBC10-8(a)	CGAA	H6d
BBC10-8(b)	CGAB/CGAC (hearth layer)	H6d
BBC M3		
BBC08-1	CP/CQA	G6d
BBC08-2	CP/CQA	G6d
BBC08-5	CP/CQA	G6c
Calcrete layers		
BBC09-1	base of CQA	F6a
BBC09-2	calcrete layer between CQ &CR	F5d
BBC09-3	calcrete layer between CR & CS	H6a
BBC09-4	calcrete layer between CR &CS	H6b
BBC08-14	calcrete layer between CQ & CR	G6a
BBC M4		
BBC09-5	CS	I6a
BBC09-6	CS	H6c

Table 3.1: A list of all samples collected and analysed for this study and their relation to the stratigraphic layer and square from which they were collected

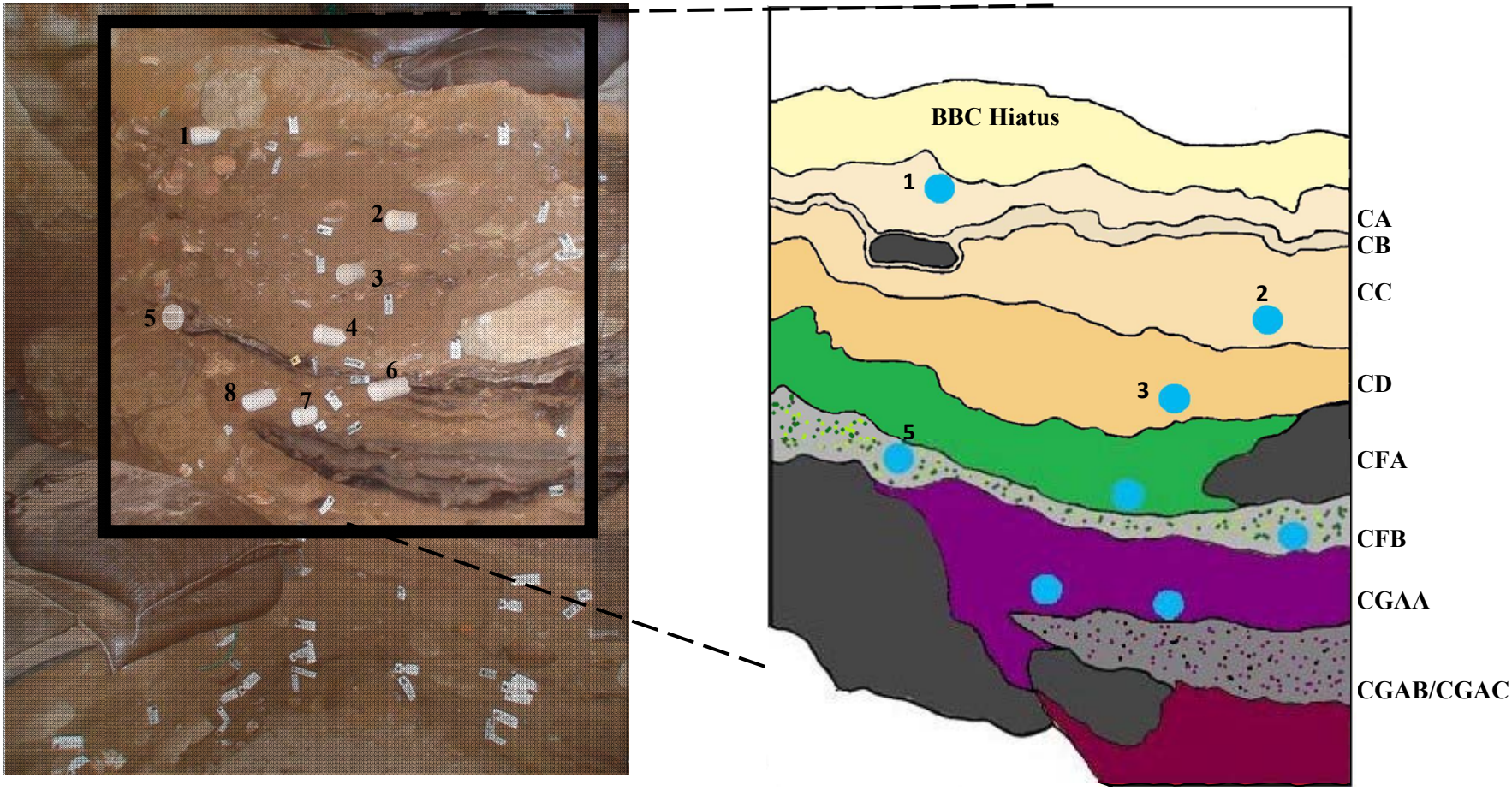

Figure 3.1 c: Locations of samples collected during the 2010 field season (Photograph Richard G. Roberts). **A)** Photograph of stratigraphic section from the front entrance of Blombos cave. The black square denotes the location of the sampling area in excavation square H6d. **B)** Illustration of the stratigraphy of the sample area showing sample tube locations of all 8 samples (represented by blue circles) extracted from the MSA "Still Bay" M1 phase and M2 (l) phase of the cave. The stratigraphical layers in the yellow/brown shade represent layers of the M1 phase; the green shades represent the upper M2 phase and the red represent the lower M2 phase. The black slabs represent rocks and the dotted layers are hearths. The numbers correspond to the sample names of the same number, i.e., 1 corresponds to BBC10-1. Tubes from position 5, 7 and 8 were subsequently divided into two sub-samples becaues the sample tube intruded into an adjacent layer.

cross-cut through two different stratigraphic layers. The two different layers comprising each of these three sample tubes had distinctly different colours that enabled us to identify in the laboratory the point at which cross-cutting occurred. The sample was able to be sub-divided and subsequently treated as two separate samples, identified as (a) and (b) (i.e. BBC 10-5(a) and BBC 10-5(b)). The block samples from the archaeologically-sterile calcrete levels were prepared by scraping off the outer 5 mm rind so that any light-exposed grains were removed. Once all samples had been removed from the tubes/bags, they were prepared for dating using standard laboratory procedures. This involved the removal of carbonates with hydrochloric acid (10%) and digestion of organic materials with 15% hydrogen peroxide (H_2O_2) solution. The sample was sieved to obtain the 180-212 μm grain-size fractions from which the feldspar and heavy minerals were separated from the quartz using sodium polytungstate solutions at a density of 2.62 and 2.70, respectively, to isolate the quartz grains. The quartz grains were then etched in 40% hydrofluoric (HF) acid for 45 minutes to remove the outer ~9 μm alpha-irradiated rind of each grain, followed by a second sieving to obtain only those grains that are >180 μm in diameter. These grains were used in all subsequent OSL measurements using single-grain dating procedures.

3.4 Single-grain OSL

The recent development of single grain dating protocols has made it possible to obtain accurate age estimates for a large number of individual sand-sized grains to determine whether they share the same luminescence age (Murray & Roberts, 1997). One of the key features of single-grain OSL dating is the ability to identify and discard any grains with aberrant OSL behaviours before D_e and age determination (e.g., Roberts et al. 1999; Yoshinda et al. 2000; Jacobs et al. 2003b, 2006a,c). Multi-grain aliquots can give rise to inaccurate D_e estimates (and OSL ages) if they contain grains with aberrant behaviours. A range of standard rejection criteria has been developed to identify and isolate these grains (see Section 3.7.1).

Once unsuitable quartz grains have been rejected, information regarding the depositional and post-depositional processes can be gleaned from the resulting D_e distributions. These may include: 1) differences in beta-dose received by individual grains in their burial environment (e.g., Murray & Roberts, 1997; Olley et al. 1997; Roberts et al. 1999; Duller et al. 2000; Jacobs et al. 2008b); this is very common in archaeological sites that may contain a range of different types of materials. 2) Insufficient or heterogeneous exposure to heat or sunlight prior to burial

(e.g. Olley et al. 1999, 2004; Duller et al. 2000; Murray & Olley, 2002). 3) Post-depositional intrusion of younger grains into older deposits, or vice-versa (e.g. David et al. 2007; Jacobs et al, 2006a,c, 2008a). 4) Decomposition of unbleached cave rock into otherwise well-bleached sediments (i.e. roof-spall contamination) (Roberts et al. 1998, 1999).

The same degree of data validation is unattainable using aliquots composed of multiple grains as these conceal the effects of the depositional and post-depositional history of a sample by averaging out the effects. In contrast, single-grain analysis can demonstrate the stratigraphic integrity of a sample or the lack thereof and subsequently treat the sample with the necessary concerns.

3.5 Single-grain equipment

All measurements were carried out using an automated Risø TL/OSL reader fitted with a single grain attachment (Fig. 3.2A-C). Individual sand-sized grains of quartz were loaded onto specially designed aluminium discs (Fig 3.3B) suitable for single-grain dating. Each disc is 9.7 mm in diameter and 1 mm thick and may hold up to 100 individual sedimentary grains arranged in a 10 x 10 grid. Single grains (usually between 180-212 μm in diameter) are retained in 100 separate chambers, 300 μm deep and 300 μm in diameter, spaced 600 μm apart so they are sufficiently far apart to keep "cross-illumination" to a minimum (Bøtter-Jensen et al., 2000). Three larger locating holes (500 μm in diameter) are situated on the outer edge of the disc (Fig. 3.3B) in order to determine the orientation of the discs once they are inside the measurement chamber.

At least 10 individual single-grain discs were prepared for each sample and placed on a 48 position sample carousel spaced by one vacant carousel position to prevent "cross-talk" between adjacent discs (i.e., the percentage dose given to an adjacent non-irradiated grain). Optical stimulation of individual quartz grains was achieved using a 10 mW Nd:YVO_4 diode-pumped green laser (532 nm) with a power density of ~50 W/cm^2 at 100 % power. The beam is focused on a ~10 μm spot using a set of three lenses to steer the laser within the measurement chamber, and two mirrors which are moved orthogonally by two motor driven stages equipped with position encoders (Fig 3.3A) (Bøtter-Jensen et al, 2000). This allows a repositioning accuracy of better than 3 μm. In addition, the reader is also fitted with a heater plate and a $^{90}Sr/^{90}Y$ beta irradiator. The heater plate is used to preheat grains and to hold them at elevated

temperatures in order to eliminate charge held in any of the thermally unstable electron traps, and the beta irradiator is used to provide different radiation doses to the grains in order to build a dose response curve for each grain. The ultraviolet OSL emission from each grain is detected by an Electron Tubes Ltd. 9235QA photomultiplier tube (Fig. 3.3C) fitted with two 3 mm thick Hoya U-340 optical filters.

3.6 Single aliquot regenerative-dose procedure (SAR)

3.6.1 *Background*

The single aliquot regenerative-dose (SAR) procedure was used to construct dose response curves, and to determine D_e values by interpolation, for individual grains from all 21 samples collected from Blombos Cave. This SAR procedure was first introduced as a method in which sensitivity-corrected estimates of an unknown dose received by sedimentary grains (quartz) may be obtained (Galbraith et al., 1999; Murray & Wintle, 2000). The method involves making repeated OSL measurements on a single grain to produce a dose response curve from which the D_e can be determined by projecting the natural OSL signal onto the curve (Fig. 3.3 b) (Galbraith et al., 1999; Murray & Wintle, 2000). Construction of a SAR dose response curve typically requires the use of three regenerative doses (R_X) bracketing the expected D_e estimate as well as a zero dose ($R_X = 0$) to monitor for recuperation and a repeat dose point to monitor the appropriateness of the sensitivity correction (Murray & Wintle, 2003; Jacobs & Roberts, 2007). In this procedure, after the natural (L_N) and each of the regenerative-dose OSL signals (L_X) have been measured for each grain, a test dose (T_D) of fixed size is applied and the induced signal measured to obtain T_N and T_X. The test dose OSL signals are used to monitor and correct for any sensitivity changes that commonly occur in quartz grains as they are repeatedly dosed, heated and illuminated as part of the SAR procedure (Fig. 3.3 a). The L_N and L_X signals are divided by their corresponding T_N and T_X signals to produce a set of 'sensitivity-corrected' values (L_N/T_N and L_X/T_X) to make up a sensitivity-corrected dose response curve from which the D_e is obtained (Fig 3.4 b). Before measuring the natural (L_N), regenerative (L_X) and test dose (T_N and T_X) signals; each grain is heated to between 160 and 300°C. The temperature and duration of these 'preheats' are optimised for a set of related samples by performing a series of routine tests. The main purpose of these preheats is to remove any accumulated trapped charge

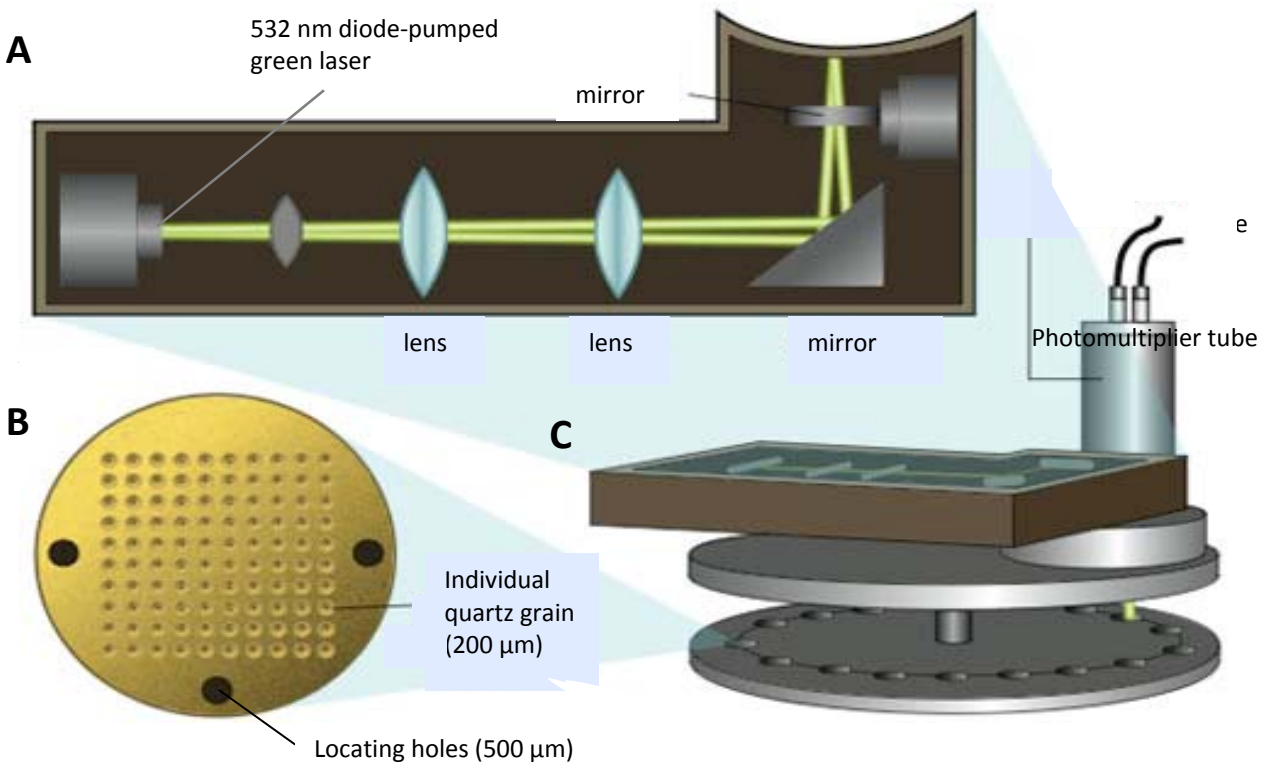

Figure 3.2: Single-grain equipment (from Jacobs & Roberts, 2009b)**. A)** The 10 mW Nd:YVO_4 diode-pumped green laser (532 nm). This is focused on a ~10 µm spot using a set of three lenses and is steered within the measurement chamber by two mirrors equipped with position encoders. This is used to stimulate quartz grains to produce a measurable luminescence signal. **B)** An example of the single-grain disc containing 100 holes in a 10 x 10 grid. Each hole is 300 µm deep and 300 µm in diameter in which an individual grain (usually between 180-212 µm in diameter) can be placed. Holes are spaced 300 µm. **C)** Single grain disc holder moving the single-grain discs below the photomultiplier tube used to measure the intensity of the luminescence signal and over a heater plate to facilitate thermal treatment of all grains. The $^{90}Sr/^{90}Y$ beta source (not shown) is used to deliver the regenerative and test doses.

within thermally unstable traps that would otherwise be absent in the natural signal, which would have thermally eroded away over the burial period. An outline of the conventional SAR procedure is provided in Fig 3.4 a. Details of the procedures and experimental conditions used to measure the quartz grains from Blombos Cave are described in the relevant sections below.

3.6.2 *SAR measurements on Blombos samples*

Jacobs et al. (2006b,c) provided detailed experimental results that supported their choice of measurement procedures. For the most part, the measurement procedure is very similar to the conventional SAR procedure proposed by Murray & Wintle (2000) as outlined in Fig 3.4 a. However, two important adaptations have been made: 1) an increase in the preheat temperature from 160°C/ 0 s to 220°C/ 5 s preceding all test dose measurements, and 2) the introduction of an additional optical stimulation at a temperature of 280°C for 40 s following the final test dose measurement in the natural and each regenerative dose cycle. The increased test dose preheat temperature was applied in order to reduce the effect that the thermally unstable slow-2 component (Singarayer & Bailey, 2003) had on the measurement of the test dose OSL signals (Jacobs et al, 2006b). The high temperature optical stimulation was added to limit the build-up of background signal (due to the presence of unbleachable slow component) between measurement cycles (Murray & Wintle, 2003). Without these adjustments to the SAR procedure, dose recovery tests performed on sample ZB4 from the SB levels at Blombos resulted in a significant underestimation of the given dose (0.87 ± 0.03) (Jacobs et al. 2006b). When these adjustments were made the measured/given dose ratio for the same sample was 1.01 ± 0.04, confirming that accurate results can be obtained using this modified SAR measurement procedure (Jacobs et al. 2006b).

The measurement procedure used for all samples is outlined in Table 3.2. All samples were given exactly the same regeneration and test doses to build the sensitivity-corrected dose response curves. The regenerative doses were ~70, 140, 210 and 280 Gy, followed by a 0 Gy dose and a repeated dose of 70 Gy. The zero dose point was used to monitor for recuperation (i.e. the thermal transfer of charge from optically insensitive traps into stable OSL traps) (Aitken, 1998). The repeat dose point was used to calculate a 'recycling ratio'

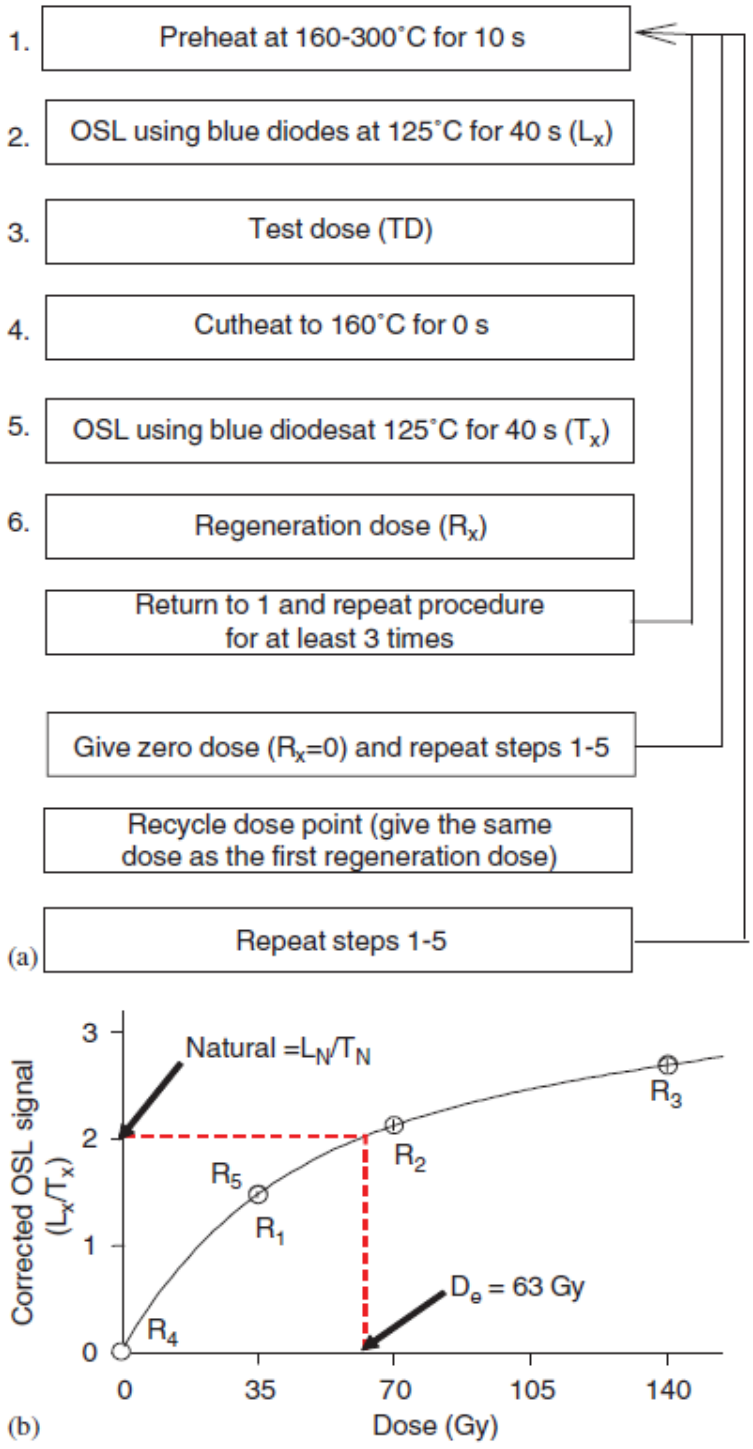

Figure 3.3. (a) Flow chart showing the conventional SAR protocol. **(b)** A hypothetical sensitivity–corrected dose response curve (from Jacobs et al., 2006c).

from which the accuracy of the sensitivity-correction could be tested. The size of the test dose was ~ 12 Gy.

Prior to measurement of the natural (L_N) and regenerative dose (L_X) signals, a preheat temperature of 260°C for 10 s was applied, and prior to measurement of the test dose signals a preheat temperature of 220°C for 5 s was used.

Optical stimulation was made at an elevated temperature of 125°C, and for 2 s using the green laser at 90% power to obtain L_N, T_N, L_X and T_X. An example decay curve is shown in Fig 3.4. After each test dose measurement the additional optical stimulation at a high temperature was applied. Here, the optical stimulation was made using the blue LEDs which stimulated all 100 grains mounted on a single disc (Fig 3.2B) simultaneously while held at a temperature of 280°C.

Finally, another repeat measurement was made at the very end of the sequence. It is almost exactly the same as for the recycling ratio, but this time, prior to the preheat of the regenerative dose, all 100 grains on a disc were simultaneously exposed for 40 s to infrared radiation at room temperature. By comparing the subsequent L_X/T_X measurement with the previous L_X/T_X, the OSL-IR depletion ratio is calculated. This produces an indication about whether or not there may be contamination of feldspar grains or inclusions in our sample (Duller, 2003).

Once this information had been gathered, dose response curves were able to be constructed for individual quartz grains by fitting the sensitivity corrected dose points with an equation that is composed of a saturating exponential plus linear term:

$$I = I_0 + I_{max}\,(1 - e^{-D/D_0}) + k.D$$

In this equation, I is the corrected luminescence intensity, D is the given laboratory dose, D_0 and k are the constants that define the shape of the dose response curve (Aitken, 1998).

The OSL intensity used to estimate D_e is from the first 0.22 s of the optical decay curve with a background signal subtracted. The background signal is the mean count rate of the last 0.33 s of the decay curve.

3.7 Single-grain analysis

3.7.1 *Single grain rejection criteria*

Due to the observed heterogeneity of sedimentary deposits and the great variability observed in the physical behaviour of individual grains from the same sample, certain measurement procedures may only be appropriate to a limited number of grains from any given sample (e.g., Roberts et al., 1999; Duller et al., 2000; Jacobs et al., 2003, 2006a,c). A series of objective rejection criteria has been proposed to separate the well-behaved from the poorly-behaved grains and remove any aberrant grains from a given sample that may provide erroneous D_e values. (e.g., Jacobs et al., 2003, 2006a,c). In this way, inappropriate grains will not adversely affect the D_e distribution of the sample. Using the single-grain method, such grains are systematically eliminated from the distribution of D_e values and not included in final age determination (Jacobs et al., 2006a).

Such rejection criteria include:

1) grains from which little or no measurable luminescence signal are obtained from the test dose (i.e. the luminescence signal is less than 3 times the background signal).
2) grains which do not provide consistent results when a repeat dose is measured, (i.e. grains with L_X/T_X values from the repeat dose that fall outside a ± 2 standard deviations of L_X/T_X values for the original dose). This indicates that our correction for sensitivity change that occurred during measurement of that grain failed.
3) grains that shows a significant OSL response when a zero-dose is measured (L_0/T_X >5% of L_N/T_N).
4) grains that show evidence for the presence of feldspar grains or inclusions (i.e. the sensitivity corrected OSL signal after exposure to infrared radiation is more than 2 standard deviations smaller than the equivalent signal without IR stimulation).
5) Grains where the L_N/T_N ratio does not intercept with the dose response curve (i.e., grains are saturated or exhibit Class-3 behaviour.

The remaining accepted grains will all be used in the final age determination. The D_e values will be displayed using radial plots, and appropriate statistical models, such as the central age model and finite mixture model, will be used to determine the final D_e value of the sample.

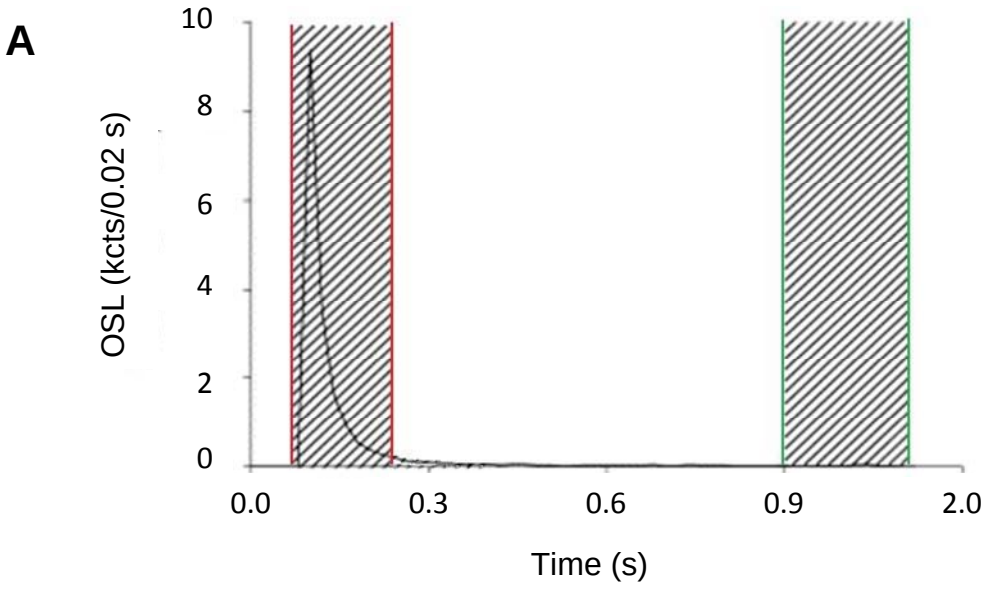

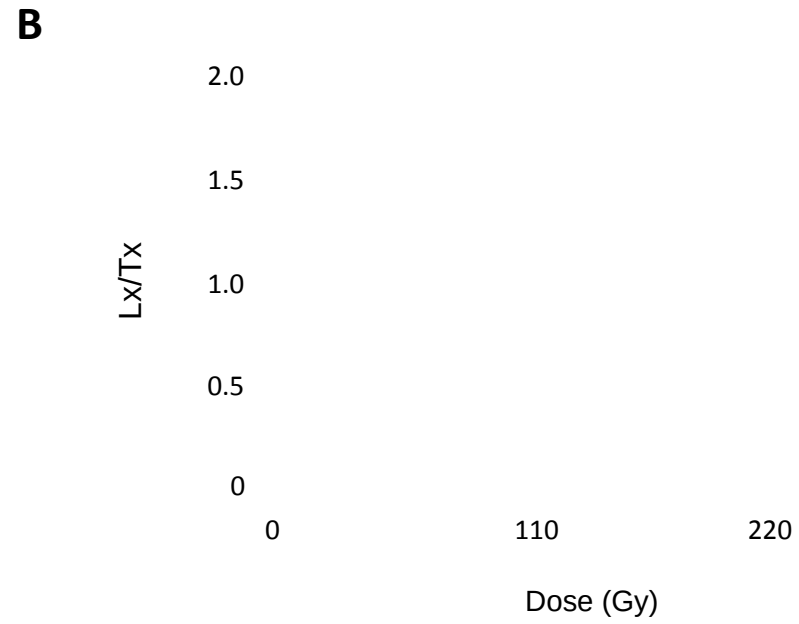

Figure 3.4A: Natural OSL decay curve for a moderately bright quartz grain from Blombos stimulated using the focused green laser (532 nm, 50 W/cm^2) (adapted from Jacobs et al, 2003b). The shaded areas represent the regions of signal integration (red bars) and background integration (green bars). **B)** OSL dose response curve. Red circles represent the regeneration doses and the yellow circle (partially exposed) represents the repeat dose.

Table 3.2: Steps of the SAR procedure used in the measurement of individual sand-sized grains of quartz from Blombos Cave

Step	Treatment	Observed
1	Preheat at 260°C for 10 s	-
2	Stimulate OSL using focused green (532 nm) laser at 125° C for 2 s	L_N or L_X
3	Test dose (T_D) for 12 Gy	-
4	Preheat to 220°C for 5 s	-
5	OSL at 125°C for 2 s using green laser light	T_N or T_X
6	OSL at 280° for 40 s using blue LEDs	
7	Regeneration dose (R_X)	-
8	Return to step 1 and repeat until all R_X have been given	-
9	Give zero dose ($R_X = 0$) and repeat steps 1-6	Check for recuperation
10	Repeat dose point ($R_1 = R_6$) and repeat steps 1-6	Check recycling ratio
11	Repeat dose point ($R_1 = R_{IR}$)	-
12	IRSL at 50 °C for 5 s using infrared diodes	
13	Repeat steps 1-5	Check for feldspar inclusions

3.8 D_e distribution analysis

3.8.1 *Radial Plots, overdispersion and age models*

Once a series of independent estimates of D_e have been obtained from individual grains, it becomes necessary to display these estimates in such a way so that it is easy to identify any patterns in the data that may help inform which D_e values correspond most accurately to the target dating event (Roberts & Galbraith, in press). It is common practice in single-grain OSL dating to use the radial plot, a graphical display method, and the value of overdispersion, a quantitative estimate of the spread of the data, to help understand the meaning of the D_e distributions. Overdispersion is the amount of spread in the data after all measurement uncertainties have been accounted for (Galbraith et al. 1999).

The radial plot provides a visual means of evaluating the D_e distribution of a sample in terms of its overall patterning and precision of individual grains (Galbraith 1988, 1990). A common feature of single-grain OSL data is the large range in precision of D_e values for grains comprising the same sample. The radial plot displays each individual D_e value separately with its associated uncertainty; this is not possible when using histograms or probability density functions. In a radial plot, the D_e for a grain is read by extending a straight line from the origin of the standardised estimate axis, through the data point onto the radial axis on the right; the intercept is the D_e value. To determine the uncertainty of the D_e value, a straight line can be extended vertically from the data point onto the x-axis; the point of the interception is the relative error (as a percentage of the D_e). The most precise D_e will, therefore, fall to the right of the plot and the least precise D_e value to the left. It is possible to evaluate whether the D_e values are statistically consistent with each other or not: if at least 95% of the D_e values fall within any two standard error bar which can be obtained by extending two lines from the ± 2 standardised estimate axis on the left to the radial scale, then all the D_e values are consistent with each other. To obtain an estimate of the spread of D_e values the overdispersion is estimated as part of the central age model (CAM) of Galbraith et al. (1999). This parameter was used for all the samples in this thesis. It is commonly accepted that D_e distributions with less than 20% overdispersion are representative of well-bleached samples; any overdispersion greater than this requires much closer scrutiny of the accompanying radial plot.

When using both the overdispersion value and the shape of the radial plot, four different types of general D_e distributions have been observed by a range of different studies:

1. Single component D_e distributions (Figure 3.5 a). These are typical of samples that have been fully bleached prior to deposition, remained undisturbed post-deposition and has a homogenous sediment matrix immediately surrounding the sample.
2. 'Mixed' D_e distributions, i.e. those that display one or more discrete dose components (figure 3.5 b). This is common in samples where well-bleached grains with different burial histories from adjacent layers have been mixed post depositionally as a result of bioturbation or other mixing processes, such as digging by humans.
3. 'Scattered' D_e distributions, i.e. those that display two or more discrete dose populations or that possess a smeared appearance (figure 3.5c). This is typical of samples that have been fully bleached prior to deposition, but subsequently exposed to varying amounts of beta-dose radiation.
4. Partially bleached D_e distribution (figure 3.5 d), i.e. those that display a continuum of D_e values with a solid base line. This occurs when grains are insufficiently bleached prior to burial and therefore contain a residual trapped charge, with those grains with the smallest D_e values, assumed to be the best bleached.

In this thesis we will visually examine each radial plot and, together with the value of overdispersion, define each distribution according to the four types listed above. The D_e distribution is interpreted in association with an understanding of the sedimentary and archaeological context of the sample. The resulting assessment and interpretation will be used to determine how best to combine the individual D_e values to obtain the best-estimate D_e value for final age calculation.

Several parametric statistical models are available to combine D_e values meaningfully for accurate age determination (Galbraith et al. 1999; Roberts et al. 2000; Roberts & Galbraith, in press). In this thesis two different statistical models will be used: i) the CAM (Galbraith et al. 1999) and ii) the finite mixture model (FMM) (Roberts et al. 2000). The choice of model is dependent on the interpretation of the shape of the radial plot and the overdispersion value. Where D_e distributions were interpreted to represent a single well-bleached population of grains, the CAM was applied. When post depositional mixing, or scatter due to the effects of beta micro-dosimetry, are identified as the most likely reason for the presence of multiple discrete components in a D_e distribution, the FMM was applied.

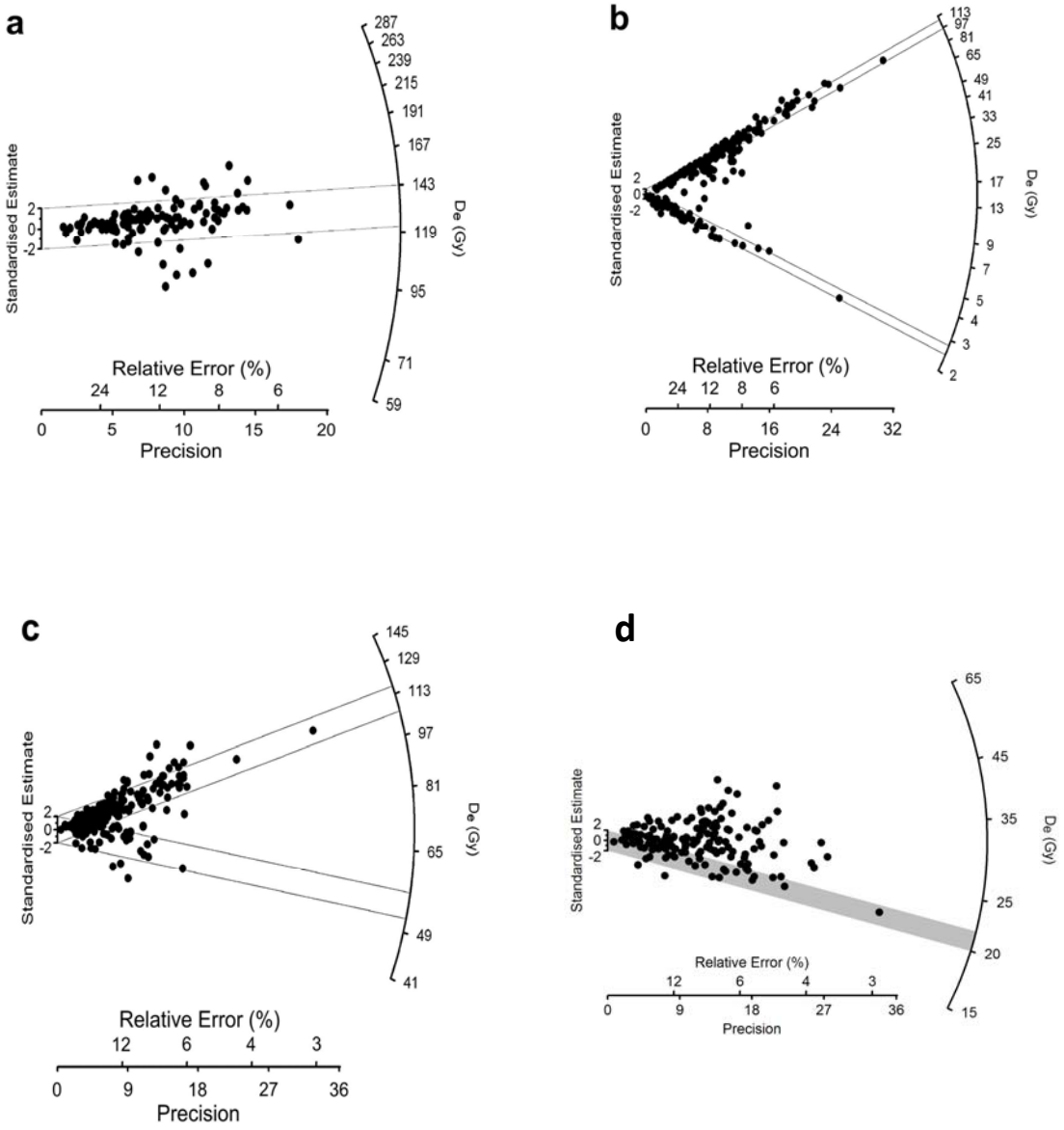

Figure 3.5: Representative radial plots of single grain D_e values from different types of D_e distributions observed at Sibudu Cave, South Africa (From Jacobs et al, 2008a). The thin grey lines bracket the 95% confidence interval for a line, or lines, projecting from the standardised estimate axis. **(a)** A single component D_e value, from well bleached sediments, **(b)** "mixed" D_e distribution resulting from mixing of MSA and Iron Age sediments; sample displays one or more dose component, **(c)** "scattered" D_e distribution from spatially inhomogeneous sources of radioactivity affecting the sample; sample displays multiple dose components. **(d)** Partially bleached D_e distribution for sediments collected from Kudjal Yolgah Cave, near Margaret River in WA (Jankowski et al., in prep).

3.8.2 *Central age model*

The CAM is the most appropriate model for those samples that have been well bleached prior to burial (Fig 3.7 a). This model assumes that the D_e values for all grains are centred on an average value of D_e (similar to the weighted mean) and the estimated uncertainty takes into account any overdispersion (Galbraith et al., 1999). This is particularly significant as well-bleached samples typically have un-explained overdispersion values of 10 to 20 per cent (e.g., Olley et al., 2004; Jacobs et al., 2006a; Galbraith, 2005).

3.8.3 *Finite mixture model*

The FMM as established by Galbraith & Green (1990) and modified for OSL dating by Roberts et al. (2000) can be applied to those samples which display a 'scattered' distribution resulting from small-scale variations in beta dose micro-dosimetry or the mixing of well-bleached grains among sediments of different ages (Jacobs et al. 2006b, 2008a; David et al. 2007; Tribolo et al. 2010). The FMM is able to determine the number of dose components (k), the D_e value of each dose component (which is the CAM of that component), and the proportion of grains belonging to each component. To obtain this information, the overdispersion value and expected number of components need to be specified. To specify these two parameters reliably, the same systematic and statistical approach developed by Galbraith (2005), David et al. (2007) and Jacobs et al. (2008a) was used. It includes the use of the Bayes Information Criterion (BIC) and maximum log likelihood (llik). When an optimum BIC and llik combination is obtained, the corresponding overdispersion and number of components are assumed to be the most appropriate. In this thesis we have varied the overdispersion values between 10 and 20% and used the dose component with the greatest proportion of grains for final age calculation.

3.9 Radionuclide measurements and dose rate determinations

Obtaining accurate age estimates requires an equally sound approximation of the environmental dose rate, i.e., the rate of supply of ionising radiation received by a given sedimentary grain. The natural radiation supply is predominately comprised of gamma (γ), beta (β) and alpha (α) radiation derived from the natural decay of radioactive elements ^{238}U, ^{235}U, ^{232}Th (and their daughter products) and ^{40}K. The environmental dose rate of a given sample can

be divided into (i) an internal dose rate (resulting from alpha and beta radiation from within sedimentary grains themselves) and (ii) an external dose rate (resulting from alpha, beta and gamma radiation in the bulk sediment matrix surrounding the grains). The internal dose rates of quartz sediments are likely to be low, as these grains contain inherently low uranium, thorium and potassium concentrations (Aitken, 1998). The external dose rate component, however, is of crucial importance and may be determined using a range of different techniques. Some techniques such as beta counting provide a direct measurement of the external beta dose rate, whereas other techniques such as thick-source alpha counting (TSAC) and X-ray fluorescence (XRF) provide radionuclide concentrations that must be converted into dose rates. Each form of nuclear radiation has a different penetration range (Aitken, 1998). Alpha particles, for example, ionise heavily and lose energy quickly, causing a localised sphere of influence of approximately 0.02 mm from the emitting nucleus. Beta particles and gamma rays are lightly ionising and, therefore, can penetrate up to between 2-3 mm and 30 cm respectively. Cosmic-ray radiation, which only has minimal influence on the natural radiation flux, has a penetrating range of several tens of metres (Fig. 3.8). The contribution of external alpha radiation may be effectively removed by etching the outermost 0.02 mm rind of the mineral grain using hydrofluoric (HF) acid. The OSL signals derived from the etched grains are thus the product of external beta, gamma and cosmic-ray radiation with a small contribution from alpha radiation internal to the grains.

To obtain accurate dose rate (D_r) values, Blombos dosimetry samples were dried and milled to produce a fine powder suitable for radioactivity measurements. They were then left for at least one week prior to any measurements to allow for the in-growth of short-lived daughter nuclides.

In this thesis, I have used four different methods to determine the total dose rate for the samples from Blombos. Two of the methods, GM-25-5 beta counting and *in situ* gamma spectrometry, provide a direct measure of the beta and gamma dose rates, respectively. The other two methods, TSAC and XRF, provide estimates of U, Th and K from which dose rates can be calculated using the conversion factors of Adamiec & Aitken (1998). In the following sections, I will discuss the basic principles of each method and how it was used to assist in determination of the total dose rate of each sample.

3.9.1 *Thick-source alpha counting (TSAC)*

TSAC measures the total combined contribution from all the alpha particles from the U and Th decay chains (Aitken, 1985) and can be used to obtain estimates of U and Th in a sample; the beta and gamma dose rates can then be calculated, providing that there is an independent estimate of K. TSAC was applied to all samples collected during all three field seasons. All measurements were carried out using a Daybreak-538 thick source alpha counter. A sample holder containing a zinc sulphide (ZnS) phosphor screen 4.34 cm in diameter (14.79 cm^2) is placed within the alpha counter above a photomultiplier tube (PMT). As alpha particles from the sample strike the ZnS screen scintillations are produced which result in the emission of photons detected by the photocathode of the PMT. Each scintillation reaching the Zn screen can, therefore, be measured. The total number of scintillations per unit area of the counting screen for a specific counting threshold is thus determined and provides an average estimate of the alpha-particle dose rate of the sample. We are, however, not interested in obtaining an alpha particle dose rate, since we removed this contribution using HF acid solution. But, of the total number of alpha counts in the U and Th concentrations in a sample, about 3% of the counts in the ^{232}Th decay series occur in 'pairs'. The 'pairs' record successive alpha decays that occur within 0.2 s of each other when ^{220}Rn decays to ^{216}Po (Fig 3.10A), and acts as a measure of Th activity in the sample. Once the total number of alpha counts and the total number of 'pairs' have been determined, a difference calculation can be made to determine the U activity from the sample (Huntley & Wintle, 1981; Aitken, 1985). By knowing the U and Th activities from a sample, the beta and gamma dose rates from U and Th can be calculated. An estimate of K is essential in the determination of the total beta and gamma dose rates.

Prior to any sample measurements, the background of the ZnS screens were recorded by placing two ZnS screens face to face for a period of 24 hours, immediately prior to the measurement of the sample. The background count rate for each screen is therefore half the measured value. Such measurement procedure allows the determination of a background-subtracted 'true' count rate for the sample (Jacobs, 2004). Once background counts were obtained, powdered sample material was placed in an alpha-thick layer (>1mm) on top of the ZnS screen and measured as an 'unsealed' sample (this involved placing two toothpick fragments between the sample holder and the sample holder lid) in order to allow free radon escape from the sample. The build-up of radon in a sealed cell can lead to significant over-counting (Aitken, 1985). The unsealed sample was measured until at least 2000 counts were obtained.

3.9.2 *X-ray fluorescence (XRF)*

XRF analysis measures the concentrations of different elements within a given sample. This method was carried out in order to determine the concentrations of ^{238}U, ^{232}Th and ^{40}K. A total of 30 samples were measured using XRF, including all samples prepared by the author, BBC08-14, BBC09-1 – 6 and BBC10-1 – 8 and an additional 15 samples collected from 2008 prepared previously. For minor element analysis, providing estimates of ^{238}U and ^{232}Th, five grams of sample were mixed with several drops of PVA glue and compressed into aluminium containers (diameter = 3 cm). These sediment 'pellets' were then dried overnight in a 100°C oven prior to measurement.

Major element analysis was carried out to obtain an estimate of ^{40}K content for each sample. These measurements were made after the minor element analysis, so the correct flux could be used for sample preparation. The type of flux used depends upon the chemical composition of each sample. Those with >25% CaO were mixed with 57 tetraborate 43 metaborate (57/43) flux, whilst those with 45–65% SiO_2 were combined with 12 tetraborate 22 metaborate (12/22) flux. Table 3.3 displays which flux was used for each sample, along with sample and flux weights. For the major analysis, approximately 0.4 g of sample and 2.4 g of the relevant flux were combined in a platinum crucible. The crucible was then placed into a furnace set at 600°C and brought up to a temperature of 970°C. Prior to pouring, an ammonium iodide tablet was added to each crucible to decrease the viscosity. The molten sample was then poured onto a carbide surface and flattened with an aluminium press to form a glass button. The buttons were then left to anneal overnight on a ~100°C hotplate. The edges were then trimmed and the buttons stored in a desiccator until measurement.

All sample measurements were run in September 2010 using an SPECTRO 'xepos' XRF analyser located at the University of Wollongong.

3.9.3 Risø GM 25-5 Beta Counting

Beta counting using the Risø GM-25-5 beta counter, described by Bøtter-Jensen and Mejdahl (1988), includes measurement of the beta emissions coming from U, Th and K that occur naturally within a sediment sample. The instrument consists of five Geiger-Mueller (GM) detectors and a common guard counter; five sample positions located within a sample slide so that

material can be locked precisely above each of the GM detectors. This whole assembly is covered with lead shielding to minimise interference from cosmic-rays.

Three replicate pots containing equal measures of powdered material were measured for each sample. Each pot (~25 mm in diameter and ~8 mm deep) were completely filled with sample material and covered with plastic cling film. Care was taken to ensure that all sample material in pots was presented to the detectors in an identical way. All three sample pots were measured for 24 hours alongside a standard with a known beta dose rate (Nussi) and a sample of Magnesium Oxide (MgO) to estimate instrumental background. Every time the sample emits a beta particle, a pulse is recorded by the GM detector. When a pulse is recorded by a detector and the guard counter at the same time it is rejected as background interference. The beta dose rate was then calculated by subtracting the counts obtained from the MgO from the sub-samples measured at the same time, and the standard also measured at the same time, to obtain a background-corrected count rate for each of the replicate sub-samples. The background-corrected count rate for each sample was then divided by the background-corrected count rate of the standard, and multiplied by the known beta dose rate of the standard to obtain a direct estimate of the beta dose rate for the sample. The benefits in obtaining the beta dose rate this way is that any daily changes in instrument behaviour are accounted for. As such, the only uncertainties in beta dose analysis are based on the standard deviation between the three subsamples, counting statistics and the systematic uncertainty associated with the measured beta dose rate of the standard.

3.9.4 *In situ gamma spectrometry*

In situ gamma spectrometry allows the gamma dose rate to be measured accurately in the presence of an inhomogeneous radiation flux within a 30 cm gamma sphere and is, therefore, particularly useful when dealing with archaeological cave sites that contain large numbers of artefacts with possibly very different radioactivities (Aitken, 1985). *In situ* gamma spectrometer measurements were able to be obtained for five of the samples presented in this thesis (BBC08-1, BBC08-2, BBC08-5, BBC09-5 and BBC09-6). Measurements were also made for all 8 samples collected in 2010, but a mechanical error resulted in spectra that were not usable. All samples collected in 2009 were collected as cemented blocks that were thick enough to have a homogenous radiation sphere.

Sample name	Sample weight (g)	Flux Weight (g)	Type
BBC08-14	0.4001	2.4004	57/43
BBC09-1	0.4005	2.3998	12/22
BBC09-2	0.4007	2.3997	57/43
BBC09-3	0.3995	2.4002	57/43
BBC09-4	0.4006	2.4003	12/22
BBC09-5	0.3999	2.4003	12/22
BBC09-6	0.4002	2.4012	12/22
BBC10-1	0.4009	2.4005	57/43
BBC10-2	0.4002	2.4003	57/43
BBC10-3	0.4001	2.3998	57/43
BBC10-4	0.4000	2.3991	57/43
BBC10-5	0.4001	2.4003	57/43
BBC10-6	0.4005	2.4001	57/43
BBC10-7	0.4002	2.3997	57/43
BBC10-8	0.4005	2.3997	12/22

Table 3.3: Sample name along with flux value used for each sample, including sample and flux weights**.**

To obtain *in situ* gamma spectrometry measurements, an Ortec Digidart portable gamma spectrometer with a NaI crystal one inch in diameter was used. This detector assembly fitted into the holes made during collection of the OSL sediment samples. Each measurement was made for one hour to obtain a total gamma dose rate. The detector was calibrated using the 'threshold' calibration technique (Mercier & Falguères, 2007).

3.10 Dose-rate determination and corrections

In this thesis the beta dose rate for all samples was determined using GM-25-5 beta counting. The gamma dose rate was determined using *in situ* gamma spectrometry for the 5 samples that were accompanied by these measurements. For the remaining samples a combination of U and Th derived from TSAC and K derived from XRF was used to calculate the gamma dose rate. In order to use the various measurements of radioactivity described in section 3.9, a number of conversions and corrections should be, and were, made.

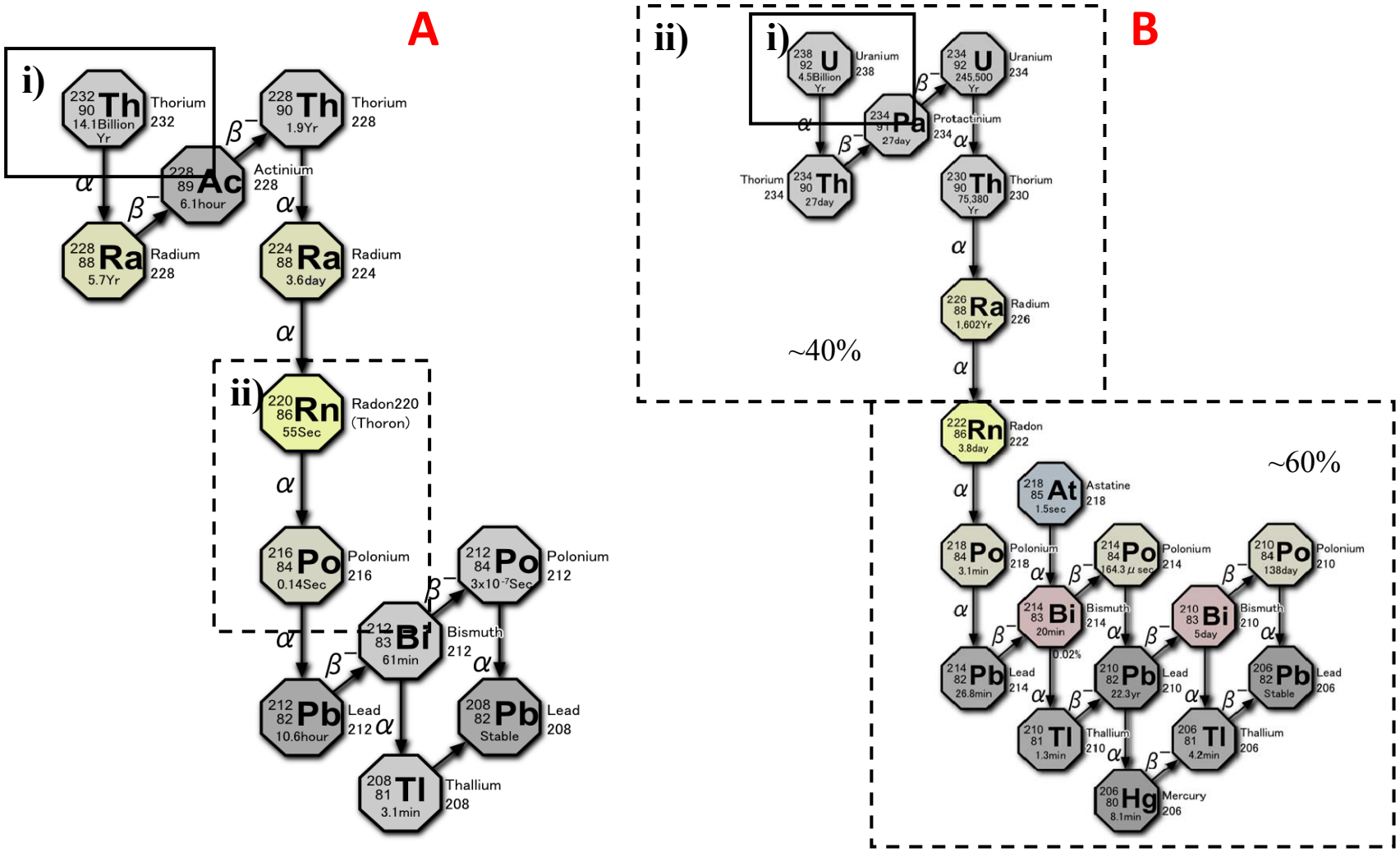

Figure 3.6: A) ^{232}Th and B) ^{238}U decay series (from Lederer et al., 1968) with i) the parent nuclides, for which concentrations can be determined using XRF analysis, and ii) daughter radionuclide decays used to determine Th pairs from which U and Th activities can be calculated. In the U-series, ~40% of the recorded counts when measured with TSAC come from the pre-radon nuclides, and the remaining ~60% from the various post-radon nuclides.

3.10.1 *Conversion from elemental concentrations to dose rates*

When the dose rate was measured directly with beta counting and *in situ* gamma spectrometry, this correction is not necessary. It is only required to convert radioelement concentrations in ppm (or %) as obtained from the XRF and TSAC measurements, to dose rates in Gy/ka. To do this, we used a set of conversion factors that were calculated by Adamiec and Aitken (1998). These conversion factors are provided in Table 3.4.

3.10.2 *Moisture content correction*

Water within the interstices of sedimentary deposits absorbs more radiation and therefore becomes an important variable in dose rate analysis (Aitken 1990, 1998; Jacobs & Roberts, 2007). Jacobs and Roberts (2007) suggest that a 1% decrease in water content produces an increase in dose rate of approximately 1% and thus a 1% decrease in age estimates for grains of quartz. Dose rates can be corrected for the beta and gamma absorption by water, using the two relations proposed by Zimmerman (1971) and recommended by Aitken and Xie (1990). In order to make this correction, the moisture content of the sample over the whole burial period is required. This may be estimated from its present day water content and by looking at the long-term climatic variations at the site and in the area (Jacobs & Roberts, 2007). Small bags of tightly sealed sediments collected from the back of each of the holes left by the OSL sample were collected for each sample individually. Samples were collected from the back of the sample hole where drying out of the excavated section walls would have had less of an effect. The sedimentary composition of each of the samples is very different, i.e. some are sandy and less likely to hold moisture, whereas others are more ashy and clayey, resulting in greater retention of moisture. Consequently, individual assessment of the moisture content for each sample is important. Moisture contents were obtained by first weighing the sample, to obtain the "wet" weight, followed by drying the sample in a 100°C oven for at least 24 hours or until it is completely dry to obtain the "dry" weight. The dry weight is then subtracted from the wet weight and divided by the dry weight to obtain the moisture content. An error of 20% has been applied to all estimates to encompass a large range of possibilities of changes through time. However, there is reason to believe that the moisture content within the cave was relatively stable during most of the burial period, since a massive dune has shielded the cave for the last ~70 ka.

	1 ppm (or % for K)
Alpha dose rate (Gy/ka)	
Uranium	2.78
Thorium	0.732
Potassium	n/a
Beta dose rate (Gy/ka)	
Uranium	0.146
Thorium	0.0273
Potassium	0.782
Gamma dose rate (Gy/ka)	
Uranium	0.113
Thorium	0.0476
Potassium	0.243

Table 3.4: Factors to convert elemental concentrations (ppm or %) to dose rate values (Gy/ka) for alpha, beta and gamma radiation. After Adamiec & Aitken (1998).

3.10.3 *Correction for grain size and HF etching*

The beta dose rate will vary depending of the size of the grain being measured for OSL. This variation arises as a result of the different proportions of radiation inflicted upon the grain and their associated sphere of penetration; very large grains may not allow complete penetration of the beta particles, which may cause some discrepancies in final dose rate determinations (Fig. 3.7). Because grains of quartz have also been etched with HF acid to remove the external alpha-irradiated rind, a small modification to the beta dose is required. The values used for correction of the dose rate due to attenuation were obtained from Bell (1979) and the effects of etching from Bell & Zimmerman (1978).

3.11 Cosmic-ray dose rate

Although the contribution from cosmic rays to the environmental dose rate is usually fairly negligible, accurate measurements of total dose rates require the inclusion of the cosmic-ray

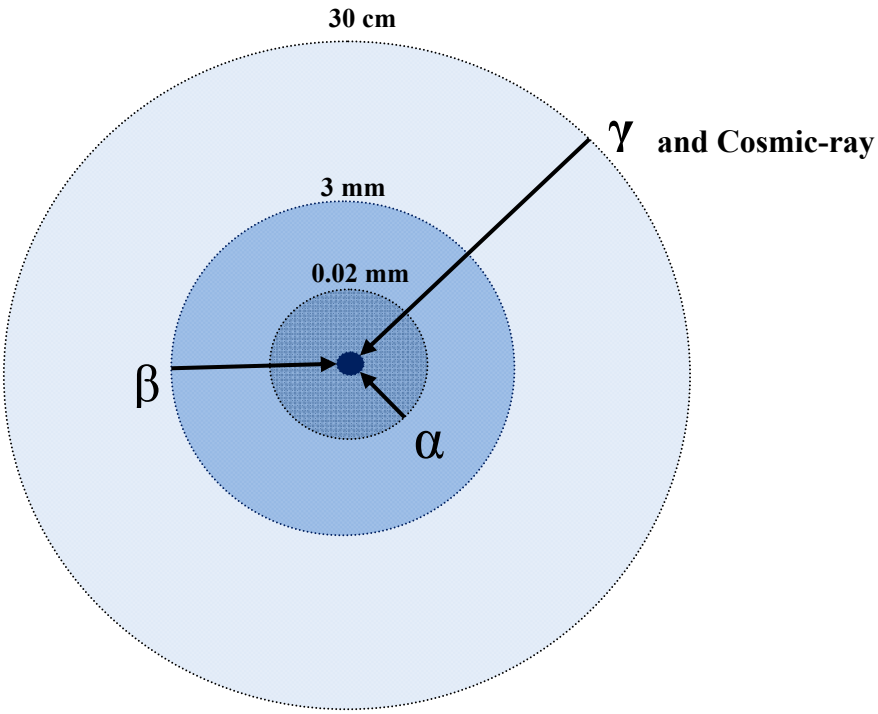

Figure 3.7: Different penetration ranges of α, β, γ and cosmic-ray radiation (not to scale). After Aitken, 1998.

component (Aitken, 1985; Prescott & Hutton, 1994). Calculation of cosmic-ray dose rate was achieved by using equations provided by Prescott and Hutton (1994). This involved making field measurements of the sample locations taking into account depth below overburden (overlying rock and sediment), as well as geomagnetic latitude and the altitude of the site. The small proportion of the cosmic flux that impinges on the surface of the cave through the cave opening was also calculated from the angular distribution of cosmic radiation (Smith et al., 1997). This contribution was minimal as the cave was sealed by a massive sand dune for most of the burial period.

3.12 Calculation of the total dose rate and application of the age equation

Calculation of the final dose rate requires integration of the internal alpha and external beta, gamma and cosmic-ray dose rates. Once dose rates have been obtained for each sample, they may be applied to the OSL age equation along with their corresponding D_e values to obtain an age. Ages for these samples were obtained using the following equation:

$$\text{Age (ka)} = \frac{\text{Equivalent dose or Palaeodose (Gy)}}{\text{Environmental dose rate (Gy/ka)}}$$

The finalised dose rates obtained from Blombos sediments are outlined in Chapter 5, and final ages are presented in Chapter 6.

3.13 Chapter Summary

Samples were collected from the relevant layers of Blombos Cave over three field seasons. Collection was performed in such a way as to preserve the OSL signal of the constituent grains. Once in the laboratory, samples were prepared under subdued red-light to isolate the 180-212 μm grain size fraction of purified quartz appropriate for OSL dating. An OSL/TL DA-15 Risø reader fitted with a single grain attachment was used to measure the OSL signal following the modified SAR procedure, resulting in the formation of an OSL dose response curve from which the D_e value for each individual grain could be obtained. These values were then plotted as a radial plot for each sample and an appropriate statistical model was applied to combine the D_e values meaningfully. A combination of *in situ* gamma spectrometry, beta counting, XRF and TSAC were used to measure and calculate the sample dose rates, taking into account the moisture content and grain size of each sample. Using the OSL age equation, ages were produced for all 21 samples, the results of which are presented in the following chapter.

Chapter 4

Chapter 4- Equivalent dose (D_e) results

4.1 Introduction

Following the methods and procedures outlined in Chapter 3, D_e values were obtained for all 21 samples collected from Blombos Cave. This chapter will describe some of the basic information generated in the course of measuring individual grains, such as decay curve shapes, dose response curve shapes and the brightness of the signal. Parallels will be drawn to the data generated for Blombos Cave samples in other studies by Jacobs (2004) and Jacobs et al. (2003, 2006a,b,c). Comprehensive listings of grain analysis will be provided. A large proportion of grains measured were rejected as they displayed malign characteristics that prevented accurate D_e determination. Finally, the D_e distributions obtained after rejection of those grains with aberrant luminescence characteristics will be presented for each sample. The individual D_e values will be plotted as radial plots, and based on the shape of the radial plot along with the overdispersion value of the sample and any contextual information, the D_e distribution will be interpreted and an appropriate statistical model will be chosen. The latter will be used to meaningfully combine the individual D_e values obtained for each sample into a single representative D_e value that will be used to calculate the final age of each sample.

4.2 OSL signal characteristics

Previous studies involving the measurement of individual grains of quartz from a range of geographical locations have shown a large grain-to-grain variability observed in almost all aspects of single-grain quartz measurements (e.g. Murray & Roberts, 1997; Roberts et al. 1999; Adamiec, 2000; Duller et al. 2000; Bulur et al. 2002; Jacobs et al. 2003, 2006a,c, 2008a,b,c; Demuro et al. 2008; Arnold et al. 2009). This grain to grain variability is particularly visible when looking at the decay curve shapes, the intensity of the OSL signal following a fixed dose, and the dose response curve shapes. Jacobs (2004) and Jacobs et al. (2003, 2006a,c) described in detail their observations for the samples from Blombos that they measured. In this study, I was interested in seeing whether the same general observations made by them were applicable to the samples I measured from 1) the same Still Bay layers, and 2) from the deeper and previously undated archaeological and geological layers. Three samples – one from the SB

levels (BBC10-3), one from the M4 level (BBC09-5) and one from the archaeologically-sterile calcrete levels that separate the M3 from the M4 phases (BBC09-3) were chosen as representative examples and will be discussed below.

4.2.1 *Optical decay curves*

Fig. 4.1 a-c shows a typical decay curve of a moderately bright grain from each of the representative examples. These OSL signals were measured following a 70 Gy regenerative dose and a preheat temperature of 260°C for 10 s using the green laser at 90% power for 2 s. These three grains give OSL signals that decay to 3.5% (BBC10-3), 4.8% (BBC09-5) and 7.3% (BBC09-3) within the first 0.2 s of optical stimulation (i.e. that part of the signal that is integrated during construction of the dose response curve). However, not every grain decays at the same rate or to the same extent. In order to investigate the range in decay rates from grains of the same sample, those grains that had more than 100 cts in the first 0.2 s of optical stimulation have been used for each representative sample as shown in Fig. 4.2 a-c. This amounted to the inclusion of 79 grains for BBC10-3, 51 grains from BBC09-3 and 115 grains from BBC09-5. For the grains from BBC10-3, the decay 'residual' varies between 1.1 and 18.6% with a median rate of 5.9%. Only limited variability can be observed (Fig. 4.2 a). This is similar to what Jacobs et al. (2006a) observed for one of their samples (ZB4) from the SB levels (layer CC) at Blombos. The shape and rate of decay also confirms that these signals, as previously found, are dominated by the 'fast' component in quartz (Bailey et al. 1997) and like Jacobs (2004) and Jacobs et al. (2006a), this may imply that there are negligible contributions from other components to the total signal for grains in this sample. There appears to be little relationship between the decay 'residual' and intrinsic brightness of grains comprising this sample (see inset in Fig 4.2 a), when % signal left after 0.2 s of optical stimulation time is plotted as a function of intrinsic signal brightness (i.e. the OSL signal measured after the same regenerative dose of ~70 Gy and a preheat of 260°C/10 s was applied). The results are given for the same 79 grains for which decay curves are plotted in Fig. 4.2 a. Apart from three of the dimmest grains with signal intensities between 100 and 200 cts, the same range of 'residual' values (1.1-12.4%) can be seen for all grains with signal intensities between 200 and 2000 cts. Only 3 grains have more counts than this and they show significantly smaller values of % signal loss. This result is not dissimilar to the pattern observed by Jacobs (2004) for 111 grains from ZB4 (Fig 4.5a in Jacobs, 2004).

For calcrete sample BBC09-3, decay 'risiduals' vary from 1.2 to 46.7% with a median value of 7%. These curves are slightly more variable than that of BBC10-3, but still appear to be dominated by the fast component (Fig 4.2 c). For this sample, the same range of signal loss is observed for all grains with intensities between 100 and 1200 cts. For sample BBC08-5, which was sampled from the archaeologically-rich M2 (l), M3 and M4 levels, decay 'residuals' range from 0.8 to 28.8% with a median decay value of 5.3%. This is very similar those determined for SB sample BBC10-5. The signal intensities for this sample also appear to more closely resemble those of the Still Bay sample, ranging (with the exception of three very bright grains that show smaller values of % 'residual' signal) – between 100 and 4000 cts (Fig. 4.2 b inset). From this, we may conclude that grains comprising the archaeologically-rich layers of Blombos (i.e., BBC10-5 and BBC08-5) are much brighter than those comprising the geological calcrete levels. Reasons pertaining to the distribution of OSL signal brightness between various samples is discussed in the following section. All three samples show consistent 'fast' components.

4.2.2 *OSL signal brightness*

4.2.2.1 OSL signal brightness distribution

Variability in the luminescence brightness of individual grains from a single sample has been observed by a large number of researchers, including the samples previously dated for Blombos (Jacobs et al. 2003b, 2006a,c). Although the reason for this variability is not well understood, it has been suggested that some of the difference may be the result of the depositional and erosional history of the sample (i.e., the more cycles of erosion and deposition, the more sensitive or 'brighter' the signal), or due to post-depositional circumstances (e.g., intense heating of grains in fireplaces) (Jacobs et al. 2008a).

Previous investigations by Jacobs et al. (2003b) and Jacobs (2004) found that for eight Blombos samples, seven had 21% of the grains contributing to 95% of the light sum. A single sample (ZB8), however, displayed a much greater proportion of grains (43%) contributing to 95% of the light sum. As this sample was obtained from within a fireplace, Jacobs et al. (2006c) has suggested that this is probably the outcome of grains being heated to high temperatures.

In order to compare grain brightness distribution patterns of the samples measured in this study to those measured by Jacobs (2004) and Jacobs et al. (2003b, 2006c), cumulative light sum plots (Duller & Murray, 2000; Duller et al., 2000) were constructed for all grains measured

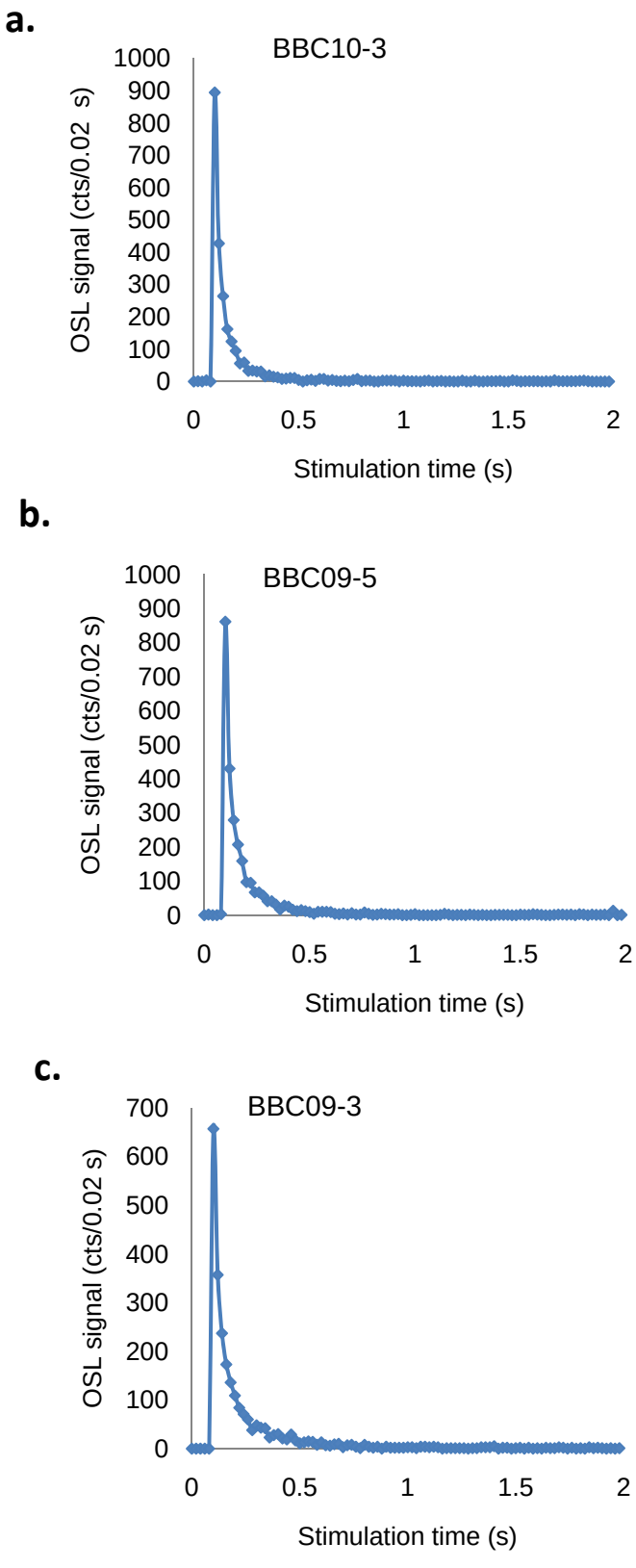

Figure 4.1: A representative decay curve for one sample from **(a)** the Still Bay layers (BBC10-3), **(b)** the deeper archaeological levels (BBC09-5) and **(c)** the calcrete level (BBC09-3). The first and last 0.15 s of optical stimulation time were dark counts, measured when the laser was not switched on.

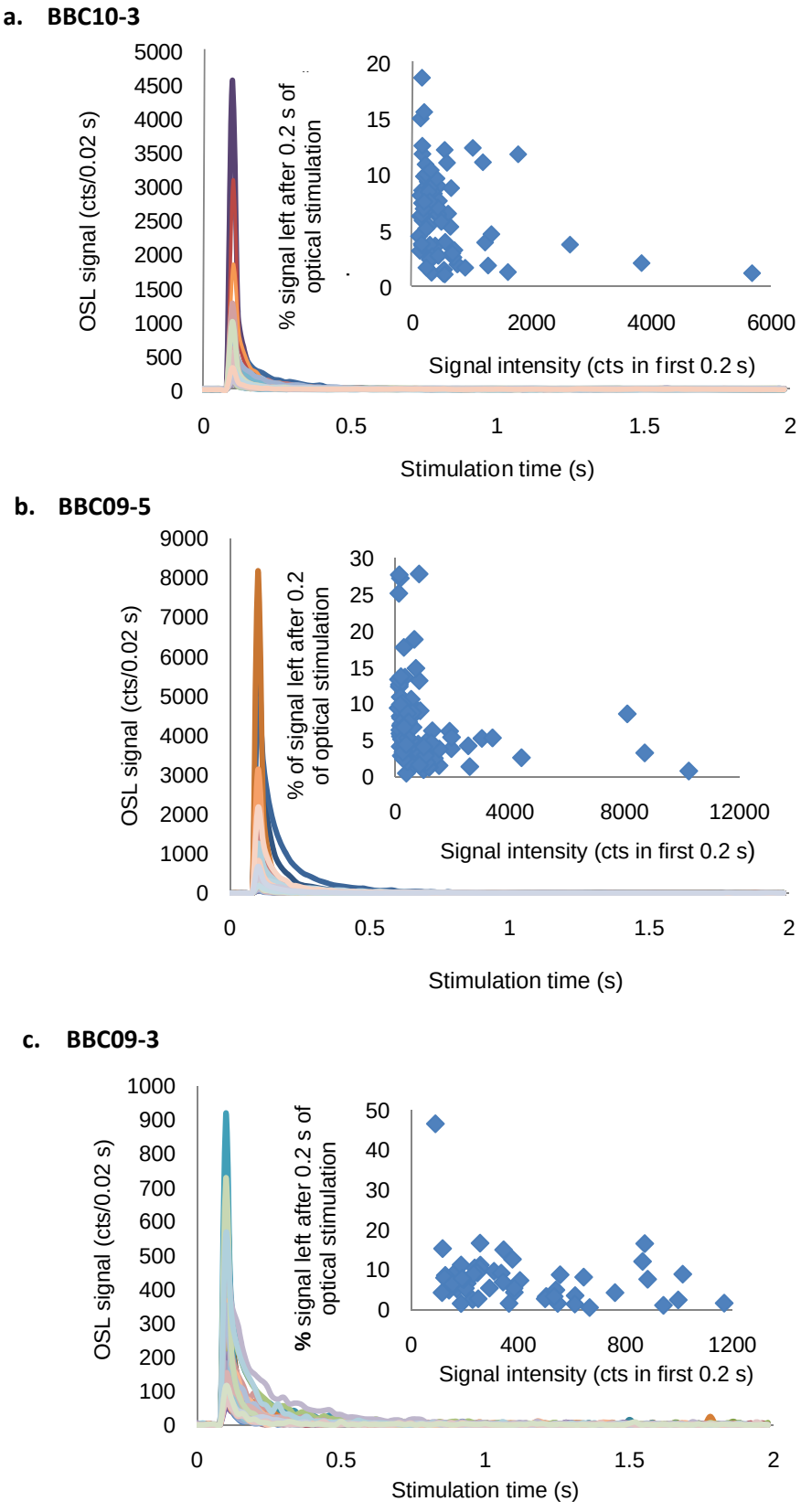

Figure 4.2 a-c: Optical decay curves for all grains with more than 100 counts when the first 0.2 s of the T_N decay curve is integrated for a representative example from **a)** Still Bay levels**, b)** M2 (l)/M3/M4 levels, and **c)** archaeologically-sterile calcrete levels. Inset plots show the relationship between the decay 'risidual' (the % signal left after 0.2 s of optical stimulation) and intrinsic brightness of the grains for which decay curves are plotted.

from each sample dated in this study. A total of 20,800 grains from the all 21 samples were measured using the same green laser for optical stimulation. To obtain an estimate of the inherent brightness of a grain, the natural test dose OSL signal (T_N) following a test dose of 12 Gy and a preheat of 220°C/5 s was measured. This assured that each grain received identical treatments prior to measurement. Any variability in the OSL signal brightness is, therefore, not a result of different doses received by the grain in nature. The OSL signal was integrated over the first 0.2 s of the optical stimulation with a background signal subtracted (obtained from the average OSL signal over the last 0.3 s of the same optical decay curve).

Fig. 4.3 a-c show the cumulative light sum plots for all 21 samples. The samples are divided into three groups: 1) SB samples (Fig. 4.3 a) (BBC10-1 – 6); 2) the samples from the archaeologically-sterile calcrete levels (Fig 4.3 b) (BBC09-1 – 4, BBC08-14); and 3) samples from M2 (l) and the previously undated M3 and M4 archaeological levels (Fig 4.3 c) (BBC08-1,2 & 5, BBC09-5 & 6). A cumulative light sum plot ranks the individual grains in order of descending brightness and the cumulative light sum (given as a percentage of the total light sum) starting from the brightest grain, is then plotted as a function of the percentage of grains measured. A sample with grains emitting equal amounts of OSL signal would plot as a diagonal line from the origin (shown as a 1:1 line in Fig 4.3 a). If grains in the same sample emit differing amounts of OSL signal, their defining line will be plotted above and to the left of the diagonal line. Both axes are expressed in percentage to facilitate comparison between samples for which different numbers of grains were measured.

The cumulative light sum plots for the seven samples measured from the SB layers have very similar signal distribution patterns (Fig. 4.3 a). Between 22.4% (BBC10-1) and 32.4% (BBC10-05a) of the grains are responsible for 95% of the light sum, or a mean of 26.8%. This is slightly higher than the mean of 21% calculated for the seven samples measured by Jacobs (2004), from the SB, M2 lower, and BBC Hiatus layers.

The cumulative light sum plots for the nine samples dated from the M2 (l), M3 and M4 archaeological levels (Fig. 4.3 b) show similar distribution patterns to each other and also with the SB samples. Eight of the nine samples have between 21.2% (BBC 09-6) and 28.8% (BBC10-8b), or a mean of 26%, of the grains contributing to 95% of the light sum. One of thesamples (BBC10-7b) has 47% of the grains contributing to 95% of the light sum, similar to the 43% reported by Jacobs (2004) for one of her samples (ZB8) from the M2 (l) levels. Interestingly, BBC10-7(b) is also from layer CGAB which is very distinctive as it is a hearth-

b. Still Bay samples

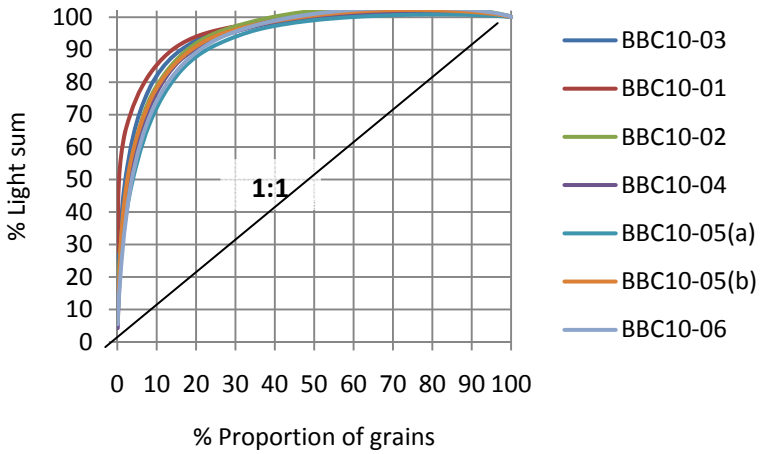

a. BBCM2 lower, BBCM3 and BBCM4

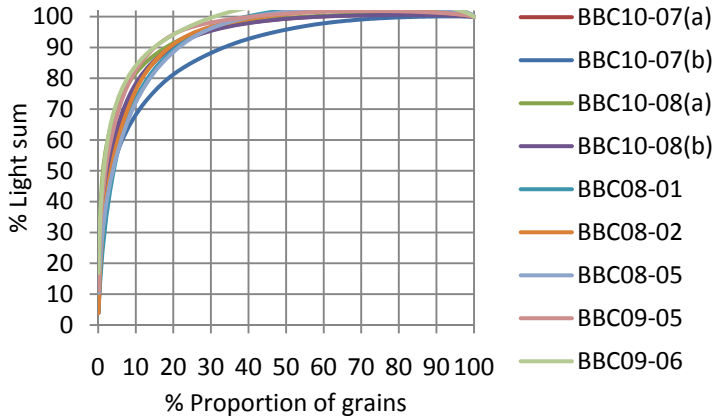

c. Calcrete samples

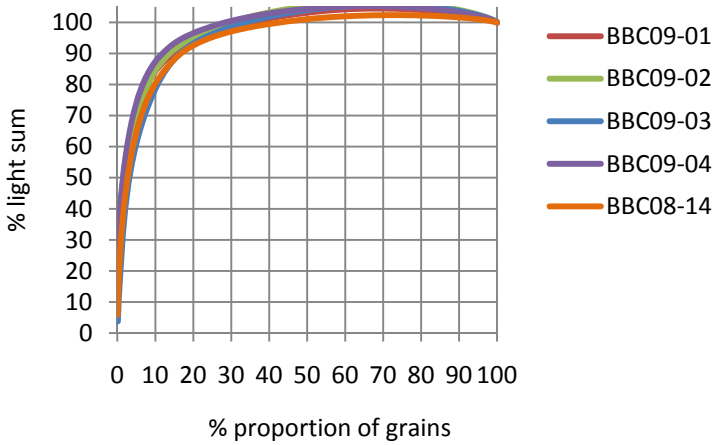

Fig 4.3: Cumulative light sum plots for all Blombos samples measured in this study, sorted into groups of: **a)** 7 samples from the Still Bay levels, **b)** 9 samples from the M2 (lower), M3 and M4 levels, and **c)** 5 samples from the archaeologically-sterile calcrete levels. A sample with grains emitting equal amounts of OSL signal would plot as a diagonal line from the origin, as shown in **a)**.

rich black lens, discernible laterally throughout the cave. Jacobs (2004) previously suggested this difference may be the result of grains being exposed to high temperatures, resulting in sensitivity change (Chen et al. 2001).

The cumulative light sum plots for the five samples collected from the archaeologically-sterile calcrete layers also display a similar pattern and range of brightness. Between 17.3% (BBC09-4) and 24.4% (BBC08-14), or a mean of 21.1%, of the grains contribute to 95% of the light sum. The similarity in the OSL signal distribution brightness for sediment samples from the archaeological and non-archaeological levels support the observation by soil micromorphology that all the sediments in the cave are of aeolian origin and from the same source (Henshilwood et al. 2001b). Slight differences may be accounted for if human practices (such as intense heating through use of fire) altered the luminescence characteristics, such as for sample BBC10-7(b).

4.2.2.2 OSL absolute signal brightness

The cumulative light sum plots do not provide any information about the absolute brightness of grains. It is the absolute brightness that places limitations on whether a grain can be included for D_e determination and also the precision with which a D_e value can be obtained. Samples from Blombos Cave are generally very weakly luminescent. Only a few grains are bright and, therefore, dominate the signal.

In Table 4.1, the numbers of grains for each of the samples that fall into one of three categories are provided. These categories include: 1) the brightest grains (i.e., those with T_N signals >1000 counts in the first 0.2 s of optical stimulation time); 2) grains with average count rates, still with a discernible decay curve (i.e. grains with counts between 100 and 1000 cts per 0.2 s of optical stimulation time) and 3) grains with <100 cts per 0.2 s, but for which the initial signal is greater than three times the corresponding background signal calculated using the average cts over the last 0.3 s of the same optical decay curve. The latter threshold is used as rejection criteria (Jacobs et al. 2006a). It was found that grains below this threshold do not produce a luminescence signal bright enough to produce dose response curves from which reliable D_e values can be obtained (Jacobs et al. 2006c).

Still Bay samples				BBCM2 lower, BBCM3 and BBCM4 samples				Calcrete samples			
Sample name	Signal intensities			Sample name	Signal intensities			Sample name	Signal intensities		
	>1000 (cts/0.2 s)	100 - 1000 (cts/0.2 s)	>3xBG signal		>1000 (cts/0.2 s)	100 - 1000 (cts/0.2 s)	>3xBG signal		>1000 (cts/0.2 s)	100 - 1000 (cts/0.2 s)	>3xBG signal
BBC10-1	5	84	277	BBC10-7(a)	18	153	302	BBC08-14	5	85	224
BBC10-2	3	63	220	BBC10-7(b)	35	315	622	BBC09-1	2	48	188
BBC10-3	5	85	270	BBC10-8(a)	12	106	292	BBC09-2	1	49	172
BBC10-4	10	111	321	BBC10-8(b)	30	176	330	BBC09-3	0	47	203
BBC10-5(a)	13	163	375	BBC08-01	2	85	305	BBC09-4	1	48	163
BBC10-5(b)	5	85	274	BBC08-02	7	102	314				
BBC10-6	2	87	280	BBC08-05	5	124	331				
				BBC09-5	7	101	236				
				BBC09-6	3	33	175				

Table 4.1: Sample name and corresponding number of grains that fall into one of three categories, including: **1)** the brightest grains (i.e., those with T_N signals >1000 counts in the first 0.2 s of optical stimulation time) **2)** grains with average count rates, still with a discernible decay curve (i.e. grains with counts between 100 and 1000 cts per 0.2 s of optical stimulation time) and **3)** grains with <100 cts per 0.2 s, but for which the initial signal is greater than three times the corresponding background signal.

From Table 4.1 it is evident that very few grains are bright. For the SB levels, only 2 to 13 grains per sample are considered bright, 2 to 35 grains from the M2 (l)/M3/M4 levels, and 1 to 5 grains from the archaeologically sterile calcrete layers. Jacobs (2004) reported a similar pattern where only 2 grains appeared to be bright for each of the measured samples. With the exception of sample BBC10-7(b), between 33 and 176 grains analysed per sample in this study have average brightness. BBC10-7(b) has many more than this, with 315 grains. This sample also has the highest amount of bright grains (35). Since 1000 grains were measured for all samples (except BBC10-2 and BBC08-5) this amounts to only 3.3 to 17.6% of grains measured. Based on these numbers, it is fair to say that one of the greatest limitations for dating sedimentary quartz grains from Blombos is their general lack of bright signals. Errors from counting statistics will limit the precision which each individual grain D_e can be measured. The similarity between the findings of this study and the previous studies by Jacobs (2004) and Jacobs et al. (2003b, 2006a,c) also suggests that even though different stimulation and detection equipment were used, the results are internally consistent. Ages produced in this study could, therefore, be integrated and compared with previous ages for Blombos sediments.

4.2.3 *OSL dose response curve shapes*

The OSL signals from individual grains extracted from all 21 samples measured in this study were collected in an identical way (see Table 3.2 and section 3.6.2). The same regenerative doses of 70, 140, 210, 280, 0 and 70 Gy, and test dose of 12 Gy, were used to construct the dose response curve for each individual grain. All usable grains could be fitted with a saturating exponential plus linear function plus linear (see Section 3.6.1). As such, each dose response curve for all grains from all samples should be directly comparable.

Four dose response curves from the four brightest grains of BBC10-3 from the SB layers are presented in Fig. 4.4. For this sample, dose response curves show a wide range of shapes, and in particular, a large range in saturation characteristics. Some of the grains have signals that continue to increase with dose, whereas others show limited growth with increasing dose.

These differences in shape and saturation values cannot easily be linked to the presence of different OSL components (i.e. fast, medium and slow). In Fig. 4.2 a-c we showed that most grains have very similar decay curve shapes and decay rates, implying a fast-component dominated signal for most grains. The inset scatter plots in Fig. 4.2 a-c also show that the

brightest grains in all three representative examples show rapid decay rates. The differences in shape as seen in Fig. 4.4 most likely relate to the saturation level of the fast component in each grain. Two of the grains shown in Fig. 4.4 are effectively saturated, so a finite D_e value cannot be obtained for them, or for any grains with similar characteristics.

4.3 Equivalent dose (D_e) determination

To determine the D_e values for single grains of quartz, the SAR procedure outlined in Table 3.2 was followed. Routine checks of protocol performance were made and grains were rejected using the criteria discussed in section 3.7.1. Table 4.2 lists the number of grains measured for each of the samples, as well as the number of grains rejected and the reasons pertaining to their rejection. The same information is also provided in graphical form in Fig 4.5a-c. Most grains were rejected on the basis of brightness, with a very low percentage of grains emitting a measurable luminescence signal. For the Still Bay and M2 (l), M3 and M4 levels, a total of 81% of the rejected grains were rejected for this reason. For the calcrete levels, the percentage of total grains rejected for this reason increases to 87%. This implies that grains obtained from the archaeologically-sterile calcrete layers are more frequently rejected on the basis of brightness, probably owing to sensitivity differences between the archaeologically-rich Still Bay and M2(l)/M3/M4 layers in which numerous ash lenses have been identified. These are the likely remnants of hearths and ancient fireplaces in which grains would have been heated to high temperatures. Thermal stimulation of the quartz grains in such layers would have enhanced their luminescence sensitivity and, as a consequence, we can expect a higher percentage of return of bright grains (Jacobs, et al. 2008a).

In total, 87% of all grains measured from the Still Bay layers were rejected following the established rejection criteria, 85% for the lower archaeological layers comprising the M2 (l), M3 and M4 levels, and 93% for the archaeologically-sterile calcrete layers. The BBCM2 (l)/M3/M4 layers had the highest percentage of return, with fewer grains being rejected on the basis of brightness, feldspar inclusions or inclusion of modern grains when compared to that of the SB levels. While the archaeologically-sterile calcrete layers had the highest overall percentage of unusable grains, very few grains (much less than that of the two archaeologically-rich phases) were rejected for reasons independent of brightness. Despite these slight differences, each collection of samples share remarkably similar grain characteristics. This demonstrates the

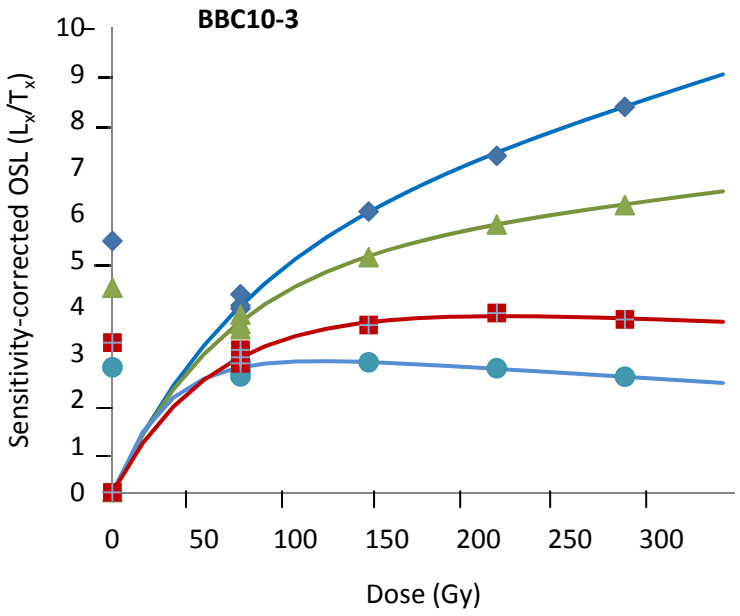

Figure 4.4: Four dose response curves from the four brightest grains of BBC10-3 from the SB layers.

effectiveness of implementing a set of systematic rejection criteria not only as a method of distinguishing between the well-behaved and poorly behaved grains, but also as a way to inform us about the inherent nature of the grains being dated.

4.3.1 *Varying the size of the test dose*

Because most of the measured grains are rejected due to their dim inherent brightness (i.e. T_N = < 3 x BG) (Fig. 4.2 a-c & Table 4.2), I was interested to determine whether a larger number of grains would be usable for D_e determination if the size of the test dose (T_D) were increased. The purpose of the T_D and the resulting OSL signal (T_X) in the SAR measurement procedure is to monitor and correct for sensitivity change (Murray & Wintle, 2000). Murray & Wintle (2000) and Roberts et al. (1999) initially recommended the use of a small T_D (10-20% of the expected burial dose). They have, however, demonstrated that the size of the T_D is not a hindrance as long as it is used in conjunction with a relatively low preheat temperature (such as

Sample name	Grains measured	*Rejected on the basis of:*						Total rejected	Total accepted	% return
		Brightness	Recycling ratio	Feldspar inclusions	Recuperation	Failure to intercept curve	Inclusion of modern grains			
i) M1 & M2 (u) (SB)										
BBC10-1	1000	723	65	44	3	16	19	870	130	13
BBC10-2	900	680	56	26	4	12	12	790	110	12.2
BBC10-3	1000	730	43	38	6	4	34	855	145	14.5
BBC10-4	1000	679	129	81	2	12	8	911	89	8.9
BBC10-5(a)	1000	625	150	26	19	15	15	850	150	15
BBC10-5(b)	1000	726	79	45	6	12	10	878	122	12.2
BBC10-6	1000	720	65	44	6	16	19	870	130	13
TOTAL	**6900**	**4883**	**587**	**304**	**46**	**87**	**117**	**6024**	**876**	**12.7**
ii) M2 (l), M3 & M4										
BBC10-7(a)	1000	698	103	50	19	11	7	888	112	11.2
BBC10-7(b)	1000	378	203	46	2	37	14	680	320	32
BBC10-8(a)	1000	708	80	37	9	16	21	871	129	12.9
BBC10-8(b)	1000	670	118	8	11	10	6	823	177	17.7
BBC08-1	1000	695	49	29	7	10	0	790	210	21
BBC08-2	1000	686	53	45	15	7	3	809	191	19.1
BBC08-5	900	569	51	31	11	14	2	678	222	24.7
BBC09-5	1000	764	53	23	2	26	18	886	114	11.4
BBC09-6	1000	825	43	69	2	12	4	955	45	4.5
TOTAL	**8900**	**5993**	**753**	**338**	**78**	**143**	**75**	**7380**	**1520**	**17.2**
iii) Calcrete layers										
BBC09-1	1000	812	62	39	1	30	3	947	53	5.3
BBC09-2	1000	828	53	27	2	45	7	956	38	3.8
BBC09-3	1000	797	45	19	2	18	8	889	111	11.1
BBC09-4	1000	837	28	26	8	17	6	922	78	7.8
BBC08-14	1000	776	42	58	6	24	9	915	85	8.5
TOTAL	**5000**	**4050**	**230**	**169**	**19**	**134**	**33**	**4629**	**365**	**7.3**

Table 4.2: Distribution summary of grains rejected according to the formal rejection criteria of Jacobs et al. (2003, 2006a, 2006c) for i) the Still Bay layers [M1 & M2 (u)]; ii) M2 (l), M3 & M4; and iii) calcrete units of Blombos Cave. See section 3.7.1 for definition and parameters of each rejection criteria.

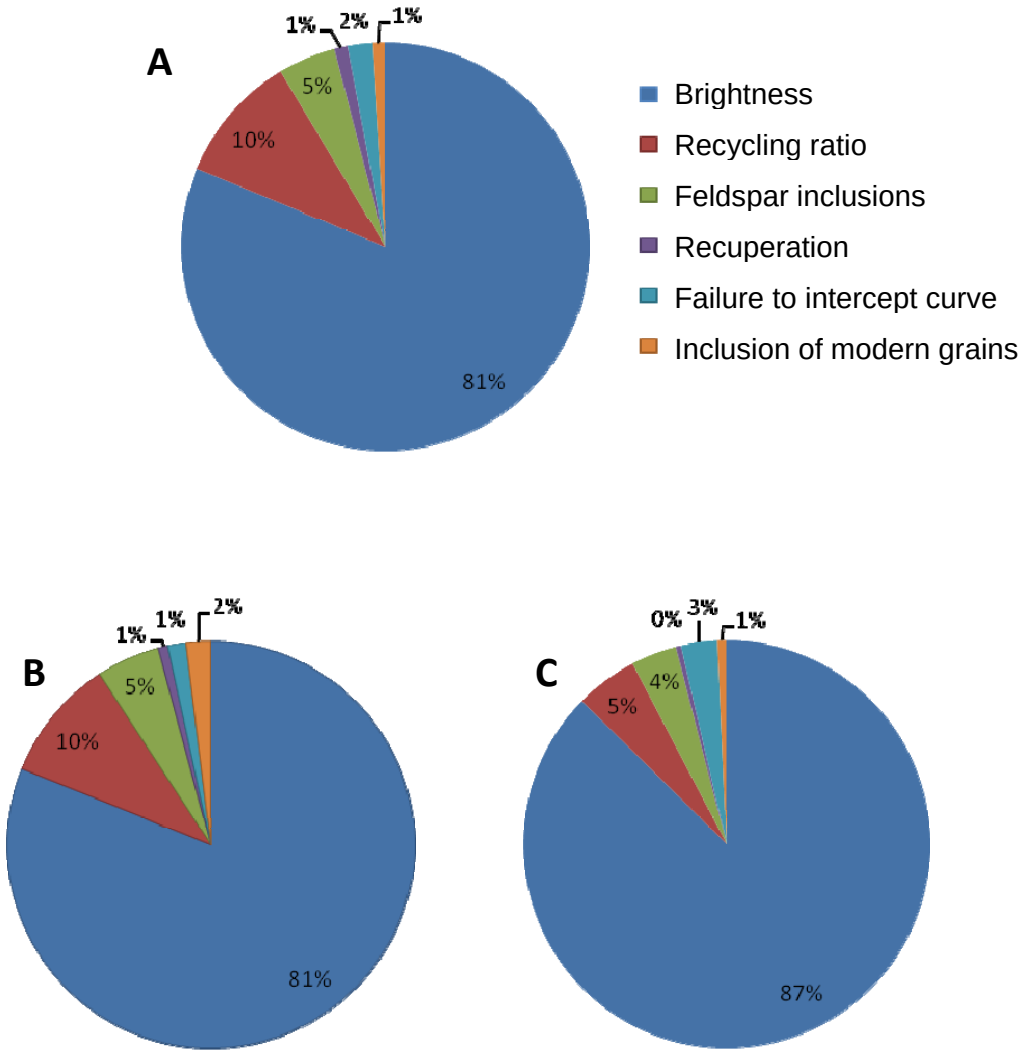

Figure 4.5: Pie graphs representing the percentage of grains rejected by the established criteria, as identified in **A)** the SB levels (M1 & M2 (u), **B)** M2 (l), M3 and M4 levels, and **C)** archaeologically-sterile calcrete layers.

220° for 5 s used in this study; see table 3.2) and does not exceed the size of the natural dose, D_e. All samples analysed in this study have D_e values ≥ 70 Gy.

To test the effect of changing the T_D, and to check whether one can obtain more grains (i.e. have a higher percent of return) if the test dose signal is increased, three separate test doses were applied to three sub-samples of the same sample. A total of 2900 grains of sample BBC09-3 were measured using the procedure outlined in Table 3.2, with various T_D intensities. Of the grains measured, 1000 received a T_D of 12 Gy, another 1000 grains a T_D of 35 Gy and 900 grains a T_D of 58 Gy. The same rejection criteria
discussed in section 3.7.1 and above were applied, and D_e values were determined for all remaining grains. As expected, the percentage grains that have a T_N signal greater than 3 times the BG signal increases with T_D, from 20.3% (12 Gy) to 23.5% (35 Gy) to 25.3% (58 Gy) (Fig 4.5). Although a small number of additional grains were accepted as a result of increased T_D, most of these grains subsequently failed one or more of the remaining rejection criteria (Section 3.7.1); no additional grains were recovered following a T_D of 35 Gy and only 1.5% more following a 58 Gy T_D. In addition, when the individual D_e values are plotted as radial plots (Fig. 4.6a-c), almost identical weighted mean D_e values of 102 ± 4 (T_D= 12 Gy), 103 ± 3 (T_D= 35 Gy) and 102 ± 4 (T_D= 58 Gy) and overdispersion values of 22 ± 4, 19 ± 3 and 24 ± 3%, respectively, were obtained (Fig. 4.6a-c and Table 4.3).

As there is no observed difference in results and number of usable grains when implementing a higher T_D, all remaining samples were given a T_D of 12 Gy in order to maintain consistency between samples and ensure direct comparability. The smaller T_D size also reduced the amount of instrument time.

4.3.2 *Varying the size of the signal integration range*

An analytical variable that may impact on determination of D_e and the resulting overdispersion value and radial plot shape is the size of the signal integration range. Typical construction of a dose response curve in most single-grain studies involves integration of the first 10 data channels (the first 0.2 s of the optical decay curve) subtracted by the background signal obtained from the last 15 data channels (the last 0.3 s of the optical decay curve). In the UOW laboratory, it is standard practice to construct dose response curves in this way. This signal integration range is assumed to preferentially include the fast component signal, as

required for the SAR procedure, which was designed to deal with this component only (Wintle & Murray, 2006). It was demonstrated in section 4.2.1 that the decay curve shapes and the rate of signal decay were variable from grain-to-grain (Fig. 4.2 a-c), so, for some grains, integration of the signal over the first 0.2 s of the optical decay curve may actually include more than just the 'fast' component. Therefore, integration of the first 10 data channels may not be appropriate for all grains, potentially affecting the overall D_e value if it is applied to grains whose signal is not completely depleted in the first 0.2 s. To test the impact that the size of the signal integration range may have on final D_e determination, one sample (BBC09-3, measured according to the SAR procedure outlined in Table 3.2 but using a T_D of 58 Gy) was analysed using four different signal integration ranges for the same set of grains: the first 0.04 s (2 data channels), the first 0.1 s (5 data channels), the first 0.2 s (10 data channels), and variable signal integration intervals, dependant on the appearance of a given decay curve. The resulting D_e values from the four different analyses are displayed as radial plots in Fig. 4.7 a-d. Also shown is the number of grains for which D_e values could be calculated, the weighted mean D_e and the overdispersion value.

The shape of the four resulting radial plots and the weighted mean D_e values, and overdispersion values are very similar for the different analyses. When integrating only the first 0.04 s of the optical decay curve, the precision with which individual D_e values can be estimated is lower due to poorer counting statistics. The overdispersion value for the data set using the first 0.2 s of the decay curve is a little higher than for the other three data sets. This is due to the single low outlier at ~40 Gy. After closer inspection, it is evident that the D_e of grain increases significantly with increasing signal integration. Because of this observation, I have, for all the samples measured in this study, checked the sensitivity of all outlying D_e values to changes in signal integration time; if the D_e changed significantly, then grain was rejected from the data set for being unstable.

This consistency in the results, regardless of the change in signal integration time, is perhaps not surprising. In section 4.2.1, it was shown that most of the decay curves for most of the grains with T_N signals > 100 cts showed little variation and were dominated by the 'fast' component (Fig. 4.2 a-c). To remain systematic, dose response curves for all samples in this study were constructed by integrating each optical decay curve over the first 0.2 s of optical stimulation time. The resulting D_e estimates will, therefore, be comparable between samples measured in the UOW luminescence laboratory.

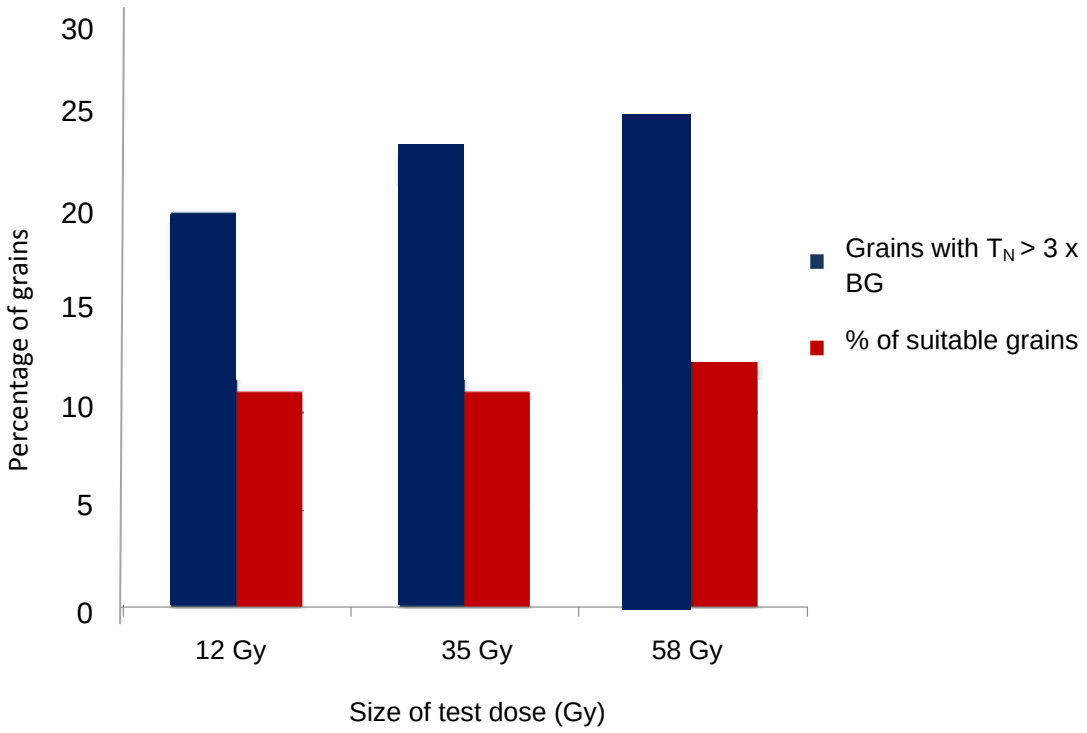

Fig. 4.6: Percentage of quartz grains resulting in a test dose OSL signal (blue column) for which the first 0.2 s is more than 3 x its corresponding last 0.3 s (BG). The percentage of usable grains after implementation of rejection criteria is displayed in the red columns as a function of their corresponding test dose size (T_D).

Test dose size	**12 Gy**	**35 Gy**	**58 Gy**
Total number of grains measured	1000	1000	900
Grains with a T_N > 3 x BG signal	203	235	228
Total number of accepted grains	111	111	114
Overdispersion value (%)	22 ± 4	19 ± 3	24 ± 3
D_e value (Gy)	102 ± 4	103 ± 3	102 ± 4

Table 4.3: Measurement results for Blombos sample BBC09-3 after receiving different size test doses: 12, 35 and 58 Gy.

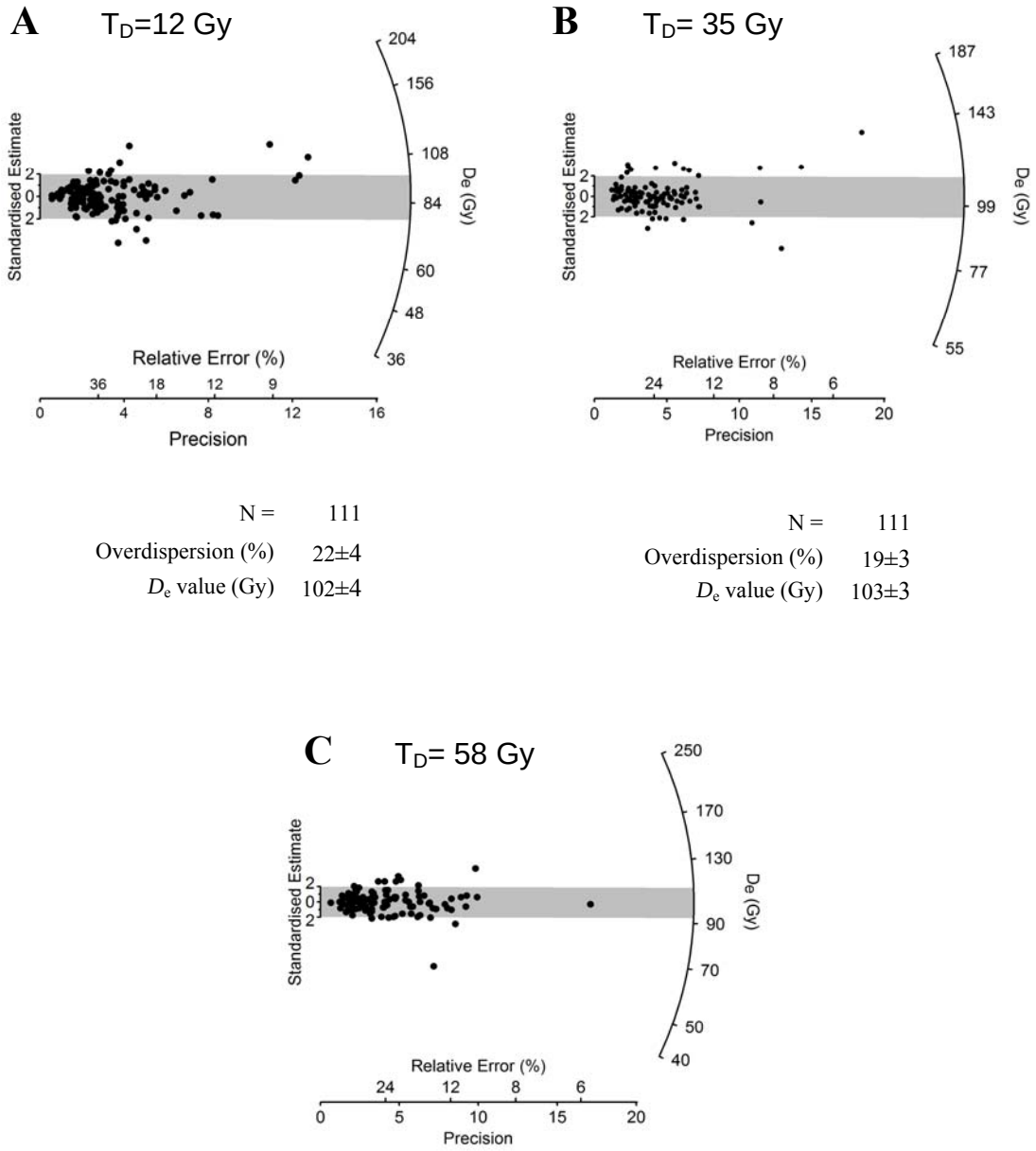

N =	111
Overdispersion (%)	22±4
D_e value (Gy)	102±4

N =	111
Overdispersion (%)	19±3
D_e value (Gy)	103±3

N =	114
Overdispersion (%)	24 ±3
D_e value (Gy)	102±4

Figure 4.7 Radial plots for Blombos sample BBC09-3. D_e values are the result of using the SAR procedure outlined in Table 3.2 but using test doses (T_D) of A) 12 Gy B) 35 Gy and 3) 58 Gy. The corresponding weighted mean D_e values, overdispersion values (%) and final number of grains accepted are also shown.

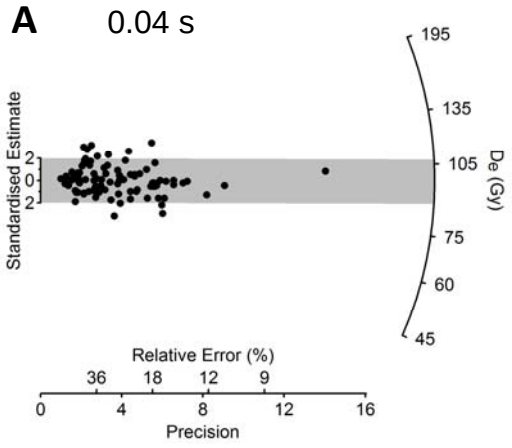

N =	95
Overdispersion (%)	18 ± 4
D_e value (Gy)	97 ± 3

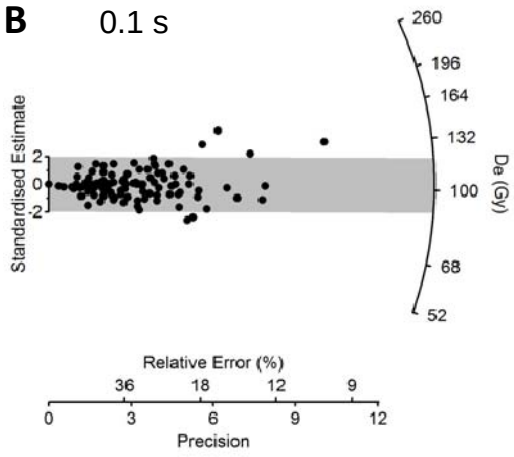

N =	109
Overdispersion (%)	16 ± 4
D_e value (Gy)	104 ± 4

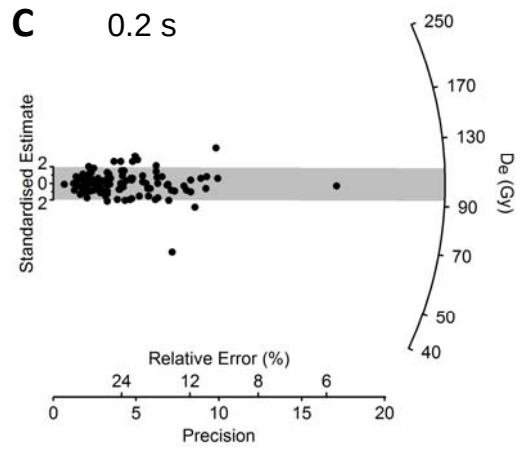

N =	114
Overdispersion (%)	22 ± 4
D_e value (Gy)	102 ± 4

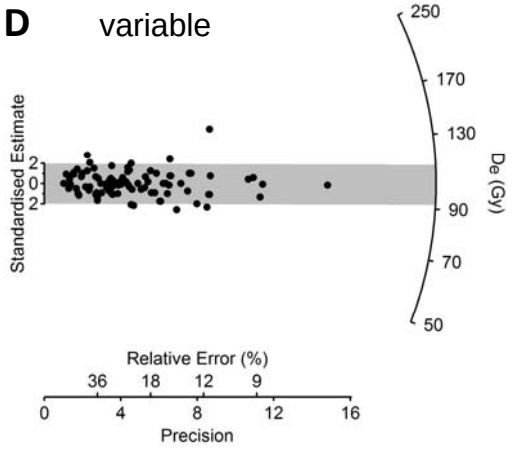

N =	96
Overdispersion (%)	14 ± 3
D_e value (Gy)	102 ± 3

Figure 4.8: D_e values shown as radial plots for individual grains of sample BBC09-3 (measured according to the SAR protocol (Table 3.2) using a T_D of 58 Gy) analysed using four different signal integration ranges: **A)** first 0.04 s of the decay, **B**) first 0.1 s, **C)** first 0.2 s, and **D)** variable integration dependent on each individual grain decay curve.

4.3.3 *Uncertainties on the D_e*

The measurement error associated with the D_e value for each grain consists of the quadratic sum of a number of random errors. The 'random error' is based on counting statistics associated with each OSL measurement (L and T) and curve fitting uncertainties related to construction of each dose response curve, obtained by Monte Carlo (Yoshinda et al. 2003; Duller, 2007). In addition, allowance is also made for uncertainties associated with instrument reproducibility, which is added in quadrature (i.e., as the square root of the sum the squared errors) to every measurement of L and T. This amounted to a 2% error for each OSL measurement (Jacobs et al. 2006a).

The standard error also includes a 'systematic error' of 2% which is added in quadrature to the total random error on the final D_e estimate to account for the uncertainty associated with calibration of the laboratory beta source. The standard error for the final D_e is reported at 1σ, which corresponds to the 68% confidence limits (i.e., there is a one in three chance that the true age will lie outside ±1σ).

4.4 Analysis and interpretation of D_e distributions

After all grains with aberrant luminescence characteristics have been rejected (Table 4.2), the single grain D_e distributions for the remaining grains still exhibit overdispersion (Table 4.4). The seven samples from the Still Bay levels had overdispersion values ranging between 22 ± 4 (BBC10-1) and 32 ± 4% (BBC10-5(b)). The nine samples analysed from the other archaeological levels (M1 (l), M3 and M4) showed a similar range of 19 ± 2, (BBc10-7(b)) and 30 ± 3% (BBC09-8(b)) – as did the five samples collected from the geological units (i.e., the archaeologically-sterile calcrete layers). These displayed overdispersion values of between 22 ± 4 (BBC09-3) and 35 ± 5% (BBC09-14). There is therefore, no clear distinction between the archaeological and non-archaeological levels, or between levels that have been heated or not. This range of overdispersion values is also very similar to the range of 13.5 to 28.6% observed by Jacobs et al. (2006c) for seven samples from Blombos Cave. For all samples, the overdispersion values are significantly greater than the ~7% obtained from laboratory-dosed grains (Jacobs et al. 2006a; Jacobs, 2004). In order to better understand this overdispersion, I have used the degree of overdispersion, the shape of the radial plot and my knowledge, and site observations, of the context of the samples, to make decisions about what the D_e distribution

may inform us about the depositional and post-depositional history of the sample. This information should help decide how best to combine the individual D_e values of each sample to obtain a single estimate of D_e for age determination (Jacobs & Roberts, 2007). Commonly proposed reasons for the extra D_e overdispersion of samples collected from archaeological contexts include:

1. Insufficient exposure to heat or light (i.e., inadequate bleaching or heating) of the grains prior to burial (e.g. Olley et al., 1999, 2004; Murray and Olley, 2002; Arnold et al., 2009).
2. Post-depositional mixing of grains from younger deposits into underlying older units, or vice versa (Roberts et al. 1998, 1999; Jacobs et al. 2006a,c, 2008a,c; Porat et al., 2006; David et al., 2007). This include possible *in situ* disintegration of roof spall that may liberate unbleached grains into otherwise well-bleached deposits.
3. Differences in the beta dose received by individual grains in their burial environment (e.g., Murray & Roberts 1997; Olley et al. 1997; Roberts et al., 1999; Jacobs et al., 2008b,c.)

4.4.1 *D_e distributions of the SB samples*

A total of 6900 grains were measured for the 7 Still Bay samples, of which between 8.9% (BBC10-4) and 15.0% (BBC09-5(a)) were usable for calculation of D_e values (Table 4.2). Six of the seven samples appear to display a single dose component representative of a single-age well-bleached D_e distribution. In all six of these samples there are a few outlier grains, but they do not form any discrete pattern. The sensitivity of the results to the inclusion or exclusion of these outliers was tested and the effect was found to be negligible, only altering the D_e value within its 1σ uncertainty. The central age model (CAM) of Galbraith et al. (1999) (section 3.8.1) was used for these samples to obtain the D_e for age calculation (Fig. 4.9 a-d, f-g). The D_e values and their 1σ uncertainties are provided in Table 4.4. The one exception to this pattern is sample BBC10-5(a), which comprises part of the split sample that cross-cut into two separate layers (CFA and CFB). Layer CFB is a hearth layer, so it may be more complex with regards to the inhomogeneous distribution of potassium (K) and, therefore, beta radiation (Jacobs et al. 2008b). Application of the finite mixture model (FMM) (Section 3.8.2) identified two discrete dose components in this sample (Fig. 4.9e). To calculate the final D_e value for this sample (Table

4.4), the weighted mean and standard error for the D_e component containing the greatest proportion of grains were used. The minor D_e is likely to be the result of spatially inhomogeneous sources of radioactivity at the beta scale, delivering different beta doses to individual grains. This occurrence is not unusual, as it has been demonstrated for other archaeological sediments, especially where there is a high abundance of ash and carbonaceous material (e.g., Jacobs et al., 2008b,c). The central D_e value and its 1σ error, alongside the proportion of grains belonging to each of the D_e components in th ecase of sample BBC10-5(a), are presented in Table 4.4. The rationale for this method, and way in which the model was implemented, is described in detail in Jacobs et al. (2008b); an identical approach was employed in this study.

4.4.2 *D_e distributions for samples from BBC M2 lower, M3 and M4*

A total of 8900 grains were measured for the nine samples collected from the BBCM2 lower, BBCM3 and BBCM4 archaeological phases (see Table 3.1 for exact layer attributions). Five of the samples (BBC10-7(a), BBC10-8(b), BBC08-5, BBC09-5 and BBC09-6) show no discrete D_e components, but they each have a single a single high precision outlier for sample BBC10-7(a) (Fig 4.10 a-i). The CAM model was used for these samples, and the single low outlier was omitted (Fig 4.10a). The central D_e value of the latter only changed by ~1 Gy, so it was not very sensitive to the inclusion or exclusion of this value. alternatively, these grains may have originated from decomposing roof spall, which is abundant throughout the deposit. However, since these grains only constitute a small percentage of the total number of grains measured for this sample, their inclusion or exclusion has little impact on D_e determination.

Interestingly, sample BBC10-7(b) shows the same high-dose components as observed by Jacobs et al. (2006c) for a sample (ZB8) from the same level (layer GGAB/CGAC). This is also the same sample for which proportionally a much greater number of grains gave measureable OSL signals (Table 4.2 and Fig. 4.3 b). In general, D_e distribution patterns obtained by Jacobs et al. (2006c) and in this study show similar distribution patterns for samples from the same archaeological layers.

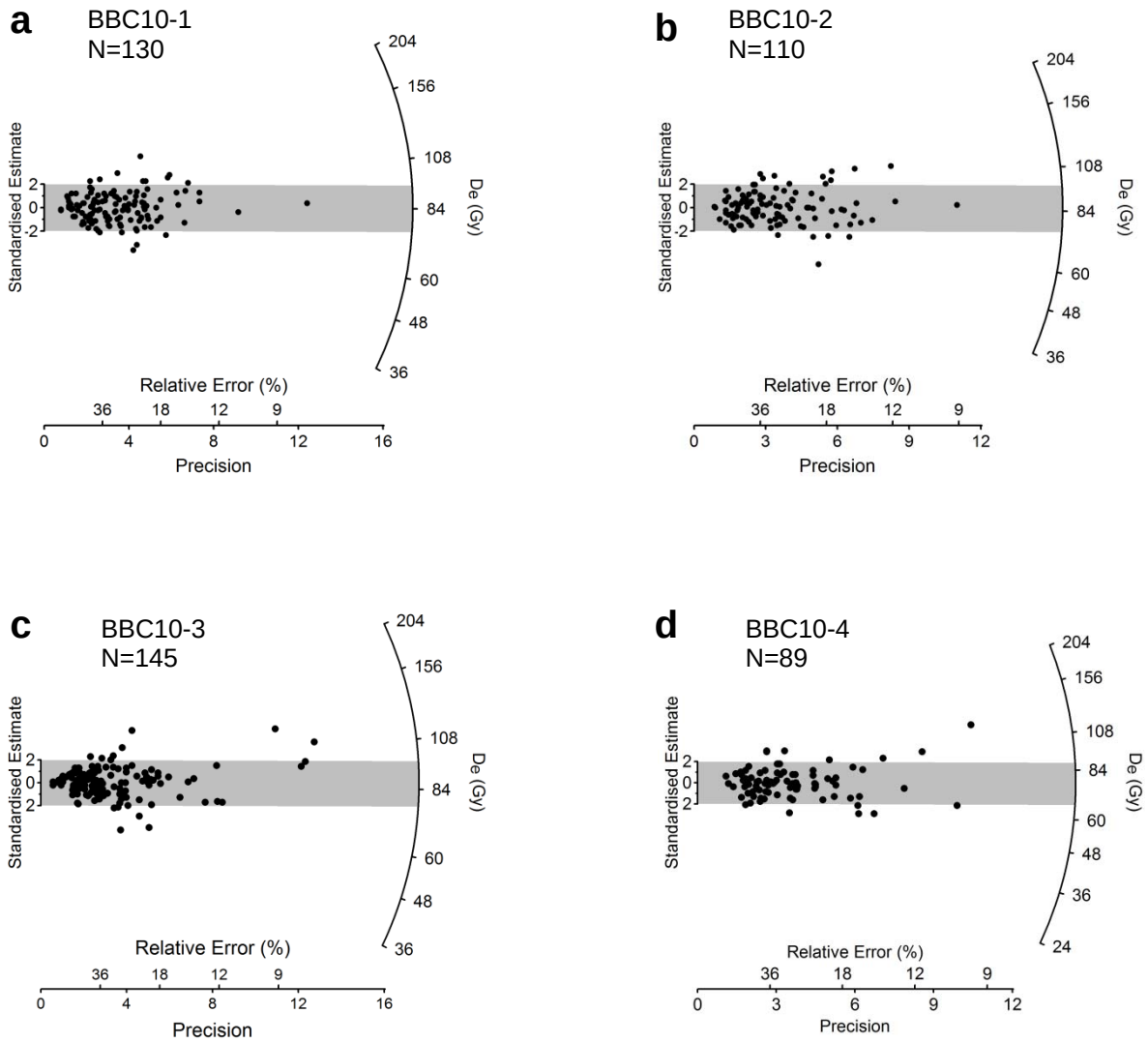
a
BBC10-1
N=130
b
BBC10-2
N=110
c
BBC10-3
N=145
d
BBC10-4
N=89
Standardised Estimate
De (Gy)
Relative Error (%)
Precision

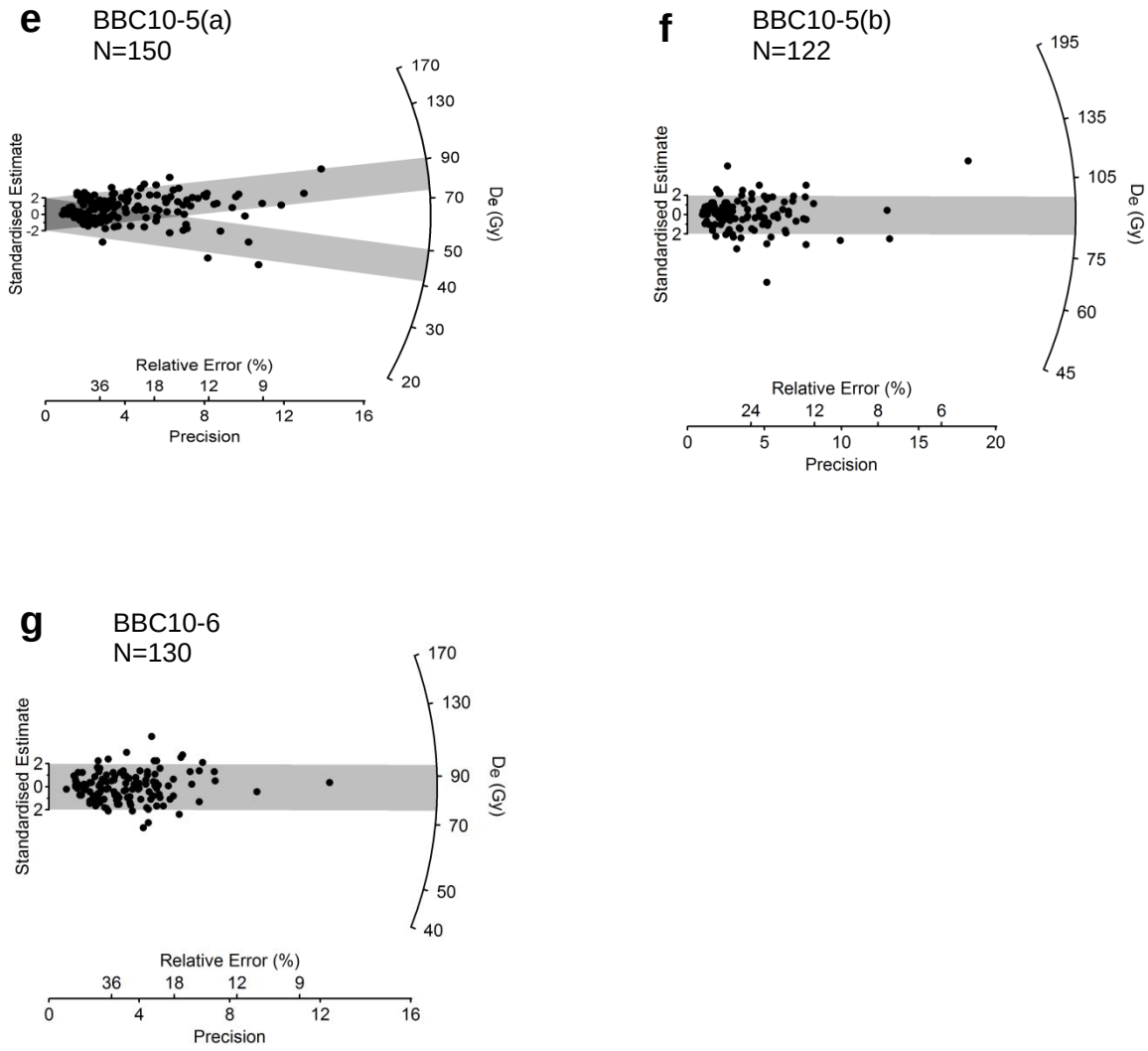

Fig 4.9a-g: Radial plots for all seven samples collected from the Still Bay levels.

The FMM was used for the remaining 3 samples (BBC10-7(b), BBC10-8(a) and BBC08-1), and two discrete D_e components were identified in all three samples. The D_e value and proportion of grains belonging to each component can be attributed to beta micro-dosimetry, but BBC10-7(b) has a D_e component with a small number (~3%) of the grains showing much higher D_e values. It is likely that these few grains were exposed to very high levels of beta irradiation;

4.4.3 *D_e distributions for samples collected from the calcrete layers*

A total of 5000 grains were measured from the five samples that relate to the calcrete layers that clearly separate the M3 archaeological deposits from the M4 layers. Only between 3.4 (BBC09-2) and 11.1% (BBC09-3) of the grains were usable for D_e determination. All five samples show scatter in D_e rates but no discrete D_e components could be observed (Fig 4.10 a-e). There is no *a priori* reason to expect partial bleaching or mixing of the sediments. Post-depositional mixing is improbable since these sediments are cemented. However, grain-to-grain variability in the beta dose rates is likely to be a significant factor in causing the spread in D_e. Not only are there areas of low beta radiation in the form of carbonate cement, but there is also a high abundance of heavy mineral grains within these samples. This can be seen in the photograph in Fig. 4.12, which shows the fresh exposure of the calcrete from where sample BBC09-2 was removed. During sample preparation it was found that ~50% of the sediment sample remaining after HCl acid digestion consisted of heavy minerals and the other 50% was quartz. Due to the range of beta radiation, some scatter in the D_e is to be expected, but the average dose rate and the average D_e value should be representative. As a result, the central age model was applied to all five samples to obtain a single D_e value for age determination. The D_e values and their standard errors are provided in Table 4.4.

4.4.4 *Conclusions*

For the most part, the D_e distributions are represented by a single dose component which suggests the samples consist of fully bleached grains that have not been mixed after burial. The majority of the SB samples exhibit this pattern, with calculated overdispersions ranging from 19 ± 2 and 32 ± 2%. Such uniform D_e values for grains within heavily occupied areas of archaeological sites are usually quite rare. But in this case it is not surprising, given the

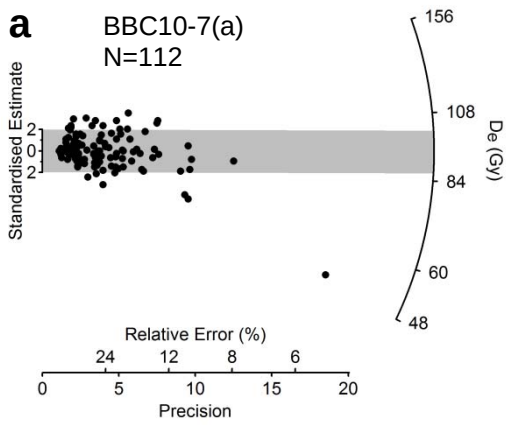
a
BBC10-7(a)
N=112
Standardised Estimate
De (Gy)
Relative Error (%)
Precision

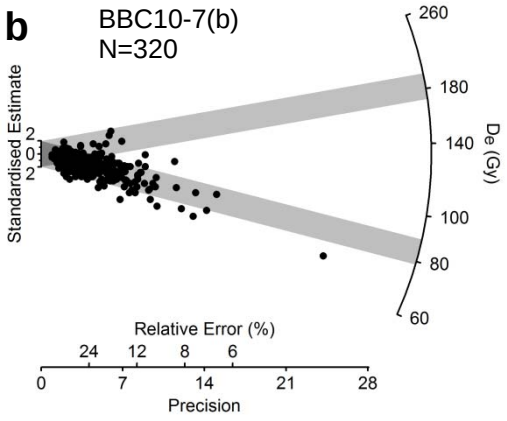
b
BBC10-7(b)
N=320
Standardised Estimate
De (Gy)
Relative Error (%)
Precision

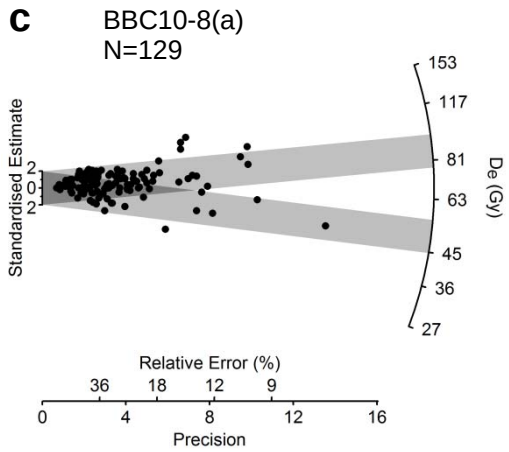
c
BBC10-8(a)
N=129
Standardised Estimate
De (Gy)
Relative Error (%)
Precision

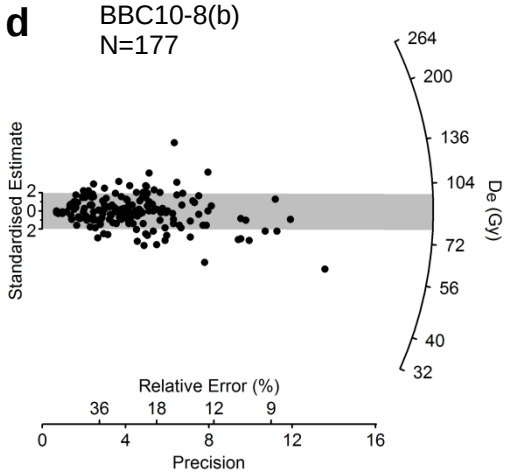
d
BBC10-8(b)
N=177
Standardised Estimate
De (Gy)
Relative Error (%)
Precision

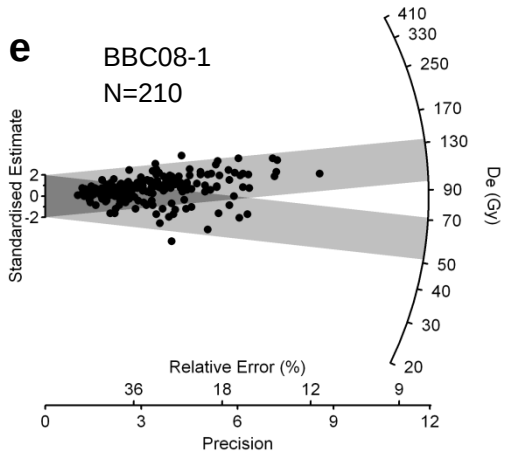
e
BBC08-1
N=210
Standardised Estimate
De (Gy)
Relative Error (%)
Precision

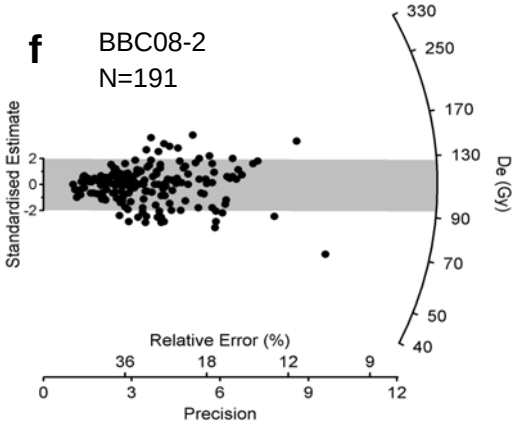
f
BBC08-2
N=191
Standardised Estimate
De (Gy)
Relative Error (%)
Precision

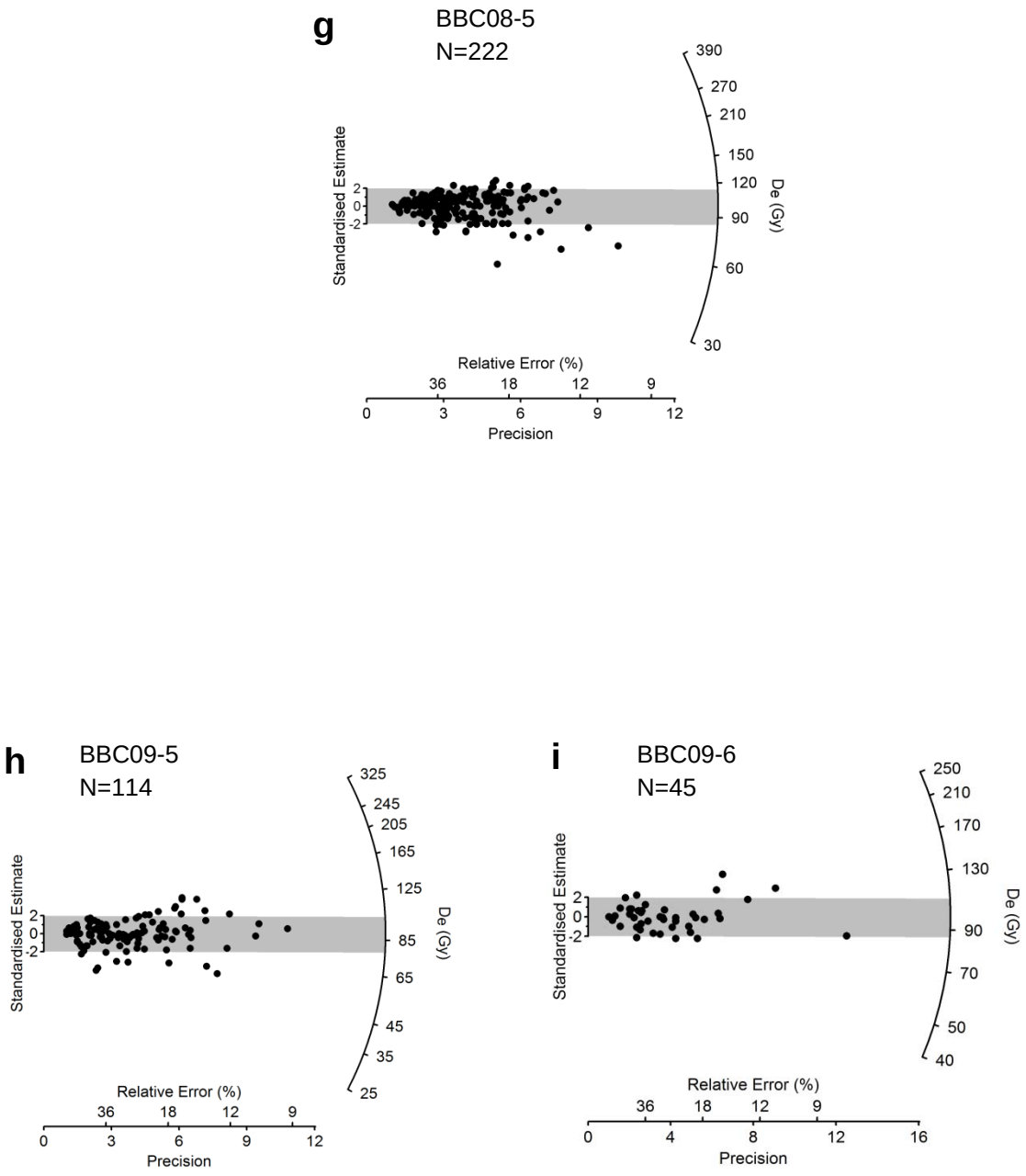

Figure 4.10: Radial plots for samples collected from within the M2 (l), M3 and M4 levels of Blombos Cave.

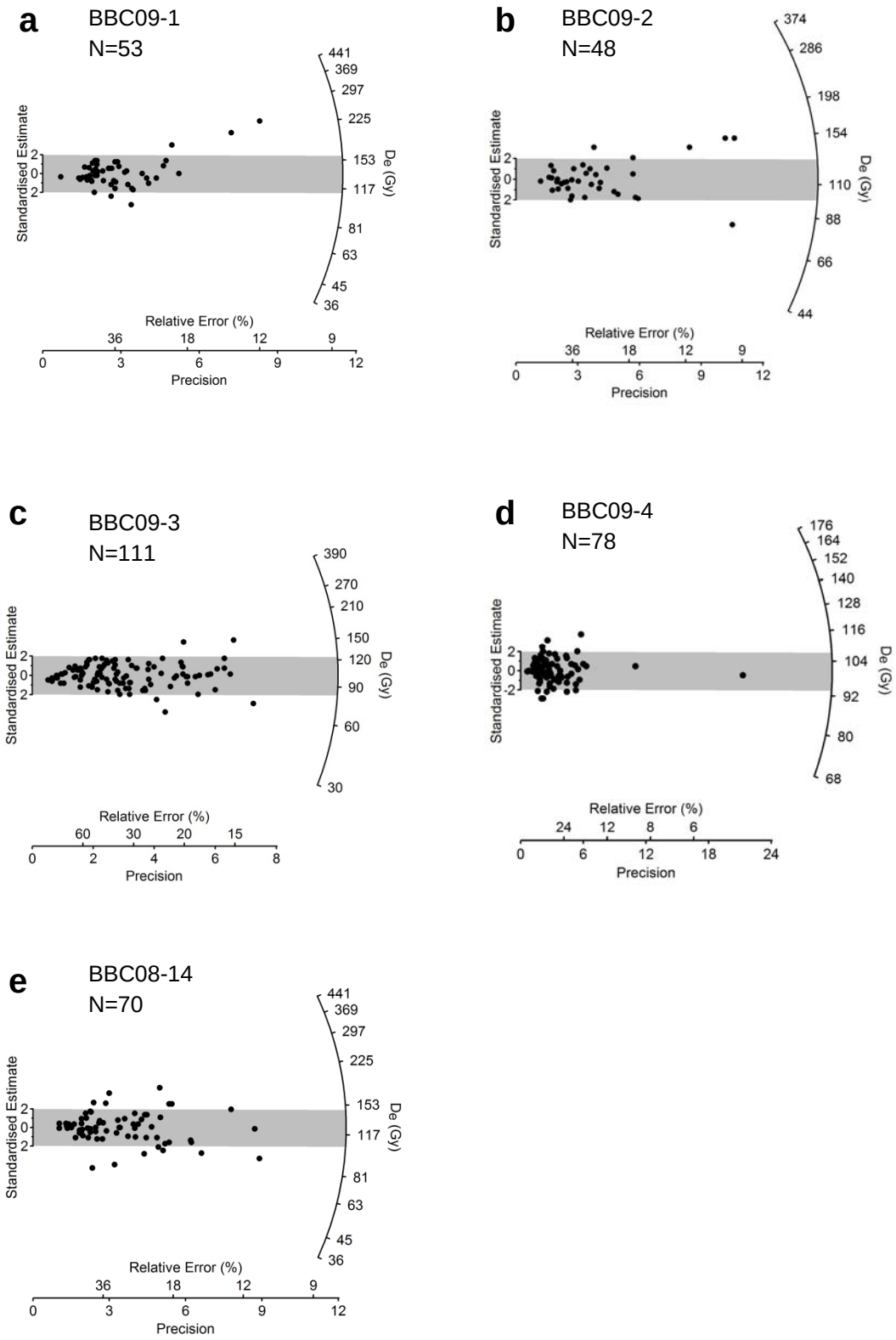

Figure 3.11: Radial plots for all five samples comprising the archaeologically-sterile calcrete layers.

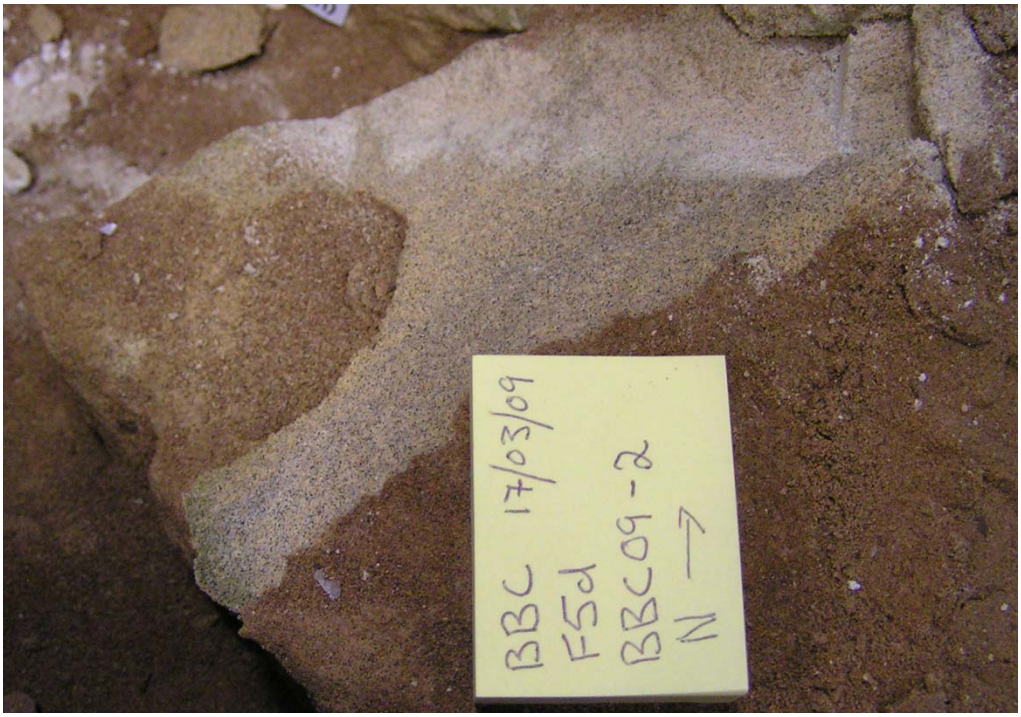

Figure 4.12: Photograph showing the fresh exposure of the geological calcrete units from which sample BBC09-2 was removed. The sediment appears to contain a high abundance of heavy minerals that are cemented together with the quartz grains by calcium carbonate. The presence of elements that may have higher (heavy minerals) and lower (carbonate) dose rates than the average beta dose rate may account for the observed spread in D_e rates for the calcrete samples.

appearance of the finely laid stratigraphic sequence being dated. These layers were well-defined and did not exhibit any obvious cross-stratigraphic contamination. In addition to this, the presence of intact features, such as hearths, within these layers argues against mixing of these deposits. Based on these observations, we can assume that mixing of sediments between adjacent layers has been minimal and, consequently, the D_e values for each of the samples in this sequence are representative of a single dose (and age) component.

Some of the samples analysed displayed two discrete D_e distributions, to which the FMM was applied. All samples analysed using the FMM contained no more than two discrete dose populations, one of which was always the dominant component with between 84 and 97% of grains belonging to that component. This population that is likely to most closely approximate the true D_e value associated with the burial event, with the remaining D_e values the possible outcome of roof spall contamination (BBC10-8(b)) or because of small-scale variations in beta dose rate received by individual grains.

4.5 Operator variance

Since single-grain OSL ages for samples from Blombos have now been obtained by both the present author and Zenobia Jacobs (ZJ), I was interested to determine whether different operators may or may not produce significantly different D_e values for the same sample. This uncertainty is important to quantify when integrating the different data sets to construct a chronology for the entire stratigraphic sequence at Blombos Cave. Although we have measured and analysed the samples in an identical way, there are still some partly subjective decisions made during the analytical process. To test whether these decisions affect the D_e outcomes and whether it is, in fact, possible to obtain internally consistent results from two operators, a sub-set of the samples measured by myself were systematically analysed also ZJ. Both of us carried out the analyses independently from start to finish without any prior discussions. The results of both sets of analyses are provided in Table 4.5, and radial plots for two representative examples – presenting the same data set, but analysed by myself and ZJ separately – are presented in Fig. 4.13 a-d.

ZJ consistently accepted a larger number of grains per sample than EH. This is likely just a difference in experience and does not appear to affect the end result. The overdispersion values showed a small amount of variation. Some of the difference here may be due to the fact that ZJ estimated the random error on the curve fit using twice the number of Monte Carlo iterations than EH. For dim grains with larger uncertainties on the individual L and T values, this may result in a larger uncertainty on the D_e and, thus, a smaller overdispersion. This effect can be best seen when all D_e values are plotted as radial plots (Fig. 4.13 a-d). The weighted mean D_e values, calculated using the central age model of Galbraith et al. (1999) are also quite consistent. The ratio of the D_e value determined by EH to the D_e value determined by ZJ is also provided in Table 4.5. Here it can be seen that for five of the seven samples, the two D_e values are consistent within 1σ of each other and for one sample (BBC10-2) within 2σ. Only one sample (BBC10-6) is significantly different. We still have to scrutinise this sample more closely to determine the reason for this difference. It is, however, interesting to note that EH almost always ended up with a higher weighted mean D_e. The reason for this is the inclusion or exclusion of grains that are saturated, or very close to saturation. Whereas EH would force the extra linear component of the curve to obtain a D_e, ZJ would in most cases interpret the dose response curve when fitted with a single saturating exponential function, as fully saturated. This problem was particularly acute in samples BBC10-1 and BBC10-2.

Sample name	Number of grains	Age Model	OD (%)	D_e (Gy)	Proportion (%)	D_e – FMM minor	Proportion (%) FMM minor
SB samples (levels M1, M2 (u)							
BBC10-1	130	CAM	22 ± 4	84.8 ± 2.8			
BBC10-2	110	CAM	25 ± 4	86.2 ± 3.3			
BBC10-3	145	CAM	24 ± 4	85.6 ± 2.9			
BBC10-4	89	CAM	25 ± 4	77.2 ± 3.2			
BBC10-5(a)	150	FMM	27 ± 3	81.5 ± 2.7	84 ± 6	45.6 ± 3.8	16 ± 6
BBC10-5(b)	122	CAM	32 ± 4	90.3 ± 3.7			
BBC10-6	130	CAM	22 ± 4	84.8 ± 2.8			
M2 (lr), M3 & M4 samples							
BBC10-7(a)	112	CAM	27 ± 3	94.2 ± 3.5			
BBC10-7(b)	320	FMM	19 ± 2	83.9 ± 1.4	97 ± 2	181.9 ± 21.5	3 ± 2
BBC10-8(a)	129	FMM	28 ± 4	86.4 ± 4.4	85 ± 1	49.8 ± 8.4	15 ± 1
BBC10-8(b)	177	CAM	30 ± 3	87.9 ± 2.7			
BBC08-1	210	FMM	19 ± 3	113.6 ±2.8	89 ± 4	60.5 ± 4.7	11 ± 4
BBC08-2	191	CAM	26 ± 3	110.4 ±3.2			
BBC08-5	222	CAM	24 ± 3	99.5 ± 2.6			
BBC09-5	114	CAM	28 ± 4	89.8 ± 3.4			
BBC09-6	45	CAM	23 ± 5	98.3 ± 5.4			
Calcrete samples							
BBC09-1	53	CAM	31 ± 7	135.4 ±9.1			
BBC09-2	38	CAM	26 ± 6	114.5 ±7.3			
BBC09-3	111	CAM	22 ± 4	101.8 ±3.9			
BBC09-4	78	CAM	23 ± 5	100.2 ±4.6			
BBC08-14	70	CAM	35 ± 5	124.8 ±7.3			

Table 4.4: Results of the D_e analysis, including the age model used, number of grains used and final D_e and overdispersion (OD) values for all samples. The D_e values and proportion of grains associated with the second (minor) De component identified by the FMM are also listed, for completeness, in the right-hand two columns.

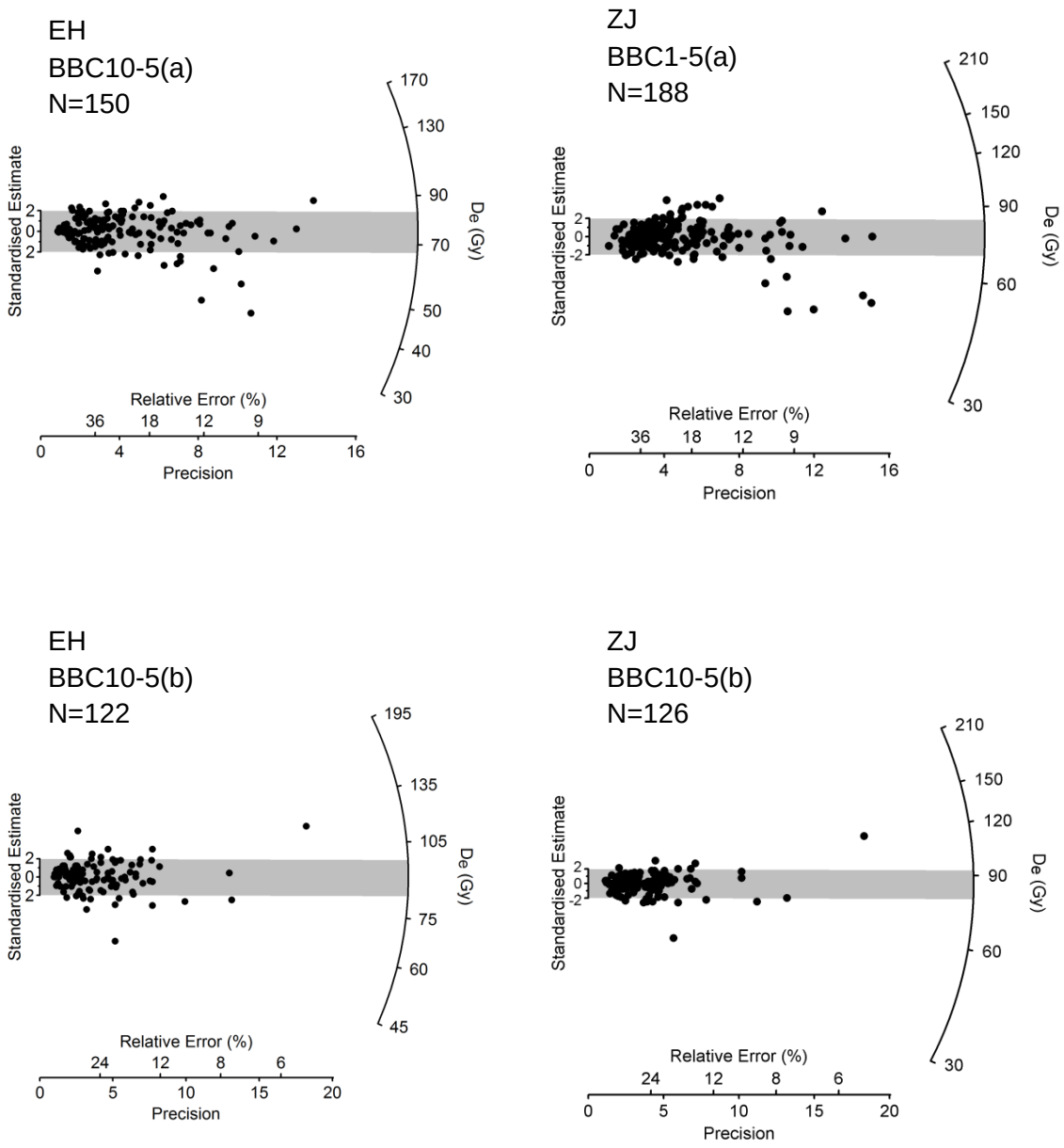

Figure 4.13: Radial plots of two samples analysed by two different operators (EH and ZJ).

Sample name	Elspeth Hayes			Zenobia Jacobs			Ratio
	N	D_e (Gy)	OD %	N	D_e (Gy)	OD %	(EH/ZJ)
BBC10-1	130	84.8±2.8	22±4	146	79.6±2.3	18±4	1.06±0.05
BBC10-2	110	86.2±3.3	25±4	130	77.4±2.8	27±4	1.11±0.06
BBC10-4	89	77.2±3.2	25±4	93	77.4±1.9	21±3	1.00±0.05
BBC10-5(a)	150	75.9±2.4	27±3	188	77.0±2.0	25±2	0.99±0.04
BBC10-5(b)	122	90.3±3.7	32±4	126	85.6±2.8	23±3	1.05±0.06
BBC10-6	130	84.8±2.8	22±4	149	71.7±2.3	25±3	1.18±0.05
BBC10-7(b)	320	86.4±1.5	27±2	366	86.9±1.3	16±2	0.99±0.02

Table 4.5: Number of accepted grains, D_e values and overdispersion values for Still Bay samples analysed by two operators; EH (myself) and ZJ Also shown is the ratio of the weighted mean D_e values calculated during both analyses.

Despite the small difference between the two operators, we consider the data generated by both researchers can be meaningfully integrated, and that this study provides evidence that ages obtained using OSL are essentially independent of operator-specific aspects of data analysis, providing that samples were measured in the same way and that the same basic analytical methods and criteria are applied.

4.6 Chapter Summary

A range of D_e values were obtained for all 21 samples collected from Blombos Cave using single-grain OSL, following the modified SAR protocol of Jacobs et al. (2006c). Grains with aberrant characteristics were rejected following a set of established rejection criteria and the remaining grains were used to determine individual D_e values. The D_e values for each sample have been presented as radial plots; based on the value of overdispersion and the shape of the radial plot, the appropriate statistical age model has been applied to estimate the final D_e value for each sample. Experimental validation checks, such as alteration of the given test dose and signal integration ranges, were also performed to determine their influence over final D_e values; the samples exhibited a lack of sensitivity to the conditions tested, which provides

confidence in the reliability of the final D_e estimates. The impact of two different operators analysing the same set of grains was also assessed, and found to be negligible.

Chapter 5

Chapter 5- Dosimetry results

5.1 Introduction

Using the different measurement techniques described in Section 3.9, a range of dose rate (D_R) values and elemental concentrations were obtained and compared for each of the Blombos samples. The inter-comparisons include measurements of elemental concentrations of K, U, and Th as well as the derived beta and gamma dose rates. Previously published estimates of the beta and gamma dose rates, and estimates of K, Th and U from Blombos Cave, used various methods and will also be compared to the data collected from this study. The similarities and differences, as well as their influence on the final age determinations, will be assessed, and reasons for the values, or combination of values, used to derive ages will be explained.

5.2 Elemental concentration comparisons

The following section provides estimates of K, U and Th concentrations using X-ray fluorescence (XRF) (section 3.9.2), thick-source alpha counting (TSAC) (Section 3.9.1) and GM-25-5 beta counting (Section 3.9.3).

5.2.1 ^{40}K comparisons

Estimates of ^{40}K, given as %K, were obtained directly by XRF for all but three of the samples, and also indirectly, by the difference in dose rates calculated from a combination of TSAC and GM-25-5 beta counting (Table 5.1A). The XRF measurements produce estimates of K_20 concentration, which have been converted here into the equivalent concentrations of ^{40}K. Table 5.1A shows the %K measured for each sample using both techniques. For each sample, the ^{40}K concentration is generally low, ranging between 0.40 and 0.76% when measured by XRF and between 0.26 and 0.70% when derived from TSAC and GM 25-5 beta counting. The ratio of %K from XRF to that estimated from TSAC and beta counting (Table 5.1A) indicates that the XRF values are consistently higher by between 8 and 53% with an average of 19% and a standard deviation of 11%. The samples from the Still Bay levels show the largest difference

between the two measurement techniques: on average, the XRF values are ~26% higher than those obtained from TSAC and beta counting. The values obtained from XRF for the SB samples are similar to those reported by Jacobs et al. (2006) using high resolution gamma spectrometry. Using these measurements, two values were reported for ZB4 and ZB10 in Bq/kg which are equivalent to 0.42 and 0.44 %K, respectively. Interestingly, Jacobs (2004) has also shown that for one of these samples (ZB10), a much lower %K value of ~0.34% was calculated using a TSAC and beta counting combination; this value is similar to those obtained in this study for the samples from the SB levels.

The samples from the M2 (l), M3 and M4 archaeological levels show %K values that are on average ~16% higher when measured with XRF. These estimates for the M2 levels fall within the range previously reported by Jacobs et al. (2006a). The values obtained from the M4 phase at the base of the current excavations are much greater (~40%) than for the samples from the M2 (l) and M3 levels, and more similar to the samples from the calcrete levels, which showed on average the highest %K concentrations and the smallest difference between the two measurement techniques (~12%).

The XRF values of %K have relative measurement uncertainties of ~0.1%. However, due to the uncertainties associated with the inhomogeneous distribution and possible re-distribution of K in archaeological contexts (e.g. Mercier et al., 1995; Jacobs et al., 2008a), a relative error of ±5% is thought to be more appropriate, and this is not dissimilar to the ~5% errors associated by the combined TSAC and beta counting estimate of K. The reason for the offset between the two values of K may relate to the subtraction method used in obtaining K from TSAC and beta counting: such an approach will not necessarily be accurate in samples that suffer from significant disequilibria in the uranium series, which I show below is the case at Blombos.

5.2.2 *U comparisons*

A summary of the U concentrations and their associated errors derived from XRF and the TSAC pairs technique is provided in Table 5.1B. In TSAC, the 'pairs' relate to radionuclide decays in the ^{232}Th series, so the U concentration is deduced by subtraction of the Th concentration (estimated from the pairs) from the total TSAC counts. Also provided in Table

	A			B			C		
Sample name	% K			U (ppm)			Th (ppm)		
	XRF	TSAC + β	ratio (XRF/TSAC+β)	XRF	TSAC	ratio (XRF/TSAC)	XRF	TSAC	ratio (XRF/TSAC)
Still Bay levels									
BBC10-1	0.43 ± 0.02	0.36 ± 0.02	1.22 ± 0.06	5.1 ± 0.3	2.2 ± 0.5	2.35 ± 0.18	2.2 ± 0.1	2.8 ± 0.5	0.80 ± 0.08
BBC10-2	0.45 ± 0.02	0.38 ± 0.02	1.16 ± 0.06	4.7 ± 0.2	2.2 ± 0.5	2.10 ± 0.16	2.8 ± 0.1	2.2 ± 0.5	1.30 ± 0.12
BBC10-3	0.47 ± 0.02	0.42 ± 0.02	1.13 ± 0.06	6.8 ± 0.3	2.4 ± 0.4	2.86 ± 0.18	3.5 ± 0.2	2.2 ± 0.4	1.62 ± 0.13
BBC10-4	0.47 ± 0.02	0.38 ± 0.02	1.21 ± 0.06	4.6 ± 0.2	2.5 ± 0.4	1.86 ± 0.12	2 ± 0.1	1.5 ± 0.4	1.36 ± 0.15
BBC10-5	0.41 ± 0.02	0.32 ± 0.02	1.29 ± 0.07	6.2 ± 0.3	2.4 ± 0.4	2.61 ± 0.17	2.1 ± 0.1	2.2 ± 0.4	0.97 ± 0.09
BBC10-6	0.40 ± 0.02	0.26 ± 0.01	1.53 ± 0.08	7.8 ± 0.4	3.5 ± 0.6	2.25 ± 0.14	2.7 ± 0.1	1.7 ± 0.6	1.62 ± 0.21
Average	**0.44**	**0.35**	**1.26**	**5.87**	**2.52**	**2.34**	**2.55**	**2.06**	**1.28**
Standard deviation	**0.03**	**0.05**	**0.15**	**1.29**	**0.48**	**0.36**	**0.57**	**0.45**	**0.34**
Standard error			**0.06**			**0.15**			**0.14**
M2 (lower), M3 & M4 levels									
BBC10-7	0.56±0.02	0.47 ± 0.02	1.19 ± 0.06	6.8 ± 0.3	3.5 ± 0.5	1.97 ± 0.12	2.7±0.1	1.2 ± 0.5	2.30 ± 0.28
BBC10-8	0.49±0.02	0.44 ± 0.02	1.12 ± 0.06	5.2 ± 0.3	3.0 ± 0.5	1.74 ± 0.12	2.6±0.1	2.0 ± 0.5	1.33 ± 0.14
BBC08-1				3.3 ± 0.2	2.4 ± 0.5	1.38 ± 0.11	1.9±0.1	1.7 ± 0.5	1.13 ± 0.13
BBC08-2				5.1 ± 0.3	3.3 ± 0.5	1.54 ± 0.10	1.8±0.1	1.3 ± 0.5	1.40 ± 0.20
BBC08-5				4.7 ± 0.2	3.0 ± 0.4	1.58 ± 0.10	2.3±0.1	1.7 ± 0.4	1.36 ± 0.13
BBC09-5	0.74±0.04	0.62 ±0.03	1.20 ± 0.06	3.4 ± 0.2	2.5 ± 0.6	1.37 ± 0.13	1.7±0.1	2.4 ± 0.6	0.70 ± 0.10
BBC09-6	0.75±0.04	0.67 ± 0.03	1.12 ± 0.06	4.2 ± 0.2	2.2 ± 0.6	1.89 ± 0.17	2.4±0.1	2.7 ± 0.6	0.90 ± 0.10
*Average **	**0.64**	**0.55**	**1.16**	**4.67**	**2.84**	**1.64**	**2.20**	**1.84**	**1.30**
Standard deviation	**0.13**	**0.11**	**0.04**	**1.21**	**0.48**	**0.24**	**0.40**	**0.55**	**0.47**
Standard error			**0.02**			**0.09**			**0.18**

	A			B			C		
Calcrete levels									
BBC08-14	0.76 ± 0.04	0.69 ± 0.03	1.10 ± 0.06	4.4 ± 0.2	2.0 ± 0.4	2.20 ± 0.14	1.9 ± 0.1	1.6 ±0.4	1.21 ± 0.12
BBC09-1	0.61 ± 0.04	0.50 ± 0.03	1.22 ± 0.06	3.3 ± 0.2	2.1 ± 0.5	1.54 ± 0.14	2 ± 0.1	2.5 ± 0.5	0.80 ± 0.08
BBC09-2	0.76 ± 0.04	0.70 ± 0.04	1.08 ± 0.06	3.3 ± 0.2	2.3 ± 0.4	1.42 ± 0.10	1.5 ± 0.1	1.4 ± 0.4	1.11 ± 0.13
BBC09-3	0.73 ± 0.04	0.67 ± 0.03	1.09 ± 0.06	3.9 ± 0.2	2.2 ± 0.4	1.74 ± 0.13	1.5 ± 0.1	2.0 ± 0.4	0.76 ± 0.09
BBC09-4	0.76 ± 0.04	0.68 ± 0.03	1.13 ± 0.06	4.8 ± 0.2	2.4 ± 0.5	1.98 ± 0.14	1.6 ± 0.1	1.7 ±0.5	0.95 ± 0.13
Average	**0.72**	**0.65**	**1.12**	**3.94**	**2.23**	**1.78**	**1.70**	**1.81**	**0.97**
Standard deviation	**0.06**	**0.08**	**0.06**	**0.67**	**0.16**	**0.32**	**0.23**	**0.44**	**0.19**
Standard error			**0.02**			**0.14**			**0.09**
ALL SAMPLES									
Average	**0.59**	**0.50**	**1.19**	**4.87**	**2.56**	**1.91**	**2.18**	**1.91**	**1.20**
Standard deviation	**0.15**	**0.15**	**0.11**	**1.31**	**0.47**	**0.43**	**0.53**	**0.48**	**0.40**
Standard error			**0.03**			**0.10**			**0.09**

Table 5.1. Elemental concentration comparisons for **A)** %K, **B)** U (ppm) and **C)** Th (ppm) following XRF and TSAC measurements. The average, standard deviation and standard error are also shown, along with the ratio of XRF over TSAC concentrations for each of the three elements measured. In the case of K, the concentration was deduced from a combination of TSAC and beta-counting.

5.1B is the ratio of the XRF values to the TSAC value for each sample, and the average for each group of samples.

The difference in U between the two techniques is very distinct. The XRF values are always higher than the TSAC values. On average they are 2.3, 1.6 and 1.8 times higher for the SB levels, the M2 (l), M3 & M4 archaeological levels, and the calcrete levels, respectively (Table 5.1B). These differences are most likely the result of disequilibria in the ^{238}U decay chain. Because XRF measures the parent radionuclide (^{238}U), only the top of this decay chain is measured. TSAC, however, measures all alpha-emitting radionuclides from the U-series chain. According to Adamiec and Aiken (1998), ~40% of the recorded alpha counts come from the pre-radon nuclides, and the remaining ~60% from the various post-radon nuclides (Fig 3.10B). Consequently, understanding the distinction between the two techniques, and which radionuclides are of interest in the derivation of beta and gamma dose rates, is very important.

An apparent excess in parental uranium (^{238}U) over its decay product ^{226}Ra was shown by Jacobs et al. (2006c) and Tribolo et al. (2006) when they measured their samples from Blombos Cave using high resolution gamma spectrometry (HRGS). They demonstrated that ^{226}Ra was in most cases in equilibrium with its daughter nuclides or never exceeded the activities of the latter by more than 20% (the threshold normally assumed) (Murray, 1981). They were able to show that significant disequilibrium between ^{238}U and ^{226}Ra occurred in the majority of their samples. The $^{226}Ra/^{238}U$ ratios for two samples from the SB levels analysed by Jacobs et al. (2006) were 0.49 (ZB4) and 0.83 (ZB10), which is not dissimilar to the TSAC/XRF ratios for U values of between 0.34 and 0.54 for the samples measured from the SB levels in this study (Table 5.1B) or the range of $^{226}Ra/^{234}Th$ ratios of between 0.46 and 0.89 reported by Tribolo et al. (2006) for sediments from the Still Bay levels. Similar results were also obtained from the M2 (lower) archaeological levels, where HRGS resulted in $^{226}Ra/^{238}U$ ratios of 0.60 (ZB7), 0.73 (ZB8) and 0.66 (ZB6) (Jacobs et al., 2006) or $^{226}Ra/^{234}Th$ ratios of between 0.68 and 0.72 (Tribolo et al., 2006), compared to TSAC/XRF ratios of between 0.51 and 0.57 for the samples measured in this study.

The Th/U ratios obtained from TSAC can also be used to suggest the existence of disequilibria in the ^{238}U decay series. These ratios are provided in Table 5.2, together with the total number of counts, the total counting time and the corrected count rate for each of the samples. For 'typical' samples (i.e., those that show no evidence of disequilibria), a ratio of ~3.4 can be found (Murray & Aitken, 1988). The samples from Blombos Cave, however, show

Sample name	Counting time (10^3 secs)	Total counts	BG corrected count rate	Ratio (Th/U)
BBC08-1	403	2127	4.793	0.701
BBC08-2	367	2477	6.141	0.387
BBC08-5	514	3180	5.777	0.568
BBC08-14	580	2609	4.082	0.786
BBC09-1	430	2256	4.778	1.159
BBC09-2	515	2550	4.520	0.581
BBC09-3	511	2625	4.683	0.877
BBC09-4	364	1934	4.845	0.691
BBC09-5	301	1756	5.315	0.977
BBC09-6	349	1921	4.991	1.194
BBC10-1	438	2389	4.955	1.273
BBC10-2	408	2141	4.768	0.960
BBC10-3	526	2885	4.989	0.906
BBC10-4	423	2254	4.836	0.594
BBC10-5	523	2883	4.996	0.908
BBC10-6	278	2009	6.572	0.482
BBC10-7	359	2494	6.325	0.339
BBC10-8	256	2318	5.921	0.656

Table 5.2: Th/U ratios obtained from TSAC, along with number of counts, the total counting time and the corrected count rate for each of the samples.

ratios that deviate substantially from this value (Table 5.2). Ratios of between 0.34 and 1.27 were obtained from the SB levels. This is similar to the range of 0.58 to 1.04 observed by Jacobs (2004). Ratios of between 0.39 and 1.19 were obtained for the samples from the M2 (l), M3 and M4 archaeological levels, and ratios of between 0.58 and 1.16 for the calcrete levels. Although consistent results were obtained in the three different studies, it is evident that disequilibrium exists in the U-series decay chain between ^{238}U and ^{226}Ra. This needs to be taken into account when dose rates are estimated for these samples to use for final age calculation. The existence of this form of U-series disequilibria also comprises the accuracy of the K concentration determination made by subtracting the TSAC estimates of U and Th concentration from the GM-25-5 estimates of the combined U, Th and K beta dose rate.

5.2.3 *Th comparisons*

A summary of the Th comparisons and their associated errors derived from XRF and the TSAC pairs technique is provided in Table 5.1C. Also provided is the ratio of the XRF value to the TSAC value for each sample, and the average for each group of samples. The ratios indicate that the two values are often quite different but, on average, these ratios are spread randomly around a value of 1. The relative error associated with the TSAC Th value is very large (between 20 and 40%) due to the poor counting statistics for the 'slow pairs' count. The number of slow pairs collected for each sample ranges from 17 (BBC10-6, BBC10-7) to 35 (BBC10-1). Due to the greater precision with which Th is measured using XRF, this may be a better estimate to use when deriving dose rates. Tribolo et al. (2006) and Jacobs et al. (2006) have previously demonstrated that the Th is in equilibrium at Blombos. Because of the short half-lives of the nuclides in the ^{232}Th decay chain, disequilibrium in this series is usually relatively unimportant in sediments that have been buried for longer than ~20 years (Murray, 1981; Olley et al. 1997) and is, thus, not a major concern for the Blombos Cave sediments.

5.3 Environmental dose-rate comparisons

Comparisons of the beta and gamma dose rates are based on the corresponding dose rates corrected for moisture content, grain size and the effects of HF acid etching (Section 3.10.3). Dose rate conversion factors were based on Adamiec and Aiken (1998). The aim of this section is to determine how the different elemental concentrations and their associated uncertainties will impact on the derived beta and gamma dose rates. This will ultimately inform us about the most appropriate estimate of the beta and gamma dose rates to use.

5.3.1 *Comparison of beta dose rates*

Beta dose rates were derived in three different ways. The first and most straightforward was through direct measurements using a GM-25-5 beta counter (see Section 3.9.3). The second method was to use the U and Th values derived from TSAC and the ^{40}K value derived from XRF (Table 5.1). The third way involved using the U value from TSAC and the Th and K values obtained from XRF; this approach was taken to avoid using the U value from XRF, given that the Blombos samples are known to have an excess of parental ^{238}U (Jacobs et al., 2006c;

Tribolo et al., 2006). Because U is not directly measured with TSAC, but rather is based on the subtraction of Th from the total counts, a correction needs to be made to the U value. This was done by determining the background-corrected count rate from the total number of counts, and from the total time the sample and the background were counted on the TSAC for each sample. These parameters are provided in Table 5.2. Once the U and Th concentrations have been estimated, the count rate per ppm of U and Th can be calculated following Table 7 in Adamiec and Aitken (1998). By replacing the TSAC estimate of Th concentration with the more precisely known XRF value, the equivalent count rate may be determined for Th; the difference between the total and new count rate would then be the corrected U count rate for that sample to estimate the beta dose rate for each sample. This corrected U value was used, together with the Th and K values derived from XRF.

The beta dose rates derived from these three approaches are provided in Table 5.3, together with the averages and standard deviations. The beta dose rates using all three methods are very consistent. The relative standard deviation is between 3.6% (BBC10-4) and 7.7% (BBC10-6) for the SB levels. For the M2 (l), M3 and M4 archaeological levels, a similar range of dose rates is observed, except for BBC09-5 which has a much higher beta dose rate from GM-25-5 beta counting and a correspondingly higher relative standard deviation (12.9%). Similar standard deviations were also obtained for the calcrete samples, but BBC09-3 (9.3%) showed greater variation (Table 5.3).

Two general trends can be observed from the data in Table 5.3. First, in the vast majority of cases, the lowest beta dose rate has been obtained from GM-25-5 beta counting. Second, the beta dose rates shows a trend with depth where the calcrete and M4 samples (i.e., those samples from the deepest excavated levels in the cave) have the highest beta dose rates.

5.3.2 *Comparisons of gamma dose rates*

Gamma dose rates were derived in four different ways. The first involved using the U and Th values obtained from TSAC, and K derived (by subtraction) from a combination of TSAC and GM-25-5 beta counting (see Section 3.9). As with the beta dose rates, the accuracy of this approach is compromised in situations where there is an excess of parental ^{238}U compared to the daughter products. The second method also involved the use of U and Th values obtained from TSAC, but included K values derived from XRF. The third method is the

Sample name	Beta dose rates (Gy/ka)			Average (Gy/ka)	Standard deviation (Gy/ka)
	β-counting	TSAC XRF (K) & (U + Th)	TSAC (U corrected) & XRF (Th + K)		
Method	**1**	**2**	**3**		
Still Bay layers					
BBC10-1	0.550 ± 0.04	0.613 ± 0.03	0.605 ± 0.03	0.589	0.034
BBC10-2	0.563 ± 0.05	0.600 ± 0.03	0.609 ± 0.03	0.591	0.025
BBC10-3	0.584 ± 0.04	0.610 ± 0.03	0.628 ± 0.03	0.607	0.022
BBC10-4	0.577 ± 0.04	0.547 ± 0.03	0.586 ± 0.04	0.570	0.020
BBC10-5	0.520 ± 0.04	0.587 ± 0.02	0.587 ± 0.03	0.565	0.039
BBC10-6	0.569 ± 0.04	0.645 ± 0.03	0.658 ± 0.04	0.624	0.048
M2 (lower), M3 & M4 layers					
BBC10-7	0.627 ± 0.05	0.671 ± 0.03	0.689 ± 0.04	0.662	0.032
BBC10-8	0.643 ± 0.05	0.678 ± 0.03	0.698 ± 0.03	0.673	0.038
BBC08-1	0.587 ± 0.04			0.587	
BBC08-2	0.587 ± 0.07			0.953	
BBC08-5	0.527 ± 0.05			0.527	
BBC09-5	0.705 ± 0.04	0.573 ± 0.03	0.573 ± 0.03	0.617	0.076
BBC09-6	0.712 ± 0.04	0.788 ± 0.04	0.785 ± 0.04	0.761	0.043
Calcrete layers					
BBC08-14	0.669 ± 0.04	0.736 ± 0.04	0.741 ± 0.04	0.715	0.040
BBC09-1	0.600 ± 0.04	0.687 ± 0.03	0.681 ± 0.04	0.656	0.048
BBC09-2	0.714 ± 0.04	0.772 ± 0.04	0.774 ± 0.04	0.753	0.044
BBC09-3	0.702 ± 0.04	0.591 ± 0.03	0.609 ± 0.03	0.634	0.060
BBC09-4	0.718 ± 0.04	0.783 ± 0.04	0.794 ± 0.04	0.765	0.041

Table 5.3. Beta dose rates obtained using three measurement approaches, along with the average and satandard deviation of all three.

same as the third method used to obtain beta dose rates as discussed above, where the Th and K values from XRF and a corrected U value from TSAC were used. The fourth way involved taking *in situ* gamma spectrometry measurements which were obtained for five samples. This approach is the most accurate, as it accounts for the existence of any present-day disequilibrium in the ^{238}U series as well as any spatial heterogeneity in the gamma radiation field. The gamma dose rates calculated using each of the methods are provided in Table 5.4, along with the average and standard deviation for each sample.

Little variation is observed for the gamma dose rates derived using the irst three of these methods. The gamma dose rates for the SB layers range between 0.43 ± 0.01 and 0.51 ± 0.01 Gy/ka when method 3 is used. The gamma dose rates for the M2 (l), M3 and M4 archaeological levels range between 0.40 ± 0.02 and 0.60 ± 0.03 Gy/ka (method 1) and the gamma dose rates for the samples from the calcrete levels range between 0.42 ± 0.01 and 0.46 ± 0.01 Gy/ka (method 3). The SB and calcrete levels are similar, whereas the values for range from the rest of the archaeological levels are mostly larger.

In situ gamma spectrometry measurements were attempted for all the samples collected in 2010 (BBC10), but unfortunately the equipment malfunctioned. During 2008 and 2009 we were able to obtain a few *in situ* measurements. These are shown as method 4 in Table 5.4. Interestingly, where these measurements were obtained, the agreement with those obtained by method 1 is not good. The *in situ* gamma spectrometry measurements are systematically smaller. Repeat *in situ* gamma spectrometry measurements were made for one of the samples (BBC09-6) and identical results were obtained. There is no evidence to suggest that the *in situ* measurements are inaccurate, so the apparent overestimation of the gamma dose rate using laboratory-based measurements may be due to the disequilibrium in the U-series decay chain (as discussed in section 5.2.2) and or the fact that these measurements were made on small samples that may not be representative of an infinite gamma sphere at the same locations.

A range of *in situ* gamma dose rates, measured using dosimeters and aluminium oxide chips, has previously been reported for the sediments from Blombos Cave (Tribolo et al., 2006; Jacobs et al., 2006c). A comparison with these could give some indication of the degree to which laboratory measurements may under or over-estimate the *in situ* gamma dose rate. Tribolo et al. (2006) reported gamma dose rates from SB levels that ranged between 0.40 and 0.53 Gy/ka. The majority of these measurements, however, were from the east, west and northern profiles of the cave, and are thus located away from the samples in this study. Jacobs

Sample name	Gamma dose measurement method				Average	Standard deviation
	β-counting	TSAC (U + Th) & XRF (K)	TSAC (U corrected) & XRF (Th + K)	In situ HRGS		
Method	**1**	**2**	**3**	**4**		
Still Bay layers						
BBC10-1	0.436 ± 0.03	0.446 ± 0.01	0.454 ± 0.03		0.445	0.009
BBC10-2	0.427 ± 0.03	0.446 ± 0.01	0.437 ± 0.03		0.432	0.010
BBC10-3	0.439 ± 0.03	0.466 ± 0.01	0.448 ± 0.03		0.443	0.014
BBC10-4	0.424 ± 0.03	0.448 ± 0.01	0.421 ± 0.03		0.431	0.037
BBC10-5	0.414 ± 0.03	0.432 ± 0.01	0.433 ± 0.03		0.424	0.010
BBC10-6	0.47 ± 0.03	0.511 ± 0.01	0.497 ± 0.03		0.484	0.021
M2 (lower), M3 & M4 layers						
BBC10-7	0.459 ± 0.02	0.492 ± 0.01	0.474 ± 0.02		0.466	0.017
BBC10-8	0.484 ± 0.03	0.501 ± 0.01	0.520 ± 0.02		0.502	0.018
BBC08-1	0.412 ± 0.02			0.363 ± 0.02	0.567	0.035
BBC08-2	0.610 ± 0.02			0.388 ± 0.02	0.499	0.157
BBC08-5	0.505 ± 0.02			0.341 ± 0.02	0.423	0.116
BBC09-5	0.494 ± 0.04	0.423 ± 0.01	0.424 ± 0.02	0.364 ± 0.01	0.459	0.041
BBC09-6	0.488 ± 0.03	0.500 ± 0.01	0.504 ± 0.03	0.330 ± 0.01	0.496	0.008
Calcrete layers						
BBC08-14	0.422 ± 0.02	0.439 ± 0.01	0.435 ± 0.02		0.428	0.009
BBC09-1	0.437 ± 0.03	0.451 ± 0.01	0.458 ± 0.03		0.447	0.010
BBC09-2	0.450 ± 0.02	0.461 ± 0.01	0.461 ± 0.01		0.455	0.006
BBC09-3	0.462 ± 0.02	0.453 ± 0.01	0.435 ± 0.02		0.449	0.013
BBC09-4	0.468 ± 0.03	0.423 ± 0.01	0.416 ± 0.02		0.442	0.028

Table 5.4. Gamma dose rates obtained using four measurement approaches, along with the average and standard deviation of all three. XRF measurements of K were not made for the three samples marked with an asterisk.

Sample	Layer	Face	Gamma dose rate (Gy/ka)
Tribolo dosimeters (Tribolo et al., 2006)			
BBC2	CA	East	0.433
D4	CAB	East	0.545
D5	CAC	West	0.421
D3	CAC	North	0.407
D1	CC	North	0.425
H	CD/CDB	West	0.400
D2	CF	North	0.446
BBC3	CFA	East	0.531
BBC4	CFA	East	0.487
D	CFA	South	0.411
D9	CFA	West	0.468
D10	CFB	South	0.527
B	CFD	West	0.397
F	CGAA	South	0.465
C	CGAC	West	0.389
D8	CGB	South	0.508
E	CH/CI	South	0.533
D6	CI		0.524
D7	CIA/CIB	South	0.557
			Range: 0.389 – 0.557
Jacobs aluminium oxide dosimeters (Jacobs et al., 2006; Jacobs, 2004)			
ZB4(L)	CC	South	0.435
ZB10(L)	CFB/CFC	South	0.402
ZB10(L)	CFD	South	0.402
ZB7(L)	CGAA	South	0.405
ZB7	CGAA	South	0.432
ZB6(L)	CGAB/CGAC	South	0.458
ZB8(L)	CGAB/CGAC	South	0.375
ZB8	CGAC/CGAC	South	0.387
ZB5(L)	CH/CI	East	0.551
ZB5	CH/CI	East	0.533
			Range: 0.375 – 0.551
Jacobs 2008 in situ gamma spectrometry measurements			
BBC08-10	CH	South	0.344
BBC08-4	CIB	South	0.35
BBC08-11	CIB	South	0.357
BBC08-12	CIBh1	West	0.333
BBC08-3	CJh1	South	0.356
BBC08-8	CL	South	0.411
BBC08-6	Upper CP sterile	South	0.461
BBC08-9	CQC	South	0.442
			Range: 0.333 – 0.461

Table 5.5. Previously published and measured field measurements from which gamma dose rates were calculated at Blombos Cave.

et al. (2006c) reported gamma dose rates of 0.40 to 0.43 Gy/ka for the SB levels, all from the southern profile, in very close proximity to the current set of samples.

Tribolo et al. (2006) and Jacobs et al. (2006c) also reported a range of *in situ* measurements for layers that make up the M2 (lower) levels and the top of the M3 levels. For the M2 (l) levels, Tribolo et al. (2006) reported values of 0.47, 0.39 and 0.50 Gy/ka and Jacobs et al. (2006c) reported gamma dose rates ranging between 0.38 and 0.46 Gy/ka. Both groups reported slightly higher gamma dose rates for the top of M3 (layer CH/CI), which ranged from 0.52 to 0.56 Gy/ka. A further eight *in situ* gamma spectrometry measurements were also made for the other M3 layers in 2008 and these gamma dose rates ranged between 0.35 and 0.44 Gy/ka.

All the known field gamma dose rate measurements are provided in Table 5.5, alongside the layer and face of the excavated profile into which the measurements were made. From this, it appears as if the laboratory values reported in Table 5.4 are not outside the range of previously published field gamma dose rates. However, because ~99% of the gamma dose rate in the ^{238}U chain originates from the post-radon daughters, any inclusion of excess U from pre-radon daughters and parental ^{238}U can lead to overestimation of the gamma dose rate when methods such as TSAC, XRF and GM-25-5 beta counting are used. The ideal would be to return to Blombos to obtain *in situ* gamma spectrometry measurements for all samples, but this is beyond the scope of this study.

5.4. Final dose rates

The final dose rates used for age determination are presented in Table 5.6. A cosmic-ray dose rate of 0.038 ± 0.008 Gy/ka has been allocated to each of the samples, following calculations based on the equations provided by Prescott and Hutton (1994) (see Section 3.11), and the same internal alpha dose rate of 0.032 ± 0.01 Gy/ka was assumed for each sample. The moisture content of each sample varied quite significantly, especially in the archaeological layers comprising the Still Bay and M2 (l), M3 and M4 levels, ranging from 5 ± 1 to 20 ± 4%. The calcrete levels showed little variability, with moisture clustered around of 10 ± 2%.

The beta dose rate of each sample was derived using the first method discussed in Section 5.3.1, that is, from direct measurements using a GM-25-5 beta counter. As this method enables direct measurements to be made of the beta dose rate, rather than the indirect

Sample name	Grain size (µm)	Moisture content (%)	Dose rates (Gy/ka))			Total dose rate (Gy kyr-1)
			Beta	Gamma	Cosmic	
Still Bay layers						
BBC10-1	180-212	6 ± 1	0.55 ± 0.04	0.45 ± 0.01	0.038 ± 0.008	1.066 ± 0.06
BBC10-2	180-212	5 ± 1	0.56 ± 0.05	0.45 ± 0.01	0.038 ± 0.008	1.079 ± 0.06
BBC10-3	180-212	7 ± 1	0.58 ± 0.04	0.47 ± 0.01	0.038 ± 0.008	1.121 ± 0.06
BBC10-4	180-212	5 ± 1	0.58 ± 0.04	0.45 ± 0.01	0.038 ± 0.008	1.096 ± 0.06
BBC10-5(a)	180-212	8 ± 2	0.52 ± 0.04	0.43 ± 0.01	0.038 ± 0.008	1.022 ± 0.06
BBC10-5(b)*	180-212	8 ± 2	0.52± 0.04	0.43 ± 0.01	0.038 ± 0.008	1.022 ± 0.06
BBC10-5(b)**	180-212	8 ± 2	0.58 ± 0.04	0.45 ± 0.01	0.038 ± 0.008	1.095 ± 0.06
BBC10-6	180-212	13 ± 3	0.57 ± 0.04	0.51 ± 0.01	0.038 ± 0.008	1.150 ± 0.07
M2 lower, M3 and M4 layers						
BBC10-7(a)	180-212	20 ± 4	0.63 ± 0.05	0.49 ± 0.01	0.038 ± 0.008	1.190 ± 0.08
BBC10-7(b)	180-212	20 ± 4	0.63 ± 0.05	0.49 ± 0.01	0.038 ± 0.008	1.190 ± 0.08
BBC10-8(a)	180-212	10 ± 2	0.64 ± 0.05	0.50 ± 0.01	0.038 ± 0.008	1.214 ± 0.07
BBC10-8(b)	180-212	10 ± 2	0.64 ± 0.05	0.50± 0.01	0.038 ± 0.008	1.214 ± 0.07
BBC08-1	180-212	10 ± 2	0.59 ± 0.04	0.36 ± 0.02	0.038 ± 0.008	1.020 ± 0.06
BBC08-2	180-212	10 ± 2	0.59 ± 0.06	0.39 ± 0.02	0.038 ± 0.008	1.044 ± 0.06
BBC08-5	180-212	10 ± 2	0.53 ± 0.05	0.34 ± 0.02	0.038 ± 0.008	0.937 ± 0.06
BBC09-5	180-212	10 ± 2	0.71 ± 0.04	0.36 ±0.01	0.038 ± 0.008	1.140 ± 0.06
BBC09-6	180-212	10 ± 2	0.71 ± 0.04	0.33 ±0.01	0.038 ± 0.008	1.112 ± 0.06
Calcrete layers						
BBC08-14	180-212	10± 2	0.67 ± 0.04	0.44 ± 0.01	0.038 ± 0.008	1.178 ± 0.06
BBC09-1	180-212	10± 2	0.60 ± 0.04	0.45 ± 0.01	0.038 ± 0.008	1.121 ± 0.06
BBC09-2	180-212	10± 2	0.71 ± 0.04	0.46 ± 0.01	0.038 ± 0.008	1.245 ± 0.07
BBC09-3	180-212	10± 2	0.70 ± 0.04	0.45 ± 0.01	0.038 ± 0.008	1.238 ± 0.06
BBC09-4	180-212	10 ± 2	0.72 ± 0.04	0.42 ± 0.01	0.038 ± 0.008	1.249 ± 0.06

Table 5.6: Final beta, gamma and cosmic dose rates, along with grain size and moisture content, used to calculate the total dose rate. The total dose rate also included an internal alpha dose of 0.032 ± 0.01 Gy/ka. The total dose rate was used in the final age calculation.

measurements achieved from XRF and TSAC, it provides a more accurate measure of the beta dose rate.

The gamma dose rates for all but five of the samples were estimated using the U and Th values obtained from TSAC combined with the K values derived from XRF (method 2 of Section 5.3.2). Although this method does not provide a direct measure of the gamma dose rate, it is the most precise method, and is less susceptible to the errors inherent in 'subtraction' methods (such as method 1). We used this method, therefore, for all samples that lacked an *in situ* estimate of the gamma dose rate. Because the remaining five samples (BBC08-1,2,5; BBC09-5,6) were accompanied by *in situ* gamma spectrometry measurements, we used the latter to obtain the gamma dose rates for these samples. Not only does this method provide direct gamma dose rate measurements, but it is also supported by previous published gamma dose rate measurements performed by Tribolo et al. (2006) and Jacobs et al. (2006c) (see Section 5.3.2).

Total dose rates for each of these samples were calculated as the sum of the beta, gamma and cosmic-ray dose rates (taking into account the grain size and moisture content of each sample) plus the internal alpha dose rate. The total dose rates, along with the final D_e values, are used in the age equation to obtain final ages, which are discussed in Chapter 6. This approach takes into account the existence of U-series disequilibrium in the sediments at the present day, and assumes that these conditions have prevailed the period of sample burial.

5.5 Chapter summary

Gamma, beta and cosmic-ray dose rates were calculated for purposes of determining OSL ages. This involved making four separate determinations of the gamma dose rate and three separate estimates of the beta dose rate, using either TSAC, GM-5-25 beta counting, XRF or *in situ* gamma spectrometry, or a combination of these methods. The results obtained have been compared and the most appropriate method of gamma and beta dose rate determination selected to calculate the total dose rates, taking into account the moisture content and grain size of each sample. Concerns about the effects of disequilibrium in the U-series remain, and should not be ignored. Future priorities are: 1) to make high-resolution gamma spectrometry measurements on these samples to better discern the nature and extent of disequilibrium; and 2) to repeat the

field gamma spectrometry measurements on all samples to obtain *in situ* gamma dose rates that take into consideration the inhomogeneous nature of the sedimentary deposits in Blombos Cave.

Chapter 6

Chapter 6- Final ages and archaeological significance

6.1 Introduction

Single-grain OSL measurements were used to derive optical ages for the 21 samples collected from Blombos Cave. From the data obtained, valuable insights regarding the timing and progression of modern behavioural innovations identified within the site were obtained. This section will present final age determinations based on the corresponding dose rate and D_e value of each sample. Chronological comparisons will be made between major environmental changes and population characteristics, which may provide insights into the key driving forces behind behavioural modernity. Any discrepancy amongst ages will also be addressed. At the end of the chapter, I will address the three aims of my thesis given in Section 1.4, to evaluate whether or not I have successfully achieved my aims.

6.2 Final age determination

Using the D_e and dose rate values obtained for each of the Blombos samples (see Table 4.4 and 5.6), the age equation was used to determine final ages (see Section 3.12). These are presented for each sample in Table 6.1. Also shown are the final beta, gamma and cosmic-ray dose rates together with the D_e value, number of grains used, age model used and the overdispersion value.

The ages for the SB levels range from between 70.5 ± 4.9 (BBC10-4) to 88.4 ± 6.3 ka (BBC10-5(b)). The latter sample was separated in the lab from BBC10-5(a) as it was believed that the sample tube had been cross-cut into an adjacent layer – layer CFA (BBC10-5(b)) and hearth layers CFB/CFC (BBC10-5(a)). Because the dose rates used on this sample were derived from the layer where the sample tube first entered, dose rates most likely pertain to the CFB/CFC hearth layer. A more appropriate measure of dose rate may be taken from the CFA layer itself, which was measured for sample BBC10-4. This would reduce the final age to 82.5 ± 5.8 ka which more closely resembles the ages of the other SB samples. This uncertainty should be kept in mind when ages are combined and conclusions drawn about the potential duration of this industry.

All seven ages for the SB levels are similar and statistically consistent with those achieved from previous OSL, TL and ESR dating studies at Blombos, which have provided ages ranging from 73 ± 3 and 77 ± 3 ka, 68 ± 6 to 82 ± 8 ka, and 50 ± 5 (early uptake) to 86 ± 11 ka (linear uptake), respectively (Jones, 2001; Jacobs, 2004; Tribolo et al., 2006, Jacobs et al., 2006a) (see Table 1.4).

The four samples analysed from the M2 (lower) phase are all systematically younger than previous single-grain OSL ages (Jacobs et al., 2006c). Two samples were collected from layer CGAA (the top of this phase) resulting in ages of 79 ± 6 (BBC10-7(a)) and 71 ± 7 ka (BBC10-8(a)). This can be compared to the age for ZB7 of 82 ± 4 ka (Jacobs et al., 2006c), which is statistically consistent with both ages determined in the other two samples were collected from layers CGAB/CGAC. Ages of 71 ± 5 (BBC10-7(b)) and 72 ± 6 (BBC10-8(b)) can be compared to the ages for ZB8 of 81 ± 4 ka and ZP6 of 85 ± 6 ka (Jacobs et al., 2006c): the ages obtained in this study is not consistent with the latter age estimate. The age of ranges is also consistent with the TL age on a single burnt stone of 76 ± 7 ka (Tribolo et al., 2006). Interestingly, with the current data set, no distinct chronological difference can be seen between the SB layers and the age of the M2 (l) layers.

The samples collected and dated in this study from the M3 archaeological layers represent only the final layer of this stage. Between layer CGAC, the lowest layer in the M2 (l) phase and layer CP/CQA, there is approximately 80-100 cm of deposit. These deposits were dated by ZJ. She obtained a weighted mean ages for layers CH/CI and CJ of 100 ± 4 (n=7) and 99 ± 5 ka (n=8) ka, respectively and also an age of 99 ± 4 ka for one sample from layer CL and another sample from CP upper, which is an archaeologically sterile layer (Z. Jacobs, pers. comm.). She also re-analysed sample ZB5 for which she previously reported an age of 143 ± 6 ka (Jacobs et al., 2006c). This age was based on multi-grain aliquots. The revised age of 97 ± 4 ka is based on measurements of individual quartz grains. The significant previous overestimation is believed to be the result of the inclusion of a large number of saturated grains, which may or may not be the result of unbleached roof spall.

The three samples from the lowermost level of the M3 phase (layer CP/CQA) dated in this study underlies Jacobs' sample from layer CP upper. These three samples (BBC08-1, 2 and 5) have ages that range between 106 ± 7 and 111 ± 8 ka and, hence, are statistically consistent with each other. They are also consistent with a U-series age of ~100 ka on thin flowstone that formed over the shell containers (C. Henshilwood, pers. comm.). They are also slightly older

than the ~99 ka ages for the deposits overlying it and are in stratigraphic order. These ages are significant as they contain the earliest evidence for MHB at Blombos Cave.

Immediately underlying layer CP/CQA, the lowest layer of the M3 phase, is a solid layer of calcrete (Fig. 3.12). One sample was collected at the base of layer CQA (BBC08-14) and gave an age of 106 ± 9 ka that is consistent with the three samples from layer CP/CQA. Two further samples were collected from the thick layers separating layers CQ and CR (BBC09-1 and BBC 09-2). One of these samples gave an age of 121 ± 11 ka, which is in stratigraphic order, whereas the other provides a younger age of 92 ± 8 ka; this is, nonetheless, statistically consistent with the ages of the overlying deposits.

The two samples from the deepest calcrete layers (BBC09-3 and BBC09-4), which separate layers CR and CS from the two samples from the deepest archaeological levels in the M4 phase (BBC09-5 and BBC09-6), show significant age inversions. The 2 calcrete samples gave ages of 87 ± 6 (BBC09-3) and 80 ± 6 ka (BBC09-4) and the two samples from layer CS gave ages of 79 ± 5 (BBC09-5) and 88 ± 7 ka (BBC09-6). Jacobs recently dated a sample from layer CR that is an archaeological level between the two calcrete levels, and obtained an age of 128 ± 6 ka (Z. Jacobs, pers. comm.).

The reason for these age reversals in the deepest levels are not understood at the present time, but it is important to note that these four samples have the highest beta dose rates of all the samples (Table 6.1). It is likely that problems associated with dose rate determination and the effects of disequilibrium in the ^{238}U decay chain may contribute to this problem and this should be further investigated, but is beyond the scope of this thesis.

6.3 Significance of ages obtained

6.3.1 *Ages for SB levels*

Jacobs et al. (2008c) determined, on the basis of four single-grain OSL ages for three sites in South Africa and Namibia (Diepkloof, Sibudu and Apollo 11; Fig 2.1), that the SB started 71.9 ka ago and ended 71.0 ka and that these ages are consistent with a short duration (<1 ka) for this industry. They, however, pointed out that there are too few data points to reliably constrain this estimate to better than ~4-5 ka at the 95% confidence interval. The

ages estimated for the SB industry in this study more than doubles the number of samples and should be useful in the re-calculation of the start and end ages and the duration of this industry. The youngest ages obtained in this study agree with the start and end date estimates of Jacobs et al. (2008c), but the oldest ages far exceeds the start date estimate. Does this mean that the SB has a much longer duration than previously proposed? Two aspects of the data set needs to be considered first: 1) there is no apparent time transgression from the uppermost (layer CA) to the lowermost (layer CFC) layers in the SB levels; all ages are randomly distributed around a mean value. 2) The differences in D_e values obtained for the same samples, but analysed by two different operators (EH and ZJ) should be considered. These ages are presented in Table 6.2. The ages are all statistically consistent between the two data sets and cover a very similar time range. The slightly older ages obtained by EH for the samples from the top layers (BBC10-1 and BBC10-2) are likely due to the inclusion of grains that are in, or close to, saturation, resulting in a slight overestimation of D_e (see discussion in Section 4.5).

With the exception of BBC10-6, the remainder of the ages obtained by ZJ are in stratigraphic order and agree well with the 73 ± 3 ka age for layer CC (ZB4) and the 77 ± 3 ka age for the bottommost layer (CFD) (ZB10) published previously (Jacobs et al., 2008c). Further work needs to be done to explore the exact difference between these two data sets and their meaning. At first pass, the results do seem to indicate a longer duration of the SB than previously estimated – a duration perhaps more similar to that reported for the HP of 5.3 ka (Jacobs et al., 2008c). Since the youngest ages have not significantly narrowed the gap between the end of the SB and the start of the HP at ~ 65 ka, it remains true to say that both industries are distinct innovative bursts. The results from this study also allow us to conclusively rule out the theory that modern behaviours were only present after ~50 ka, with our ages for the SB industry being some 20 to 30 ka earlier than this. The possible driving forces behind the appearance and disappearance of the SB industry and other periods of technological innovation are discussed below.

6.3.2. *Ages for the layer CP/CQA – the ochre container levels*

Ages obtained for samples BBC08-1, BBC08-2 and BBC08-5 are potentially very significant. These samples were collected from the basal layer of the M3 archaeological phase (layer CP/CQA) in which evidence has been found for (what is believed to be) the

Sample name	Grain size (μm)	Moisture content (%)	Dose rates (Gy/ka)			Total dose rate (Gy/ka)	D_e	Number of grains	Age model	OD (%)	Optical age (ka)
			Beta	Gamma	Cosmic						
SB layers (M1 & M2 upper)											
BBC10-1	180-212	6 ± 1	0.550 ± 0.04	0.446 ± 0.01	0.038 ± 0.008	1.066 ± 0.06	84.8 ± 2.8	130	CAM	22 ± 4	79.5 ± 5.1
BBC10-2	180-212	5 ± 1	0.563 ± 0.05	0.446 ± 0.01	0.038 ± 0.008	1.079 ± 0.06	86.2 ± 3.3	110	CAM	25 ± 4	79.9 ± 5.7
BBC10-3	180-212	7 ± 1	0.584 ± 0.04	0.466 ± 0.01	0.038 ± 0.008	1.121 ± 0.06	85.6 ± 2.9	145	CAM	24 ± 4	77.3 ± 5.2
BBC10-4	180-212	5 ± 1	0.577 ± 0.04	0.448 ± 0.01	0.038 ± 0.008	1.096 ± 0.06	77.2 ± 3.2	89	CAM	25 ± 4	70.5 ± 4.9
BBC10-5(a)	180-212	8 ± 2	0.520 ± 0.04	0.432 ± 0.01	0.038 ± 0.008	1.022 ± 0.06	81.5 ± 2.7	150	FMM	27 ± 3	79.7 ± 5.3
BBC10-5(b)*	180-212	8 ± 2	0.520 ± 0.04	0.432 ± 0.01	0.038 ± 0.008	1.022 ± 0.06	90.3 ± 3.7	122	CAM	32 ± 4	88.4 ± 6.3*
BBC10-5(b)**	180-212	8 ± 2	0.577 ± 0.04	0.448 ± 0.01	0.038 ± 0.008	1.095 ± 0.06	90.3 ± 3.7	122	CAM	32 ± 4	82.5 ± 5.8**
BBC10-6	180-212	13 ± 3	0.569 ± 0.04	0.511 ± 0.01	0.038 ± 0.008	1.150 ± 0.07	84.8 ± 2.8	130	CAM	22 ± 4	73.7 ± 5.0
M2 lower											
BBC10-7(a)	180-212	20 ± 4	0.627 ± 0.05	0.492 ± 0.01	0.038 ± 0.008	1.190 ± 0.08	94.2 ± 3.5	112	CAM	27 ± 3	79.2 ± 6.4
BBC10-7(b)	180-212	20 ± 4	0.627 ± 0.05	0.492 ± 0.01	0.038 ± 0.008	1.190 ± 0.08	83.9 ± 1.4	320	FMM	19 ± 2	70.5 ± 5.2
BBC10-8(a)	180-212	10 ± 2	0.643 ± 0.05	0.501 ± 0.01	0.038 ± 0.008	1.214 ± 0.07	86.4 ± 4.4	129	FMM	28 ± 4	71.2 ± 6.6
BBC10-8(b)	180-212	10 ± 2	0.643 ± 0.05	0.501 ± 0.01	0.038 ± 0.008	1.214 ± 0.07	87.9 ± 2.7	177	CAM	30 ± 3	72.4 ± 6.0
M3											
BBC08-1	180-212	10 ± 2	0.587 ± 0.04	0.363 ± 0.02	0.038 ± 0.008	1.020 ± 0.06	113.6 ± 2.8	210	FMM	19 ± 3	111.3 ± 7.7
BBC08-2	180-212	10 ± 2	0.587 ± 0.06	0.388 ± 0.02	0.038 ± 0.008	1.044 ± 0.60	110.4 ± 3.2	191	CAM	26 ± 3	105.7 ± 7.4
BBC08-5	180-212	10 ± 2	0.527 ± 0.05	0.341 ± 0.02	0.038 ± 0.008	0.937 ± 0.06	99.5 ± 2.6	222	CAM	24 ± 3	106.1 ±10.1
Calcrete layers											
BBC08-14	180-212	10 ± 2	0.669 ± 0.04	0.439 ± 0.01	0.038 ± 0.008	1.178 ± 0.06	124.8 ± 7.3	38	CAM	35 ± 5	105.9 ± 8.5
BBC10-1	180-212	10 ± 2	0.600 ± 0.04	0.451 ± 0.01	0.038 ± 0.008	1.121 ± 0.06	135.4 ± 9.1	111	CAM	31 ± 7	120.8 ± 10.9
BBC09-2	180-212	10 ± 2	0.714 ± 0.04	0.461 ± 0.01	0.038 ± 0.008	1.245 ± 0.07	114.5 ± 7.3	78	CAM	26 ± 6	92.0 ± 7.8.
BBC09-3	180-212	10 ± 2	0.702 ± 0.04	0.453 ± 0.01	0.038 ± 0.008	1.238 ± 0.06	101.8 ± 3.9	70	CAM	22 ± 4	82.2 ± 5.6
BBC09-4	180-212	10 ± 2	0.718± 0.04	0.423 ± 0.01	0.038 ± 0.008	1.249 ± 0.06	100.2 ± 4.6	53	CAM	23 ± 5	80.3 ± 5.7
M4											
BBC09-5	180-212	10 ± 2	0.705 ± 0.04	0.364 ± 0.01	0.038 ± 0.008	1.140 ± 0.06	89.8 ± 3.4	114	CAM	28 ± 4	78.8 ± 5.4
BBC09-6	180-212	10 ± 2	0.712 ± 0.04	0.330 ± 0.01	0.038 ± 0.008	1.112 ± 0.06	98.3 ± 5.4	45	CAM	23 ± 5	88.4 ± 6.8

* ages obtained using dose rates from dosimetry sample BBC10-5(a); **ages obtained using dose rates from dosimetry sample BBC10-4

Figure 6.1: Table showing final dose rates, D_e values and ages for all samples analysed in this study. Samples are listed in stratigraphic order in the phases to which they belong.

Sample name	Elspeth Hayes		Zenobia Jacobs	
	D_e (Gy)	Age (ka)	D_e (Gy)	Age (ka)
BBC10-1	84.8 ± 2.8	79.5 ± 5.1	79.6 ± 2.3	71.8 ± 4.5
BBC10-2	86.2 ± 3.3	79.9 ± 5.7	77.4 ± 2.8	71.7 ± 5.1
BBC10-4	77.2 ± 3.2	70.5 ± 4.9	77.4 ± 1.9	70.7 ± 4.6
BBC10-5(a)	75.9 ± 2.4	79.7 ± 5.3	77.0 ± 2.0	75.3 ± 4.8
BBC10-5(b)	90.3 ± 3.7	82.5 ± 5.8	85.6 ± 2.8	78.2 ± 5.4
BBC10-6	84.8 ± 2.8	73.7 ± 5.0	71.7 ± 2.3	62.3 ± 4.8

Table 6.2: D_e values and ages obtained for the SB samples after analysis by two different operators. For each sample, the same dose rate was used by EH and ZJ.

earliest evidence for MHB in Blombos and possibly elsewhere. The evidence consists of two large abalone shells used as containers in which ochre and other ingredients were mixed together to produce paint (see Section 1.2.3). The containers are filled with residues of the mixture that are currently being studied by a group of international scholars. It is believed that these analyses may confirm the ingredients were used as paint and inform us more about the composition of the paint. In addition to the containers, a bone spatula made from a seal scapula as well as other tools have been found alongside these containers, smeared in ochre; these tools were likely the mixers. The whole sedimentary layer is also packed with powdered ochre and when it was first excavated appeared bright red. Such tools would generally be interpreted as unambiguous evidence for MHB and advanced cognition. The ages for these samples range between 106 ± 7 and 111 ± 8 ka. This pushes back the earliest evidence for MHB at Blombos by at least 20-25 ka and place it at the same time, if not slightly earlier, as the early shell beads found in the Levant (Vanhaeren et al., 2006). This also refutes the idea that the SB industry is related to the first wave of modern cognition, and thus supports the idea that modern behaviour likely developed gradually during the MSA in Africa.

6.3.3 *Ages for layer CS – the deepest and oldest archaeological levels*

The two ages obtained for the deepest archaeological levels at the base of the current excavations gave ages that are significantly younger than the overlying levels. The reason for this is not currently fully understood and will be further explored. As a consequence, determining the age of the oldest archaeological levels, one of the aims of my thesis (see Section 1.4), has not been fulfilled. However, based on the ages of the overlying levels, it is likely to by >110 ka and possibly >125 ka.

6.4 Driving forces of behavioural modernity

The possible driving forces behind the sudden appearance and disappearance of the SB industry and other indicators of MHB as identified at Blombos and other MSA sites southern Africa have been argued to pertain to two main factors: 1) environmental change, and 2) demographic change. These will be discussed in the following section.

6.4.1 *Environmental change*

As discussed in section 2.9.2, intense climatic fluctuations have been proposed as a key mechanism behind the appearance and disappearance of the SB industry (e.g. d'Errico et al., 2009; Thackeray, 2009; Fisher et al., 2010). Temperature indices for both the Vostok core in Antarctica (Petit et al., 1999) and Klasies River in South Africa (Thackeray, 2007) have enabled past climatic records to be produced. Given the OSL agess in relation to temperature indices, it would appear that the SB period corresponds with periods of warmer (although cooling) temperatures occurring toward the end of and immediately following oxygen isotop stage (OIS) 5. In addition to this, it has been noted that another period of innovative technologies, associated with the HP industry, occurred when temperatures were several degrees warmer (Thackaray, 2009). It has been argued, however, that the temporal resolution of the Vostok ice core is not congruent over the relevant time period, as data obtained from other Antarctic ice cores such as the Byrd and the EPICA Dronning Maud Land, do not display consistent temporal resolutions (See Fig. 2.8) (Jacobs & Roberts, 2009a). Consequently, there has been hesitation to link the SB industry with warmer temperatures.

Another potential influence that may have impacted on early modern humans and their behaviour relates to sea level change. Using integrated bathymetric datasets, geographical information systems (GIS) and a relative sea level curve, Fisher et al. (2010) have produced a model of the South African coastline position through time. Sea levels were believed to be higher during OIS 5 and lower during OIS 4. Figure 6.1 shows the ages of each of the SB levels plotted on a sea level curve against the OIS in which they occurred, as well as the estimated sea level (Pillans et al., 1998). The diagram reveals the SB industry was present during OIS 4 to OIS 5c, when sea levels were lower. The lower sea levels correspond to periods of marine regression, likely occurring when temperatures were cooler. As such we cannot conclude the SB industry occurred during significant warming periods. Furthermore, if warmer temperatures were the driving force behind behavioural and technological innovations, we would expect to see distinctive sets of innovative technologies throughout the MSA archaeological record corresponding to other periods of warmer temperatures. The ages obtained for the ochre containers, which are believed to reflect cognitive sophistication, are associated with OIS 5d, when sea levels were higher than during OIS 4 (Fisher et al., 2010). This would imply warmer temperatures. However, because two subsequent periods of warming have occurred after the SB and HP industries, and these later periods are not notable for particularly advanced innovations, climate factors alone are insufficient to explain bursts of technological and behavioural innovation, although climate was likely a significant factor in the occupation of certain sites.

6.4.2 *Demographic change*

Increased human population size and settlement density in Africa has also been proposed as a key mechanism behind technological innovation (see Section 2.9.1). According to Powell et al. (2009), skill accumulation increases with increasing population density, and the degree of interaction of constituent sub-populations ensures the inheritance of culturally inherited skills among communities. Consequently, one would expect to see increased complexity in innovations during periods of population expansion. OSL ages achieved in this study reveal the SB industry occurred during a period of population growth (86 to 61 ka) (Atkinson et al., 2008, 2009). This would also be sufficient to explain the appearance of the HP industry which is also associated with MHB. However, no such growth in human population size is recorded for the period of between 115 and 100 ka, which is the age range of the newly uncovered ochre

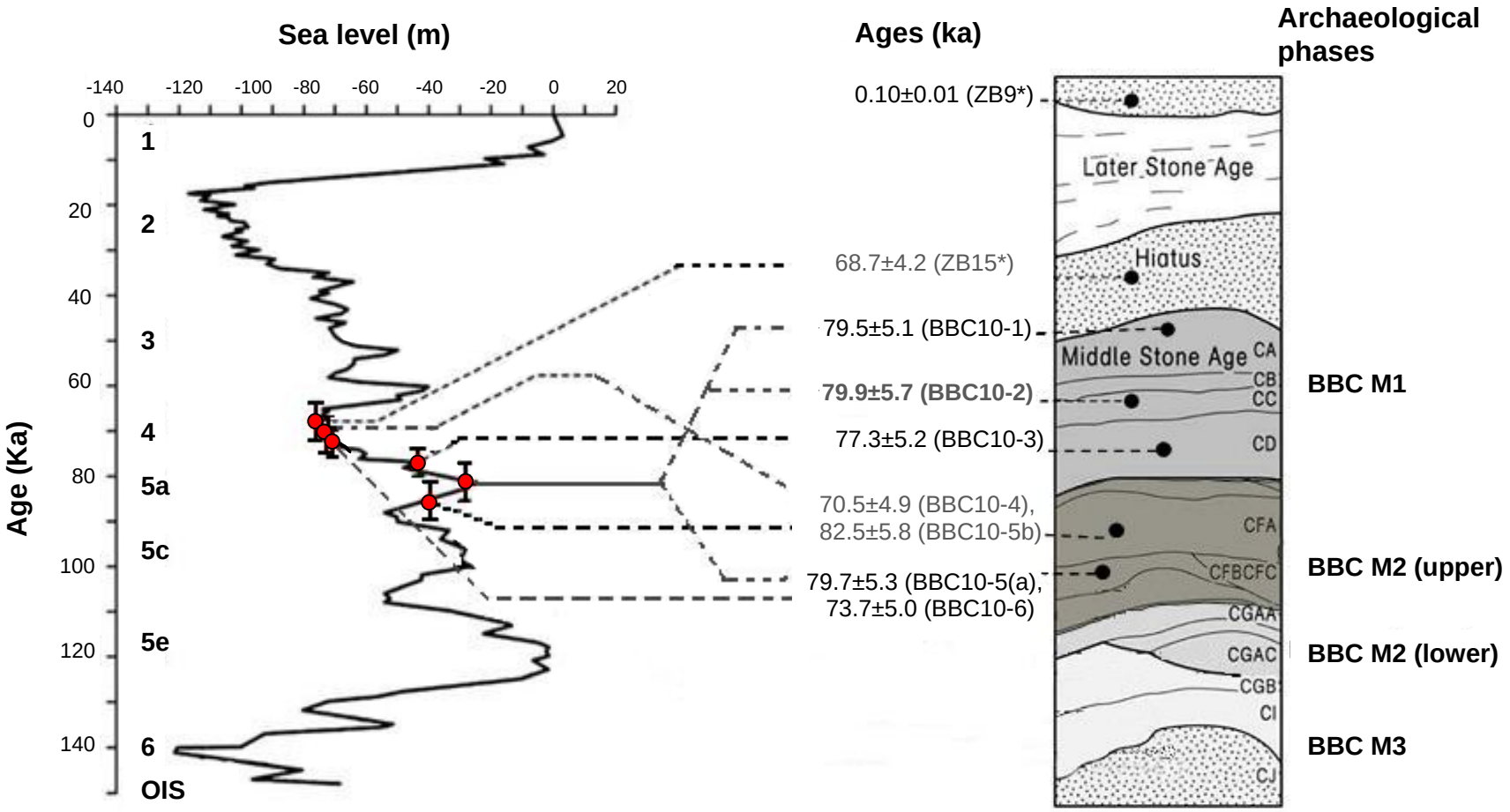

Figure 6.1: SB sample ages and corresponding sea level and oxygen isotope stage (OIS). After Jacobs et al. (2006c).

containers. Although increased population may explain the onset of both the SB and HP industries, it cannot explain this earlier occurrence of behavioural innovation.

6.5 Conclusions

MHB was present in southern Africa at least ~100 ka ago. This evidence comes in the form of ochre containers which contain evidence of the production and use of paint for symbolic expression. The SB industry began abruptly perhaps as early as ~82 ka and lasted until ~70 ka. The abrupt appearance and disappearance of such an industry implies that MHB does not occur in a linear or gradual fashion over time, but rather in the form of abrupt, sporadic events. The most likely cause of this mosaic appearance of MHB through time is a combination of both increased population size and more favourable climatic conditions. Based on the ages obtained from this study, it is likely that the former has greatly influenced the appearance and disappearance of the SB industry. Once more accurate terrestrial temperature records for sub-Saharan Africa are produced for this time period, a greater understanding of the impact of climate and its influence on the emergence of MHB may be achieved.

Section 1.4 presented 3 key aims of this study:

1) *to date the new finds in the deeper and recently excavated deposits, to push back the timing of MHB.*

This aim has been partially achieved by systematically dating layers that contain the recent discovery of the ochre containers as well as the lower, previously undated calcrete layers and the highest layer of the M4 phase. Ages obtained for the levels containing the ochre containers are very significant, as they confirm the presence of MHB at least 25 ka earlier than previously asserted. Ages obtained for the lower calcrete and M4 layers, however, show significant age inversions. Reliable age estimates can, therefore, not be produced for these deeper, recently excavated layers. Further work is required to obtain reliable age estimates.

2) *To collect and date samples from previously excavated layers to more finely resolve the existing evidence for MHB from this site*.

This aim has been achieved by systematically dating each layer within the M1 and M2 (u) phases of the cave. These layers comprise the SB, which contain significant indicators of

MHB. Ages obtained from this phase have enabled determination of any more ages from this industry, which will further help a more reliable estimate for the duration of the SB.

3) *To integrate the new Blombos chronology with ages of modern human behavioural indicators at other sites across Africa and the Levant, and to use this chronology to facilitate comparisons of the archaeological record with demographic and environmental records for the same period.*

Using the chronology achieved from this study, it has been possible to test a number of proposed models believed to initiate or be part of the driving force behind MHB. The ages produced have been compared to past climate and genetic data, so that any pattern in the timing of these events may be observed. From this, suggestions have been made as to the key mechanisms behind behavioural innovation. Investigations carried out in this study imply that a key driving force behind behavioural modernity is related to demographic growth, facilitating the expansion of populations and connectivity between communities.

References

Adamiec, G. 2000. Variations in luminescence properties of single quartz grains and their consequences for equivalent dose estimation. *Radiation Measurements* **32:** 427-432.

Adamiec, G., Aitken, M.J. 1998. Dose–rate conversion factors: update. *Ancient TL* **16:** 27-50.

Aitken, M.J., 1985. Thermoluminescence dating. Academic Press, London.

Aitken, M.J. 1989. Luminescence dating: a guide for non-specialists. *Archaeometry* **31:** 147-159.

Aitken, M.J. 1990. Science-based dating in archaeology. Longman House, London.

Aitken, M.J. 1998. An introduction to optical dating: the dating of Quaternary sediments by the use of photon-stimulated luminescence. Oxford University Press, New York.

Aitken, M.J., Valladas, H. 1992. Luminescence dating relevant to human origins. *In* Aitken, M.J., Stringer, C.B. & Mellars, P.A. eds. *The Origin of Modern Humans and the Impact of Chronometric Dating*, pp. 27-39. Princeton University Press, Princeton, New Jersey.

Aitken, M.J., Xie, J. 1990. Moisture correction for annual gamma dose. Ancient TL 8: 6-9.

Ambrose, S.H. 1998. Chronology of the Later Stone Age and food production in east Africa. *Journal of Archaeological Science* **25:** 377-392.

Appenzeller, T. 1998. Art: evolution or revolution? *Science* **282:** 1451-1454.

Arnold, L.J., Roberts, R.G., Galbraith, R.F., DeLong, S.B., 2009. A revised burial dose estimation procedure for optical dating of young and modern age sediments. *Quaternary Geochronology* **4**: 306–325.

Atkinson, Q.D., Gray, R.D., Drummond, A.J. 2008. MtDNA variation predicts population size in humans and reveals a major southern Asian chapter in human prehistory. *Molecular Biology and Evolution* **25:** 468-474.

Atkinson, Q.D., Gray, R.D., Drummond, A.J. 2009. Bayesian coalescent inference of major human mitochondrial DNA haplogroup expansions in Africa. *Proceedings of the Royal Society B* **276:** 367-373.

Backwell, L., d'Errico, F., Wadley, L. 2008. Middle Stone Age bone tools from the Howiesons Poort layers, Sibudu Cave, South Africa. *Journal of Human Evolution* **35:** 1566-1580.

Bailey, R.M., Smith, B.W, .Rhodes, E.J. 1997. Partial bleaching and the decay from characteristics of quartz OSL. *Radiation Measurements* **27:** 123-136.

Bar-Yosef Mayer, D.E., Vandermeersch, B., Bar-Yosef, O. 2009. Shells and ochre in Middle Palaeolithic Qafzeh Cave, Israel: indications for modern behaviour. *Journal of Human Evolution* **56:** 307-314.

Bell, W.T. 1979. Thermoluminescence dating - radiation dose-rate data. Archaeometry 21: 243-245.

Bell, W.T., Zimmerman, D.W. 1978. Effect of HF acid etching on morphology of quartz inclusions for Thermoluminescence dating. Archaeometry 20: 63 - 65.

Binford, L.R. 1989. Isolating the transition to cultural adaptations: an organisational approach. *In* Trinkaus, E. ed. *The emergence of modern humans: bicultural adaptations in the later Pleistocene*, pp. 18-41. Cambridge University Press, Cambridge.

Bøtter-Jensen, L., Bulur, E., Duller, G.A.T., Murray, A.S. 2000. Advances in luminescence instrument systems. *Radiation Measurements* **32:** 523-528.

Bøtter-Jensen, L., Mejdhal, V. 1985. Determination of potassium in feldspars by beta counting using GM multicounter system. *Nuclear Tracks and Radiation Measurements* **10:** 663-666.

Bøtter-Jensen, L., Mejdahl, V. 1988. Assesment of beta dose-rate using a GM muliticounter system. *Nuclear Tracks and Radiation Measurements* **14:** 187-191.

Bouzouggar, A., Barton, N., Vanhaeren, M., d'Errico, F., Collcutt, S., Higham, T., Hodge, E., Parfitt, S., Rhodes, E., Schwenninger, J., Stringer, C.B., Turner, E., Ward, S., Moutmir, A., Stambouli, A. 2007. 82,000-year-old shell beads from north Africa and implications for the origins of modern human behaviour. *Proceedings of the National Academy of Sciences of the USA* **104:** 9964-9969.

Bowler, J.M., Johnston, H., Olley, J.M., Prescott, J.R., Roberts, R.G., Shawcross, W., Spooner, N.A. 2003. New ages for human occupation and climatic change at Lake Mungo, Australia. *Nature* **421:** 837-840.

Brooks, A.S., Helgren, D.M., Cramer, J.M., Franklin, A., Hornyak, W., Keating, J.M., Klein, R.G., Rink,W.J., Schwarcz, H.P., Smith, J.N.L., Stewart, K., Todd, N.E., Verniers, J.,Yellen, J.E. 1995. Dating and the context of three Middle Stone Age sites with bone points in the upper Semliki Valley, Zaire. *Science* **268:** 548-553.

Brown, K.S., Marean, C.W., Herries, A.I.R., Jacobs, Z., Tribolo, C., Braun, D., Roberts, D. L., Meyer, M.C., Bernatchez, J. 2009. Fire as an engineering tool of early modern humans. *Science* **325:** 859-862.

Brumm, A.F., van den Bergh, G.D., Morwood, M.J., Moore, M.W., Kurniawan, I., Hobbs, D.R. Fullagar, R. 2006. Early stone technology on Flores and its implications for *Homo floresiensis*. *Nature* **441:** 624-628.

Bulur, E., Duller, G.A.T., Solongo, S., Bøtter-Jensen, L., Murray, A.S. 2002. LM-OSL from single grains of quartz: a preliminary study *Radiation Measurements* **35:** 79-85.

Byers, A.M. 1994. Symbolling and the Middle-Upper Palaeolithic Transition. *Current Anthropology* **35:** 369-399.

Byers, A.M. 1999. Communication and material culture: Pleistocene tools as action cues. *Cambridge Archaeological Journal* **9:** 23-41.

Cann, R.L., Stoneking, M., Wilson, A.C. 1987. Mitochondrial DNA and human evolution. *Nature* **325:** 31-36.

Chappell, J., Omura, A., Esat, T., McCulloch, M., Pandolfi, J., Ota, Y., Pillans, B. 1996. Reconciliation of late Quaternary sea levels derived from coral terraces at Huon Peninsula with deep sea oxygen isotope records. *Earth and Planetary Science Letters* **141:** 227-236.

Chase, P.G. 1991. Symbols and Paleolithic Artifacts: Style, Standardization, and the Imposition of Arbitrary Form. *Journal of Anthropological Archaeology* **10:** 193-214.

Chase, P.G. 2006. The Emergence of Culture: The Evolution of a Uniquely Human Way of Life. *PalaeoAnthropology* **2006:** 95-97.

Chase, P.G. & Dibble, H.L. 1987. Middle Paleolithic symbolism: a review of current evidence and interpretations. *Journal of Anthropological Archaeology* **6:** 263-296.

Chen, G., Murray, A.S., Li, S.-H. 2001. Effect of heating on quartz dose-response curve. *Radiation Measurements* **33:** 59-63.

Clark, J.D. 1993. African and Asian perspectives on the origins of modern humans. *In* M. J. Aitken, C. B. Stringer and P. A. Mellars. eds. *The Origin of Modern Humans and the Impact of Chronometric Dating*, pp. Princeton University Press, Princeton, New Jersey.

Dansgaard, W., Johnsen, S. J., Clausen, H. B., Dahl-Jensen, D., Gundestrup, N. S., Hammer, C. U., Hvidberg, C. S., Steffensen, J. P., Sveinbjörnsdottir, A. E., Jouzel, J., Bond, G. 1993. Evidence for the general instability of past climate from a 250-kyr ice-core record. *Nature* **364:** 218-220.

David, B., Roberts, R.G., Magee, J., Mialanes, J., Turney, C., Bird, M., White, C., Fifield, K., Tibby, J. 2007. Sediment mixing at Nonda Rock: investigations of stratigraphic integrity at an early archaeological site in northern Australia and implications for the human colonisation of the continent. *Journal of Quaternary Science* **22:** 449-479.

Davidson, I. & Noble, W. 1989. The archaeology of perception. Traces of depiction and language. *Current Anthropology* **30:** 125-55.

Davidson, I. and Noble, W. 1993 Tools and language in human evolution. In K. Gibson and T. Ingold (eds) *Tools, Language and Cognition in Human Evolution*, pp. 363-388. Cambridge: Cambridge University Press.

Deacon, H. J. 2001. Modern human emergence: An African archaeological perspective *In* P. V. Tobias, M. A. Raath, Maggi-Cecchi and G. A. Doyle. eds. *Humanity from African naissance to coming millennia: Colloquia in human biology and palaeoanthropology*, pp. 217-226. University of Florence Press, Florence.

Demuro, M., Roberts, R. G., Froese, D. G., Arnold, L. J., Brock, F., Bronk Ramsey, C. 2008. Optically stimulated luminescence dating of single and multiple grains of quartz from

perennially frozen loess in western Yukon Territory, Canada: comparison with radiocarbon chronologies for the late Pleistocene Dawson tephra. *Quaternary Geochronology* **3:** 346-364.

d'Errico, F. 2003. The invisible frontier. A multiple species model for the origin of behavioural modernity. *Evolutionary Anthropology* **12:** 188-202.

d'Errico, F., Henshilwood, C.S. 2007. Additional evidence for bone technology in the southern African Middle Stone Age. *Journal of Human Evolution* **52:** 142-163.

d'Errico, F., Henshilwood, C., Lawson, G., Vanhaeren, M., Tillier, A.-M., Soressi, M., Bresson, F., Maureille, B., Nowell, A., Lakarra, J., Backwell, L. & Julien, M. (2003). Archaeological Evidence for the Emergence of Language, Symbolism, and Music–An Alternative Multidisciplinary Perspective. Journal of World Prehistory 17: 1-70.

d'Errico, F., Henshilwood, C.S., Nilssen, P.J. 2001. An engraved bone fragment from *c.* 70,000-year-old Middle Stone Age levels at Blombos Cave, South Africa: implications for the origin of symbolism and origin. *Antiquity* **75:** 309-318.

d'Errico, F., Henshilwood, C.S., Vanhaeren, M., van Niekerk, K. 2005. Nassarius Kraussianus shell beads from Blombos Cave: evidence for symbolic behaviour in the Middle Stone Age. *Journal of Human Evolution* **48:** 3-24.

d'Errico, F., Vanhaeren, M., Barton, N., Bouzouggar, A., Mienis, H., Richter, D., Hublin, J., McPherron, S. P., Lozouet, P. 2009. Additional evidence on the use of personal ornaments in the middle Palaeolithic of north Africa. *Proceedings of the National Academy of Sciences of the USA* **106:** 16051-16056.

d'Errico, F., Vanhaeren, M., Wadley, L. 2008. Possible shell beads from the Middle Stone Age layers of Sibudu Cave, South Africa. *Journal of Archaeological Science* **35:** 2675-2685.

Duller, G.A.T. 1991. Equivalent dose determination using single aliquots. *Nuclear Tracks and Radiation Measurements* **18:** 371.

Duller, G.A.T. 1994. Luminescence dating of sediments using single aliquots: new procedures. *Quaternary Science Reviews* **13:** 149-156.

Duller, G.A.T. 1995. Luminescence dating using single aliquots: methods and applications. *Radiation Measurements* **24:** 217-226.

Duller, G.A.T. 2004. Luminescence dating of Quaternary sediments: recent advances. *Journal of Quaternary Science* **19:** 183-192.

Duller, G.A.T. 2007. Assessing the error on equivalent dose estimates derived from single aliquot regenerative dose measurements. *Ancient TL* **25:** 15-24.

Duller, G.A.T. 2008. Single-grain optical dating of Quaternary sediments: why aliquot size matters in luminescence dating. *Boreas* **37:** 589-612.

Duller, G.A.T., Bøtter-Jensen, L., Murray, A.S., 2000. Optical dating of single sand-sized grains of quartz: sources of variability. *Radiation Measurements*. **32:** 453–457.

Duller, G.A.T., Murray, A.S. 2000. Luminescence dating of sediments using individual mineral grains. *Geologos* **5:** 88-106.

Feathers, J.K. 1996. Luminescence dating and modern human origins. *Evolutionary Anthropology* **5:** 25-36.

Feathers, J.K. 1997. The application of luminescence dating in American archaeology. *Journal of Archaeological Method and Theory* **4:** 1-65.

Feathers, J.K. 2002. Luminescence dating in less than ideal conditions: case studies from Klasies River Mouth and Duinefontein, South Africa. *Journal of Archaeological Science* **29:** 177-194.

Feathers, J.K., Bush, D. A. 2000. Luminescence dating of Middle Stone Age deposits at Die Kelders. *Journal of Human Evolution* **38:** 91-119.

Feathers, J.K., Migliorini, E. 2001. Luminescence dating at Katanda – a reassessment. *Quaternary Science Reviews* **20:** 961-966.

Fisher, E.C., Bar-Matthews, M., Jerardino, A., Marean, C.W. 2010. Middle and Late Pleistocene paleoscape modelling along the southern coast of South Africa. *Quaternary Science Reviews* **29:** 1382-1398.

Forster, P., Matsumura, S. 2005. Did early humans go north or south? *Science* **308:** 965-966.

Galbraith, R.F. 1988. Graphical display of estimates having differing standard errors. *Technometrics* **30:** 271-281.

Galbraith, R.F. 1990. The radial plot: graphical assessment of spread in ages *Nuclear Tracks and Radiation Measurements* **17:** 207-214.

Galbraith, R.F., 2005. Statistics for Fission Track Analysis. Chapman & Hall, London.

Galbraith, R.F. 1998. The trouble with "probability density" plots of fission track ages. *Radiation Measurements* **29**: 125-131.

Galbraith, R.F., Green, P.F. 1990. Estimating the component ages in a finite mixture. *Radiation Measurements* **17:** 197-206.

Galbraith, R.F., Roberts, R.G., Laslett, G.M., Yoshida, H., Olley, J.M. 1999. Optical dating of single and multiple grains of quartz from Jinmium Rock Shelter, Northern Australia: Part I, experimental design and statistical models. *Archaeometry* **41:** 339-364.

Galbraith, R.F., Roberts, R. G., Yoshida, H. 2005. Error variations in OSL palaeodose estimates from single aliquots of quartz: a factorial experiment. *Radiation Measurements* **39:** 289-307.

Grine, F.E., Henshilwood, C. S. 2002. Additional human remains from Blombos Cave, South Africa: (1999-2000 excavations). *Journal of Human Evolution* **42:** 293-302.

Grün, R., Stringer, C.B. 1991. Electron spin resonance dating and the evolution of modern humans. *Archaeometry* **33:** 153-199.

Hammer, M.F. 1995. A recent common ancestry for human Y chromosome. *Nature* **378:** 376-378.

Henshilwood, C.S. 2001. Stratigraphic integrity of the Middle Stone Age levels at Blombos Cave. *In* F. d'Errico and L. Blackwell. eds. *From Tools to Symbols: From Early Hominids to Modern Humans* pp. 441-458. Witwatersrand University Press, Johannesburg.

Henshilwood, C.S. 2004. Marine shell beads from 75 000 year old levels at Blombos Cave *South African Archaeological Society* **21:** 1-4.

Henshilwood, C.S., d'Errico, F., Marean, C.W., Milo, R.G., Yates, R. 2001a. An early bone tool industry from the Middle Stone Age at Blombos Cave, South Africa: implications for the origins of modern human behaviour, symbolism and language. *Journal of Human Evolution* **41:** 631-678.

Henshilwood, C.S., d'Errico, F., Yates, R., Jacobs, Z., Tribolo, C., Duller, G.A.T., Mercier, N., Sealy, J.C., Valladas, H., Watts, I., Wintle, A.G. 2002. Emergence of Modern Human Behaviour: Middle Stone Age engravings from South Africa. *Science* **295:** 1278-1280.

Henshilwood, C.S., d'Errico, F., Vanhaeren, M., Van Niekerk, K., Jacobs, Z. 2004. Middle Stone Age Shell Beads from South Africa. *Science* **304:** 404.

Henshilwood, C.S., d'Errico, F., Watts, I. 2009. Engraved ochres from Middle Stone Age levels at Blombos Cave, South Africa. *Journal of Human Evolution* **57:** 27-47.

Henshilwood, C.S., Marean, C.W. 2003. The origin of modern human behaviour: critique of the models and their test implications. *Current Anthropology* **44:** 627-651.

Henshilwood, C.S., Sealy, J.C. 1997. Bone artefacts from the Middle Stone Age at Blombos Cave, Southern Cape, South Africa. *Current Anthropology* **38:** 890-895.

Henshilwood, C.S., Sealy, J.C., Yates, R., Cruz-Uribe, K., Goldberg, P., Grine, F.E., Klein, R.G., Poggenpoel, C., van Niekerk, K., Watts, I. 2001b. Blombos Cave, Southern Cape, South Africa: Preliminary report on the 1992-1999 excavations of the MSA levels. *Journal of Archaeological Science* **28:** 421-448.

Huntley, D.J., Godfrey-Smith, D.I., Thewalt, M.L.W. 1985. Optical dating of sediments. *Nature* **313:** 105-107.

Huntley DJ and Lamothe M, 2001. Ubiquity of anomalous fading in K-feldspars and the measurement and correct. *Canadian Journal of Earth Science* **38**: 1093-1106,

Huntley, D.J., Wintle, A.G. 1981. The use of alpha scintillation counting for measuring Th-230 and Pa-231 contents of ocean sediments. *Canadian Journal of Earth Sciences* **18:** 419-432.

Ingham, M., Kaessmann, H., Pããbo, S., Gyllensten, U. 2000. Mitochondrial genome variation and the origin of modern humans. *Nature* **408:** 708-713.

Jacobs, Z. 2004. Development of luminescence techniques for dating Middle Stone Age sites in South Africa. PhD thesis, University of Wales (unpublished).

Jacobs, Z., Duller, G.A.T., Wintle, A.G. 2003b. Optical dating of dune sand from Blombos Cave, South Africa: II – single grain data. *Journal of Human Evolution* **44:** 613-625.

Jacobs, Z., Duller, G.A.T., Wintle, A.G. 2006a. Extending the chronology of deposits at Blombos Cave, South Africa, back to 140-ka using optical dating of single and multiple grains of quartz. *Journal of Human Evolution* **51:** 255-273.

Jacobs, Z., Duller, G.A.T., Wintle, A.G. 2006b. Interpretation of single grain D_e distributions and calculations of D_e. *Radiation Measurements* **41:** 264-277.

Jacobs, Z., Roberts, R.G. 2007. Advances in optically stimulated luminescence dating of individual grains of quartz from archeological deposits. *Evolutionary Anthropology* **16:** 210-223.

Jacobs, Z., Roberts, R.G. 2009a. Catalysts for Stone Age innovations. *Communicative and Integrative Biology* **2:** 191-193.

Jacobs, Z., Roberts, R.G. 2009b. Human history written in stone and blood. *American Scientist* **97:** 302-309.

Jacobs, Z., Roberts, R.G. 2009c. Were environmental or demographic factors the driving force behind Middle Stone Age innovations in southern Africa? *South African Journal of Science* **105:** 333-334.

Jacobs, Z., Roberts, R.G., Galbraith, R.F., Deacon, H.J., Grün, R., Mackay, A., Mitchell, P., Vogelsang, R., Wadley, L. 2008b. Ages for the Middle Stone Age of southern Africa: implications for human behavior and dispersal. *Science* **322:** 733-735.

Jacobs, Z., Wintle, A.G., Duller, G.A.T. 2003a. Optical dating of dune sand from Blombos Cave, South Africa: I – multiple grain data. *Journal of Human Evolution* **44:** 599-612.

Jacobs, Z., Wintle, A.G., Duller, G.A.T. 2006c. Evaluation of SAR procedures for D_e determination using single aliquots of quartz from two archaeological sites in South Africa. *Radiation Measurements* **41:** 520-533.

Jacobs, Z., Wintle, A., Duller, G.A.T., Roberts, R.G., Wadley, L. 2008a. New ages for the post-Howiesons Poort, late and final Middle Stone Age at Sibudu, South Africa. *Journal of Archaeological Science* **35:** 1790-1807.

Jacobs, Z., Wintle, A.G., Roberts, R.G., Duller, G.A.T. 2008c. Equivalent dose distributions from single grains of quartz at Sibudu, South Africa: context, causes and consequences for optical dating of archaeological deposits. *Journal of Archaeological Science* **35:** 1808-1820.

Jankowski, N., Jacobs, Z., Roberts, R., Prideaux, G., Gully, G. (in prep). Photons and fauna: Optical dating of palaeontological sites in southwest Western Australia.

Jones, H.L. (2001). *Electron spin resonance dating of tooth enamel at three Palaeolithic sites*. M.Sc thesis, McMaster University, Hamilton, Canada (unpublished).

Klein, R.G. 1995. Anatomy, behaviour, and modern human origins. *Journal of World Prehistory* **9:** 167-198.

Klein, R.G. 2000. Archaeology and the evolution of human behaviour. *Evolutionary Anthropology* **9**:17-36.

Klein, R.G. 2008. Out of Africa and the evolution of human behaviour. *Evolutionary Anthropology* **17:** 267-281.

Lederer, C.M., Hollander, J.M., Perlman, I. 1968. *Table of Isotopes*, 6th ed., Wiley & Sons, New York.

Li, S.H. 1994. Optical dating: insufficiently bleached sediments. *Radiation Measurements* **23:** 563-567.

Lombard, M. 2005. Evidence of hunting and hafting during the Middle Stone Age at Sibudu Cave, KwaZulu-Natal, South Africa: a multianalytical approach. *Journal of Human Evolution* **48:** 279-300.

Lombard, M. 2007. The gripping nature of ochre: The association of ochre with Howiesons Poort adhesives and Later Stone Age mastics from South Africa. *Journal of Human Evolution* **53:** 406-419.

Lombard, M. 2008. Finding resolution for the Howiesons Poort through the microscope: micro-residue analysis of segments from Sibudu Cave, South Africa. *Journal of Achaeological Science* **35:** 26-41.

Mackay, A., Welz, A. 2008. Engraved ochre from Middle Stone Age context at Klein Kliphuis in Westen Cape of South Africa. *Journal of Archaeological Science* **35:** 1521-1532.

Marean, C.W., Bar-Matthews, M., Bernatchez, J., Fisher, E., Goldberg, P., Herries, A.I.R., Jacobs, Z., Jerardino, A., Karkanas, P., Minichillo, T., Nilssen, P.J., Thompson, E., Watts, I., Williams, H.M. 2007. Early human use of marine resources and pigment in South Africa during the middle Pleistocene. *Nature* **449:** 905-908.

McBrearty, S., Brooks, A.S. 2000. The revolution that wasn't: a new interpretation of the origin of modern human behaviour. *Journal of Human Evolution* **39:** 453-563.

McDougall, I., Brown, F.H. Fleagle, J.G. 2005. Stratigraphic placement and age of modern humans from Kibish, Ethiopia. *Nature* **433:** 733-736.

Mellars, P.A. 2006. Why did modern human populations disperse from Africa *ca*. 60,000 years ago? A new model. *Proceedings of the National Academy of Sciences of the USA* **103:** 9381-9386.

Mercier, N., Falguères, C. 2007. Field gamma dose-rate measurement with a NaI (Tl) detector: re-evaluation of the "threshold" technique. *Ancient TL* **25**: 1-4.

Mercier, N., Valladas, H., Joron, J. L., Schiegl, S., Bar-Yosef, O., Weiner, S. 1995. Thermoluminescence dating and the problem of geochemical evolution of sediments- a case study- the Mousterian levels at Hayonim. *Israel Journal of Chemistry* **35:** 137-141.

Milo, R.G. 1998. Evidence for hominid predation at Klasies River Mouth, South Africa, and its implications for the behaviour of early modern humans. *Journal of Archaeological Science* **25:** 99-113.

Minichillo, T. 2006. Raw material use and behavioural modernity: Howiesons Poort lithic foraging strategies. *Journal of Human Evolution* **50:** 356-364.

Murray, A.S. 1981. Environmental radioactivity studies relevant to thermoluminescence dating. PhD thesis, University of Oxford (unpublished).

Murray, A.S., Aitken, M.J. 1988. Analysis of low-level naturally occurring radioactivity in small samples for use in thermoluminescence dating using high-resolution gamma spectrometry. *International Journal of Applied Radiation and Isotopes* **39:** 145-158.

Murray, A.S., Marten, R., Johnston, A., Martin, P. 1987. Analysis of naturally occurring radionuclides at environmental concentrations by gamma spectrometry. *Radioanalytical and Nuclear Chemistry Articles* **115:** 263-288.

Murray, A.S., Olley, J.M. 2002. Precision and accuracy in the optically stimulated luminescence dating of sedimentary quartz: a status review. *Geochronometria* **21:** 1-16.

Murray, A.S., Roberts, R.G. 1997. Determining the burial time of single grains of quartz using optically stimulated luminescence *Earth and Planetary Science Letters* **152:** 163-180.

Murray, A.S., Roberts, R.G. 1998. Measurement of equivalent dose in quartz using a regenerative-dose single-aliquot protocol *Radiation Measurements* **29:** 503-515.

Murray, A.S., Wintle, A.G. 2000. Luminescence dating of quartz using improved single-aliquot regenerative-dose protocol *Radiation Measurements* **32:** 57-73.

Murray, A.S., Wintle, A.G. 2003. The single aliquot regenerative dose protocol: potential for improvements in reliability. *Radiation Measurements* **37:** 377-381.

Noble, W., Davidson, I. 1996. Human evolution, language and mind: a psychological and archaeological inquiry. Cambridge University Press, Cambridge.

Norton, C.J., Jin, J.J.H. 2009. The evolution of modern human behaviour in east Asia; current perspectives. *Evolutionary Anthropology* **18:** 247-260.

Olley, J.M., Caitcheon, G.G., Roberts, R.G. 1999. The origin of dose distributions in fluvial sediments, and the prospect of dating single grains from fluvial deposits using optically stimulated luminescence. *Radiation Measurements* **30:** 207-217.

Olley, J.M., Roberts, R.G., Murray, A. S. 1997. Disequilibria in the uranium decay series in sedimentary deposits at Allen's Cave, Nullarbor Plain, Australia: implications for dose rate determinations. *Radiation Measurements* **27:** 433-443

Olley, J.M., Pietsch, T., Roberts, R.G. 2004. Optical dating of Holocene sediments from a variety of geomorphic settings using single grains of quartz. *Geomorphology* **60:** 337-358.

Partridge, T.C., Demenocal, P.B., Lorentz, S.A., Paiker, M.J., Vogel, J.C. 1997. Orbital forcing of climate over South Africa: a 200,000 year rainfall record from the Pretoria saltpan. *Quaternary Science Reviews* **16:** 1125-1133.

Pienaar, M. 2005. Dating the Stone Age at Rose Cottage Cave in South Africa- An exercise in optical dating cave sediments. MSc thesis, University of Pretoria (unpublished thesis).

Pillans, B.P., Chappell, J., Naish, T.C. 1998. A review of the Milankovitch climatic beat: template for Pilo-Pliestocene sea-level changes and sequence stratigraphy. *Sedimentary Geology* **122**: 5-21.

Plug, I. 2004. Resource exploitation: animal use during the Middle Stone Age at Sibudu Cave, KwaZulu-Natal. *South African Journal of Science* **100:** 151-158.

Porat, N., Rosen, S.A., Boaretto, E., Avni, Y. 2006. Dating the Ramat Saharonim Late Neolithic desert cult site *Journal of Archaeological Science* **33:** 1341-1355.

Powell, A., Shennan, S., Thomas, M.G. 2009. Late Pleistocene demography and the appearance of modern human behaviour. *Science* **324:** 1298-1301.

Prescott, J.R., Hutton, J.T. 1994. Cosmic ray contributions to dose rates for luminescence and ESR dating: large depths and long–term time variations. . *Radiation Measurements* **23:** 497-500.

Prescott, J.R., Robertson, G.B. 1998. Sediment dating by luminescence: a review. *Radiation Measurements* **27:** 893-922.

Reynolds, T.E.G. 1991. Revolution or resolution? The archaeology of modern human origins. *World Archaeology* **23:** 155-166.

Robbins, L.H., Murphy, M.L., Ivester, A.H., Campbell, A.C., Klein, R.G., Milo, R.G., Stewart, K.M., Downey, W.S., Stevens, N.J. 2000. Archaeology, palaeoenvironment, and chronology of the Tsodilo Hills White Paintings Rock Shelter, northwest Kalahari Desert, Botswana. *Journal of Archaeological Science* **27:** 1085-1113.

Robbins, L.H., Murphy, M.L., Stewart, K.M., Campbell, A.C., Brook, G.A. 1994. Barbed bone points, paleoenvironment, and the antiquity of fish exploitation in the Kalahari Desert, Botswana. *Journal of Field Archaeology* **21:** 257-264.

Roberts, R.G. 1997. Luminescence dating in archaeology: from origins to optical. *Radiation Measurements* **27:** 819-892.

Roberts, R.G. & Galbraith, R.F. (in press) Statistical aspects of equivalent dose and error calculation. In: Krbetschek, M. (Ed.), Luminescence Dating: an Introduction and Handbook (Springer, Berlin).

Roberts, R.G., Galbraith, R.F., Olley, J.M., Yoshida, H., Laslett, G.M. 1999. Optical dating of single and multiple grains of quartz from Jinmium Rock Shelter, Northern Australia: Part II, results and implications. *Archaeometry* **41:** 365-395.

Roberts, R.G., Galbraith, R.F., Yoshida, H., Laslett, G.M., Olley, J.M. 2000. Distinguishing dose populations in sediment mixtures: a test of single-grain optical dating procedures using mixtures of laboratory-dosed quartz. *Radiation Measurements* **32:** 459-265.

Roberts, R.G., Jacobs, Z. 2008. Dating in landscape archaeology. *In* Davis, B. and Thomas, J. eds. *Handbook of landscape archaeology*, pp. 347-364. Berg Publishers, Oxford.

Roberts, R.G., Yoshida, H., Galbraith, R.F., Laslett, G.M., Jones, R., Smith, M.A. 1998. Single–aliquot and single–grain optical dating confirm thermoluminescence age estimates at Malakunanja II rock shelter in northern Australia. *Ancient TL* **16:** 19-24.

Scholz, C.A., Johnson, T.C., Cohen, A.S., King, J.W., Peck, J.A., Overpeck, J.T., Talbot, M.R., Brown, E.T., Kalindekafe, L., Amoako, P.Y.O., Lyons, R.P., Shanahan, T. M., Castañeda, I.S., Heil, C.W., Forman, S.L., McHargue, L.R., Beuning, K.R., Gomez, J., Pierson, J. 2007. East African megadroughts between 135 and 75 thousand years ago and bearing on early modern human. *Proceedings of the National Academy of Sciences of the USA* **104:** 16416-16421.

Schwarcz, H.P., Rink, W.J. 2001. Dating methods for sediments of caves and rockshelters with examples from the Mediterranean region. *Geoarchaeology: An International Journal* **16:** 355-371.

Seely, M. 1975. Thermoluminescent dating and its application in archaeology: a review. *Journal of Archaeological Science* **2:** 17-43.

Singarayer, J.S., Bailey, R.M. 2003. Further investigations of the quartz optically stimulated luminescence components using linear modulation. *Radiation Measurements* **37:** 451-458.

Singhvi, A.K., Meldahl, V. 1985. Thermoluminescence dating of sediments. *Nuclear Tracks and Radiation Measurements* **10:** 137-161.

Smith, M.A., Prescott, J.R., Head, M.J. 1997. Comparison of ^{14}C & luminescence chronologies at Puritjarra Rock Shelter, Central Australia. *Quaternary Science Reviews* **16**: 299-320.

Stokes, S. 1999. Luminescence dating applications in geomorphological research. *Geomorphology* **29:** 153-171.

Stokes, S., Colls, A.E.L., Fattahi, M., Rich, J. 2000. Investigations of the performance of quartz single aliquot D_e determination procedures. *Radiation Measurements* **32:** 585-594.

Stringer, C.B. 1999. Has Australia backdated the revolution? *Antiquity* **73:** 876-879.

Stringer, C.B. 2002. Modern human origins: progress and perspectives. *Philosophical Transactions of the Royal Society of London B: Biological Sciences.* **357:** 563-579.

Tattersall, I. 2008. An evolutionary framework for the acquisition of symbolic cognition by *Homo sapiens*. *Comparative Cognition and Behaviour Reviews* **3:** 99-114.

Tattersall, I. 2009. Human origins: Out of Africa. *Proceedings of the National Academy of Sciences of the USA* **106:** 16018-16021.

Texier, P., Parkington, J., Rigaud, J., Poggenpoel, C., Miller, C., Tribolo, C., Cartwright, C., Coudenneau, A., Klein, R.G., Steele, T., Verna, C. 2010. A Howiesons Poort tradition of engraving ostrich eggshell containers dated to 60,000 years ago at Diepkloof rock shelter, South Africa. *Proceedings of the National Academy of Sciences of the USA* **107:** 6180–6185.

Thackeray, J.F. 2009. Chronology, climate and technological innovation associated with the Howiesons Poort and Still Bay industries in South Africa. *South African Journal of Science* **105:** 90.

Tribolo, C., Mercier, N., Rasse, M., Soriano, S. Huysecom, E. 2010. Kobo 1 and L'Abri aux Vaches (Mali, West Africa): Two case studies for the optical dating of bioturbated sediments. *Quaternary Geochronology* **5:** 317-323.

Tribolo, C., Mercier, N., Selo, M., Valladas, H., Joron, J.L., Reyss, J.L., Henshilwood, C.S., Sealy, J.C., Yates, R. 2006. TL dating of burnt lithics from Blombos Cave (South Africa): Further evidence for the antiquity of modern human behaviour. *Archaeometry* **48:** 341-357.

Tribolo, C., Mercier, N., Valladas, H., Joron, J. L., Guibert, P., Lefrais, Y., Selo, M., Texier, P.-J., Rigaud, J.-P., Porraz, G., Poggenpoel, C., Parkington, J., Texier, J.-P. Lenoble, A. 2009. Thermoluminescence dating of a Stillbay–Howiesons Poort sequence at Diepkloof Rock Shelter (Western Cape, South Africa). *Journal of Archaeological Science* **36:** 730-739.

Valladas, G., Reyss, J.L., Joron, J.L., Valladas, G., Bar-Yosef, O., Vandermeersch, B. 1988. Thermoluminescence dating of Mousterian 'Proto-Cro-Magnon' remains from Israel and the origin of modern man. *Nature* **331:** 614-616.

Vanhaeren, M., d'Errico, F., Stringer, C.B., James, S.L., Todd, J.A., Mienis, H.K. 2006. Middle Palaeolithic shell beads in Israel and Algeria. *Science* **312:** 1785-1788.

Vigilant, L., Stoneking, M., Harpending, H., Hawkes, K., Wilson, A. 1991. African populations and the evolution of human mitochondrial DNA. *Science* **253:** 1503-1507.

Villa, P., Soressi, M., Henshilwood, C.S., Mourre, V. 2009. The Still Bay points of Blombos Cave (South Africa). *Journal of Archaeological Science* **36:** 441-460.

Wadley, L., Hodgskiss, T., Grant, M. 2009. Implications for complex cognition from the hafting of tools with compound adhesives in the Middle Stone Age, South Africa. *Proceedings of the National Academy of Sciences of the USA* **106:** 9590-9594.

Wadley, L. 2010. Were snares and traps used in Middle Stone Age and does it matter? A review and a case study from Sibudu, South Africa. *Journal of Human Evolution* **58:** 179-192.

Wallinga, W., 2002. Optically stimulated luminescence dating of fluvial deposits: a review. *Boreas* **31:** 303-322.

Watson, E., Forster, P., Richards, M., Bandelt, H.-J. 1997. Mitochondrial footprints of human expansions in Africa. *American Journal of Human Genetics* **61:** 691-704.

White, T.D., Asfaw, B., DeGusta, D., Gilbert, H., Richards, G.D., Suwa, G., Howell, F.C. 2003. Pleistocene *Homo sapiens* from Middle Awash, Ethiopia. *Nature* **423:** 742-747.

Wintle, A.G. 1973. Anomalous fading of thermoluminescence in mineral samples. *Nature* **245:** 143-144.

Wintle, A.G. 1993. Luminescence dating of aeolian sands: an overview. *Geological Society of London, Special Publications* **72:** 49-58.

Wintle, A.G. 1996. Archaeologically relevant dating techniques for the next century. *Journal of Archaeological Science* **23:** 123-138.

Wintle, A.G. 2008. Fifty years of luminescence dating. *Archaeometry* **50:** 276-312.

Wintle, A.G., Murray, A.S., 2006. A review of quartz optically stimulated luminescence characteristics and their relevance in single-aliquot regeneration dating protocols. *Radiation Measurements* **41:** 369-391.

Wurz, S.J.D. 1999. The Howiesons Poort backed artefacts from Klasies River: an argument for symbolic behaviour. *South African Archaeological Bulletin* **54:** 38-50.

Wurz, S.J.D. 2000. The Middle Stone Age at Klasies River. PhD thesis, University of Stellenbosch (unpublished).

Wynn, T. 2009. Hafted spears and the archaeology of mind. *Proceedings of the National Academy of Sciences of the USA* **106:** 9544-9545.

Yellen, J.E., Brooks, A.S., Cornelissen, E., Mehlman, M.J. Stewart, K. 1995. A Middle Stone Age worked bone tool industry from Katanda, Upper Semliki Valley, Zaire. *Science* **268:** 553-556.

Yoshida, H., Roberts, R.G., Olley , J.M. 2003. Progress towards single-grain optical dating of fossil mud-wasp nests and associated rock art in northern Australia. *Quaternary Science Reviews* **22:** 1273-1278.

Yoshida, H., Roberts, R.G., Olley, J.M. Galbraith, R.F. 2000. Extending the age range of optical dating using single 'supergrains' of quartz. *Radiation Measurements* **32:** 439-446.

Zielinski, S. (July, 2008). Showing their age: dating the fossils and artefacts that mark the great human migration. Smithsonian magazine online.

Zilhão, J. 2007. The emergence of ornaments and art: an archaeological perspective on the origins of "behavioural modernity". *Journal of Archaeological Science* **15:** 1-54.

Zimmerman, D.W. 1971. Thermoluminescent dating using fine grains from pottery. *Archaeometry* **13**: 29-52.